DOKUZ EYLUL UNIVERSITY

GRADUATE SCHOOL OF NATURAL AND APPLIED

SCIENCES

FAILURE ANALYSIS OF BOLTED AND PINNED COMPOSITE JOINTS UNDER TEMPERATURE EFFECTS

by

İbrahim Fadıl SOYKÖK

October, 2012

İZMİR

FAILURE ANALYSIS OF BOLTED AND PINNED COMPOSITE JOINTS UNDER TEMPERATURE EFFECTS

A Thesis Submitted to the
Graduate School of Natural and Applied Sciences of Dokuz Eylül University
In Partial Fulfillment of the Requirements for the Degree of Doctor of
Philosophy in Mechanical Engineering, Mechanics Program

by
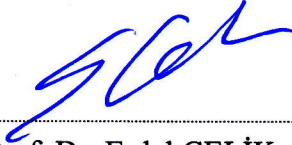İbrahim Fadıl SOYKÖK

October, 2012
İZMİR

Ph.D. THESIS EXAMINATION RESULT FORM

We have read the thesis entitled **"FAILURE ANALYSIS OF BOLTED AND PINNED COMPOSITE JOINTS UNDER TEMPERATURE EFFECTS"** completed by **İBRAHİM FADIL SOYKÖK** under supervision of **PROF. DR. ONUR SAYMAN** and we certify that in our opinion it is fully adequate, in scope and in quality, as a thesis for the degree of Doctor of Philosophy.
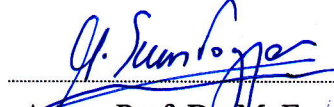
Prof. Dr. Onur SAYMAN

Supervisor

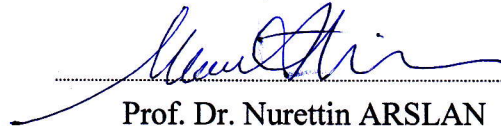Prof. Dr. Erdal ÇELİK

Thesis Committee Member

Assoc. Prof. Dr. M. Evren TOYGAR
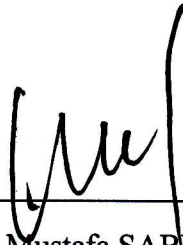
Thesis Committee Member

Prof. Dr. Ramazan KARAKUZU

Examining Committee Member

Prof. Dr. Nurettin ARSLAN

Examining Committee Member

Prof. Dr. Mustafa SABUNCU

Director

Graduate School of Natural and Applied Sciences

ACKNOWLEDGMENTS

İbrahim Fadıl SOYKÖK

FAILURE ANALYSIS OF BOLTED AND PINNED COMPOSITE JOINTS UNDER TEMPERATURE EFFECTS

ABSTRACT

In the first part of the study, experimental failure analysis has been carried out to determine the effects of high temperatures and tightening torques on the failure load and failure behavior of single lap double serial fastener glass fiber / epoxy composite joints. 40, 50, 60, 70, and 80 degrees centigrade temperatures were exposed to the specimens during tensile tests. It was seen that the load-carrying capacity of the joint is decreased gradually by increasing temperature level. In proportion to the room temperature, the maximum decrease of failure loads occurs at 70 and 80 degrees centigrade with the rate of nearly 55 and 70 percent respectively, because of the heat damage to the resin matrix. In the second part of the study, experimental investigations were conducted on failure responses of single lap double serial fastener joints in glass fiber / epoxy composite laminates when subjected to low temperature environment. The results of experiments, implemented at five different low temperature levels ranging from 0 to -40 degrees centigrade, were evaluated in comparison with room temperature tests. Joints exhibited relatively higher load-carrying capacities with increased stiffness by decreasing temperature. Both in the first and second part of experiments, bolts were fastened under M= 6 Nm and M= 0 Nm (finger tightened) torques in order to examine tightening torque effects at each temperature condition. As expected, a greater amount of bearing load could be carried by the joints with pre-tightened fasteners. The results proved that, tightening torque is still effective at elevated and low temperature conditions, Furthermore, any reduction in temperature at subzero degrees centigrade is observed to lift the effectiveness of tightening torque on the joint strength. In addition, bearing mode, the most desirable failure type in mechanically fastened joints was monitored as the main failure mode, regardless of the temperature exposed.

Keywords: glass fiber composites, composite joints, high temperature, low temperature

CIVATALI VE PİMLİ KOMPOZİT BAĞLANTILARIN SICAKLIK ETKİLERİ ALTINDA HASAR ANALİZİ

ÖZ

Çalışmanın ilk bölümünde, yüksek sıcaklığın ve sıkma momentinin tek katlı, çift seri cıvatalı cam elyaf / epoksi kompozit bağlantıların hasar yükleri ve hasar davranışları üzerindeki etkilerini belirlemek için deneysel hasar analizleri gerçekleştirilmiştir. Çekme testleri sırasında numunelere 40, 50, 60, 70 ve 80 santigrat derecelerinde sıcaklık kademeleri uygulanmıştır. Görülmüştür ki, sıcaklık seviyesinin yükselmesiyle birlikte, bağlantının yük taşıma kapasitesi de kademeli olarak düşmüştür. Reçine matristeki ısıl deformasyon nedeniyle, oda sıcaklığındakine oranla hasar yükündeki en yüksek azalma 70 ve 80 santigrat derece sıcaklıklarında sırasıyla yaklaşık yüzde 55 ile 70 seviyelerinde gerçekleşmiştir. Çalışmanın ikinci bölümünde, düşük sıcaklık ortamına maruz bırakıldığında tek katlı, çift seri cıvatalı cam elyaf / epoksi kompozit plaka bağlantıların hasar davranışları üzerine deneysel araştırmalar gerçekleştirilmiştir. 0 ile -40 santigrat dereceleri arasında değişen beş farklı sıcaklık kademesinde gerçekleştirilen deneylerin sonuçları oda sıcaklığındaki test sonuçlarıyla karşılaştırmalı olarak değerlendirilmiştir. Bağlantılar sıcaklık düşüşüne karşılık rijitlik artışı ile birlikte, nispeten daha yüksek yük taşıma kapasiteleri sergilemişlerdir. Deneylerin birinci ve ikinci bölümünün her ikisinde de her bir sıcaklık ortamındaki sıkma momenti etkisini sınayabilmek için cıvatalar M= 6 Nm ve M= 0 Nm (el ile sıkılmış) momentleri ile sıkılmıştır. Beklendiği üzere, daha yüksek seviyedeki çekme yükleri ön gerilme uygulanmış cıvatalara sahip bağlantılar tarafından taşınabilmektedir. Sonuçlar, sıkma momentinin, yüksek ve düşük sıcaklıklarda da halen etkili olduğunu ispat etmektedir. Ayrıca, sıfır santigrat altındaki sıcaklıklarda, sıcaklıktaki herhangi bir azalmanın sıkma momentinin bağlantı dayanımı üzerindeki etkisini yükselttiği gözlemlenmiştir. Buna ek olarak, uygulanan sıcaklığa bağlı olmaksızın, ana hasar mekanizması olarak mekanik bağlantılarda en çok tercih edilen hasar tipi olan yatak ezilme hasarı gözlemlenmiştir.

Anahtar sözcükler: cam elyaf kompozitler, kompozit bağlantılar, yüksek sıcaklık, düşük sıcaklık

CONTENTS

CHAPTER ONE
INTRODUCTION

1.1 Overview

Because of rapid technological development and increased competition in industry, lightweight, high strength materials with high performance have been the main need in real applications. The use of composite materials which meets the need has an ever-expanding trend of variety such as for military and commercial air vehicles, robot arms, and automotive industry. Especially for use in aviation and aerospace industry, composite materials, which are lighter than metals and higher strength in terms of weight, are designed and produced. Trusses, optical benches, equipment-panels, solar array support systems, and radiators, are some typical spacecraft structures which should have high specific stiffness, low coefficient of thermal expansion and dimensional stability during operation. High-performance composites satisfy these requirements, and also offer the minimum weight material solution for these structures (Park, 2001). They are also becoming more commonly used with every generation of aircraft. The Boeing 787 is a prime example, which is set to include 50% composite material by weight. (Pearce et al., 2010).

It is generally impossible to produce a structure without using joints because of the limitations of material sizes, and conformity for manufacture or transportation. Joints are usually the weakest points of a construction so they determine the stability of composite structure. Composite structures can be assembled by using adhesively bonded and / or mechanically fastened joints. Although leading to a weight penalty due to stress concentration created by drilling a hole in the laminate, mechanical fasteners are widely used in composite joints owing to their unique characteristics such as lower cost of producing, testing and maintaining and convenience to inspect load carrying capacity etc.

The above mentioned stress concentrations lead to high tensile stresses in pinned and bolted composite parts. On the other hand, the front side of the hole is deformed

under pressure and the interface between the fastener and the laminate change as applied load increasing, which results in altering the force distribution in the interface. Depending on its geometry, a pinned or bolted composite joint can exhibit four different failure modes, namely the net tension, bearing, shear-out, and cleavage failure. In practice, combinations of these failure modes are observed. The bearing and shear-out failure modes are usually more or less ductile, but the net-section and cleavage ones are brittle and abrupt. The net tension failure mode is defined by fracture of a laminate across its width from the hole to its edges, the shear-out failure mode is described by the pull-out fracture between the hole and laminate end, and the cleavage failure mode is defined by the simultaneous fracture across the width to one edge and between the hole and the laminate end. The bearing failure mode is thought to be the desirable mode, since it generally gives a higher strength, and the failure is less brittle. The other three modes are often considered as premature ones, which should be prevented through a proper design of the joint geometry and the composite material it self. These failure types are undesirable, giving rise to an abrupt damage growth. Finally, a serious problem in designing the joints is the selection of their geometrical parameters suitable to force the bearing failure (Pekbey, 2008).

An understanding of the stiffness, strength and failure mode of bolted joints is critical to an efficient design of composite structures. The strength of pinned or bolted joints depends on many factors, including joint geometry, fiber orientation, stacking sequence, through thickness pressure, etc. Similarly, the particular failure mode that is observed in a pinned or bolted connection is also dependent on geometry, lay up, and loading direction. A large part of the research that has been done on mechanically fastened joints has been concerned with the experimental and numerical determination of the influence of geometric factors on the joint strength and failure type. Several authors carried out the effects of joint geometry, ply orientation and geometrical parameters such as the end distance-to-diameter (E/D), width-to-diameter ratios (W/D) on the failure strength and failure modes of mechanically fastened laminated composite plates (Asi, 2010).

Karakuzu et al. (2008) investigated the effects of geometrical parameters such as the edge distance-to-hole diameter ratio (E/D), plate width-to-hole diameter ratio (W/D), and the distance between two holes-to-hole diameter ratio (M/D) on the failure loads and failure modes in woven-glass–vinyl ester composite plates with two serial pin-loaded holes, experimentally and numerically. In the numerical analysis, they used the Hashin failure criterion in order to determine failure loads and failure modes. LUSAS commercial finite element software was utilized during their analysis. After experimental and numerical studies they showed that the ultimate load capacity of woven glass– vinyl ester laminates with pin connections increased by increasing ratios E/D, W/D, and M/D. Besides geometrical parameters, Sayman & Ozen (2011) investigated the first failure load and the bearing strength behavior of pinned joints of glass fiber reinforced woven epoxy composite prepregs with two serial holes subjected to traction forces by two serial rigid pins for immersed and unimmersed conditions. There was almost no difference between the results of the immersed and unimmersed specimens under preload moments.

Aktaş et al. (2009) analyzed experimentally and numerically failure mode and failure load of glass-epoxy plates with single and double parallel-pinned joints. The distance from the free edge of plate to the diameter of the first hole (E/D) ratios (2, 3, 4, 5) and the width of the specimen to the diameter of the holes (W/D) ratios (2, 3, 4, 5) were investigated during analyses. Experiments were carried out according to ASTM D953-D and numerical study was performed by means of ANSYS program. According to experimental and numerical results, from which a good agreement obtained, the pin hole farthest from the free edge is subjected to the highest stress.

Okutan (2006) investigated the effects of joint geometry and fiber orientation on the failure strength and failure mode in pinned joint laminated composite plate. E/glass-epoxy laminated composites were loaded through pins. The specimens were loaded by single hole and tested to evaluate width to hole diameter (W/D) and the edge distance to hole diameter (E/D) effects. Six different composite configurations ([0/±45]s–[90/±45]s, [0/90/0]s–[90/0/90]s and [90/0]2s–[±45] 2s) were used. E/D ratios from 1 to 5 and W/D ratios from 2 to 5 were tested. Testing results showed that

the fiber orientations have definite influence on the position around hole circumference at which failure initiated. Another result was that the ultimate load capacities of E/glass-epoxy laminate plates with pin connection were increased by increasing W and E, but if E/D and W/D are increased beyond a critical value it has not a significant effect on the ultimate load capacity of the connection.

Asi (2010) studied pinned joints of glass fiber reinforced composite filled with different proportions of Al_2O_3 particles (as function of filler loading and joint geometry) and investigated the bearing strength behavior. The weight fractions of the filler in the matrix were 7,5,10 and 15 %. The single hole pin loaded specimens were tested in tension. The test results showed that the increase of Al_2O_3 particle in the matrix improves the bearing strength of composites. Beyond a critical value of particle content the bearing strength began to decrease but remained above that of the unfilled glass reinforced epoxy composites.

In order to determine the influence of the preload moment, the edge distance to the pin diameter ratio, and the specimen width to the pin diameter ratio on the strength of the material, Pekbey (2008) investigated the failure strength of a bolted joint e-glass/epoxy composite plate.   Load-displacement curves were obtained for each test. Experimental results showed that the maximum bearing strength was reached at max preload moment 4 Nm, max W/D ratio 6 and max E/D ratio 5. At W/D=2 the most dangerous mode net tension developed and at E/D<2 the shear-out failure mode occurred, which is another undesirable failure mode.

Ling (1986) considered the effect of clamping on bolted joints and presented a way to predict critical bearing strength of single-hole joints on the basis of observing and analyzing the results of experiments. The comparison between the experimental and the calculated value showed that the estimate method of the ultimate bearing load is available for bolted joints.

Dano at al. (2000) presented a finite element model including the characteristics friction, non-linear shear behavior, large deformation theory and property

degradation. In particular, the influence of the failure criteria and the inclusion of geometric and shear non-linearities was discussed in the paper. The deformation behavior of the pin loaded joint was predicted using a two dimensional finite element model developed in the commercial software ABAQUS. The composite plate was modeled using a single layer of CPS4 elements since shell element couldn't be used to simulate in plane-contact problems. Because the technique allowed computing the stresses in each ply, propagation of damage from ply-to-ply could be studied. Then the progressive failure analysis used to study damage propagation around the hole was described. To predict the progressive ply failure, the analysis combined Hashin and the maximum stress failure criteria. From the theoretical and the experimental results of the study, it can be concluded that when the shear stress-strain relationship is linear, the use of maximum stress criterion for fiber failure leads to higher and more realistic strength than Hashin criterion. When a non-linear shear stress-strain relationship is considered, the predictions from the different failure analysis converge toward the same predictions. When using mixed failure criteria, including a non-linear shear behavior has a slight effect for the quasi-isotropic $[(0/\pm45/90)_3]$s laminate whereas for the $[(0/90)_6]$s and $[(\pm45)_6]$s laminates the increase in the strength prediction was quite important.

Park (2001 a) developed a methodology for assessing the delamination bearing strength of mechanically fastened joints in finite carbon-epoxy composite laminates in conjunction with accurate three dimensional contact stress analysis via a quasi-three-dimensional finite element procedure based on the layer wise theory. The contact phenomena and stress distribution in the vicinity of joints in composite laminates were investigated. The lamination bearing failure strengths of mechanically fastened joints in composite laminates were predicted using modified Ye-delamination failure criterion based on layer wise finite element contact stress analysis. Comparisons of the numerical results with experimental data showed the accuracy and applicability of the analysis.

Park (2001b) examined the effects of stacking sequence and clamping force on delamination bearing strength and ultimate bearing strength of mechanically fastened

joints in carbon/epoxy composite laminates using the acoustic emission (AE) technique. Two orthotropic and three quasi-isotropic laminate lay-up configurations and four clamping forces were examined. Based on the experiments, the effects of stacking sequence and clamping force on joint strengths were systematically investigated. Guidelines for effective stacking sequences and maximum clamping forces for mechanically fastened joints in composite laminates were suggested based on delamination bearing strength and ultimate bearing strength. According to the experimental investigation it was found that: a) the stacking sequence and clamping pressure have a great influence on the delamination and the ultimate bearing strength of bolted and pinned joints of composite laminates. b) The stacking sequence of the lay-up $[90_6/0_6]s$ with 90º layers on the surface would be more advantageous than the lay-up $[0_6/90_6]s$ with 0º layers on the surface, in the aspect of delamination failure of composite laminates on bearing plane. c) The stacking sequence of $[90_3/0_3/\pm45_3]s$, which has the highest delamination bearing strength and the second highest ultimate bearing strength, should be preferred from the view-point of its characteristics of the fail-safe delamination failure. d) The delamination bearing strength of the lay-up with 90º layers on the surface is stronger than the one with 90º layers located at the center of laminate. e) The lateral clamping pressure increases both the delamination and ultimate failure strengths of bolted joints in composite laminates. f) As the clamping pressure increases, the ultimate bearing strength shows a significant increase toward saturation, while the delamination bearing strength shows a progressive increase. The ultimate bearing strengths do not increase after the saturated bolt clamping pressure. Hence, it is desirable that the clamping torque of a bolted joint in a composite laminate should not exceed the saturated bolt clamping pressure.

A methodology to predict the onset of damage, final failure and failure mode of mechanically fastened joints in composite laminates was introduced by Camanho & Lambert (2006). The stress distribution at each ply was obtained using semi-analytical or numerical methods. The elastic limit of the joint was predicted using the ply strengths and stress distribution in failure criteria. Final failure and failure mode were predicted using point or average stress models. Standardized procedures to

measure the characteristic distances used in the point or average stress models were proposed. The statistical analysis of the experimental results showed that the characteristic distances in tension are a function of both the hole diameter and specimen width. It was also concluded that the characteristic distances in compression are a function of the clamping conditions applied to the joints and of the hole diameter. The methodology proposed was proved that it is practical in double-shear mechanically fastened joints using quasi-isotropic laminates under uniaxial or multi-axial loading. The predictions were compared with experimental data obtained in pin-loaded and bolt-loaded joints, and the results indicated that the methodology proposed could accurately and effectively predict ultimate failure loads as well as failure modes in composite bolted joints.

Bolt-hole clearance effects on failure behavior have been another issue of interest, the researchers are dealing with. Kelly and Hallström (2004), examined the effect of bolt-hole clearance on the bearing strength at 4% hole deformation and at ultimate load. Significant reduction in bearing strength at 4% hole deformation was found for both pin-loaded and clamped laminates as a result of bolt-hole clearance. It was concluded that the effect of bolt-hole clearance is significant with regard to the design bearing strength of mechanically fastened joints. The magnitude and distribution of stress at the hole was found to be significantly dependent on the level of clearance.

Sen et al. (2008) investigated the failure mode and bearing strength of mechanically fastened bolted-joints in glass fiber reinforced epoxy laminated composite plates, experimentally. Two different geometrical parameters which are the edge distance-to-hole diameter ratio (E/D) and plate width-to-hole diameter ratio (W/D) were studied. E/D ratios were selected from 1 to 5, whereas W/D ratios were chosen from 2 to 5. Laminated plates were stacked as three different group which are $[0°/0°/45°/–45°]s$, $[0°/0°/45°/45°]s$ and $[0°/0°/30° /30°]s$, to determine material parameters effect. In addition, the preload moments were applied as 0, 3 and 6 Nm, to observe the changing of failure mechanism under various preloads. The experiments were also performed under a clearance, thus the diameters of the bolt

and the circular bolt hole were fixed 5 and 6 mm, respectively. Results showed that failure modes and bearing strengths were affected by the increasing of preloads to a considerable extent. The maximum values of bearing strengths were calculated for the group of having 3 Nm torque. Furthermore, when the material and geometrical parameters of composite bolted joints were changed, the failure behavior and the values of bearing strengths were fully influenced from this change.

A similar study was conducted by Kishore et al. (2009). The study was aimed to obtain failure modes and failure loads for multi-pin joints in unidirectional glass fiber/epoxy composite laminates by finite element analysis and validating the results with the experimental work. The effect of variation in pitch-to-diameter ratio (P/D), in addition to side width-to-diameter (S/D) and edge-to-diameter (E/D) ratios were studied in multi-pin joints. Developing a two-dimensional finite element model with ANSYS software, Tsai–Wu failure criteria associated with material property degradation was used in the analysis to predict failure load and to differentiate failure modes.

An artificial neural network (ANN) method was developed by Sen et al. (2010) to predict the bearing strength of two serial pinned / bolted E-glass reinforced epoxy composite joints. The experimental data with different geometrical parameters and under various applied torques were used for developing the ANN model. Comparisons of ANN results with desired values showed that ANN is a valid powerful tool to prediction of bearing strength of two serial pinned / bolted composite joints. In another study, Sen & Sayman (2011) investigated the effects of material parameters, geometrical parameters and magnitudes of preload moments on the failure response of two serial bolted joints in composite laminates. Some geometrical ratios were found out to be unfavorable and the increasing of preloads was seen very convenient for safe design of two serial bolted composite joint.

Lie et al. (2000) developed a boundary element formulation for analyzing a mechanically bolted composite. Boundary equations were formulated for all the member panels of the composite joints. These equations were solved together with

the fastener equations to get the resultant contact forces for all the fasteners involved. The fasteners were then modeled as 1D springs that are governed by linear relationship between the fastener forces and the displacements of member panels at the respective fastener centers. After obtaining all the fastener forces from the global analysis, detailed stress analysis was performed for region around an individual fastener. The stress distributions around fastener holes were then used to evaluate the margin of safety of the composite panels. The numerical predictions on the fastener forces, failure modes and failure loads of two typical bolted composite joints using the proposed method were compared and it was found that they agree well with that of the experimental results.

The onset of local damage in joints, such as delamination, cracking and fastener loosening can often be difficult to detect and has long-term implications on the performance of the structure. To develop an innovative technique to monitor the state of damage in composite structures, Thostenson et al. (2008) reported the capability of carbon nanotube networks as in situ sensors for sensing local composite damage and bolt loosening in mechanically fastened glass/epoxy composite joints. According to their research it was possible to detect the onset and progression of damage in the joint through careful design of the specimen.

Ekh & Schön (2006) developed a three-dimensional finite element model in order to determine the load transfer in multi fastener single shear joints. The model was based on continuum elements and accounted for the mechanisms involved in load transfer, such as bolt-hole clearances, bolt clamp-up and friction. They conducted an experimental program in order to validate the finite element model through measurement of fastener loads, by means of instrumented fasteners. The results showed that simulations and experiments agreed well and the bold-hole clearance is the most important factor in terms of load distribution between the fasteners. Any variation in clearance between the different holes implies that the load is shifted to the fastener where the smallest clearance occurs. It was also found that sensitivity to this variation was large, so that temperature changes could significantly affect the load distribution if member plates with different thermal expansion properties are

used. It was concluded that, good accuracy in load transfer predictions requires that all factors would be taken into consideration and nonlinear kinematics should be accounted for the solution process.

In some cases, the joints transferring large mechanical loads between composite panels of advanced vehicles need to be operated at high and low temperature extremes. Mechanical properties of polymer matrix joints are usually influenced by the thermal environment. In particular, it is known that temperatures exceeding the glass transition temperature (Tg) seriously degrade the material properties. The amount or rate of material degradation varies depending on the material (Song et al., 2008). At the other end of spectrum, an application of composite joint in a cryogenic environment would be possible. A computational study investigating thermal effects on pin bearing behavior of IM7/PETI5 composite joints was reported by Walker (2002). Pin-bearing tests of several lay-ups at the operating temperatures of -129, 21, and 177 °C were conducted to generate data on the effect of temperature changes on the pin-bearing behavior. Thermal residual stresses were combined with the state of stress due to pin-bearing loads at three-dimensional solution. The presence of thermal residual stresses intensify the inter laminar stresses predicted at the hole boundary in the pin-bearing problem. The research showed that changes in material properties drive pin-bearing strength degradation with increasing temperature.

Sánchez-Sáez et al. (2002) tested carbon fiber reinforced epoxy laminates to determine the effect of low temperature on the mechanical behavior. Tensile and bending static tests were carried out on two laminate lay-ups (quasi-isotropic and cross-ply laminates), determining properties such as the mechanical strength, stiffness and strain to failure. The results reveal the changes in the mechanical behavior of this material at different test temperatures (20, -60 and -150 °C). As a result, three different test temperatures affected the mechanical behavior of the material. The stiffness of the quasi-isotropic laminate grows as the temperature decreases. At room temperature, the matrix fails first. As the temperature decreases, the fiber–matrix interface becomes much weaker and thus the fibers debond from the matrix.

Hirano et al. (2007) investigated the effects of temperature on the bearing failure of a pinned joint in CF/epoxy quasi-isotropic laminates. Two stacking sequences, namely, $[0/45/{-}45/90]_{3S}$ and $[90/{-}45/45/0]_{3S}$, were loaded at room temperature (25℃), high temperature (150℃), and low temperature (-100℃); then, the internal damages were evaluated. It was found that the bearing failure of a pinned joint is composed of various damages depending on environmental temperatures; further, the strength of the pinned joint is closely related to the compressive kinking failure of all the inner layers.

1.2 Objectives of the Study

As seen in related literature, many authors were interested in material and geometrical parameters influencing the failure behaviors of mechanically fastened composite joints. However, a few of them have taken into account the environmental effects, particularly the temperature extremes that composite joints are exposed during operation. Among these studies, those associated with glass-fiber reinforced composites are even more limited.

Through the current experimental study it was intended to investigate the failure responses of mechanically fastened joints in glass fiber – epoxy composite laminates at varying high and low temperature levels. The bolted joints were initially subjected to tensile loadings together with the effects of high thermal conditions from 40 ℃ up to 80 ℃, gradually increasing chamber temperatures for each test. In the second phase of experiments, the joints were exposed to low temperature environments, which were gradually decreased down to – 40 ℃ during tensile tests. Carefully observing failure behaviors of joints at varying temperature levels, it was finally reached to some significant conclusions about mechanically fastened joints under thermal effects.

CHAPTER TWO
COMPOSITE MATERIALS

2.1 Introduction

Composite materials can be defined as materials consisting of two or more constituents (phases) that are combined at the macroscopic level and are not soluble in each other. Modern synthetic composites using reinforcement fibers (one phase) and matrices (another phase) of various types have been introduced as replacement materials to metals in civilian, military, and aerospace applications (Sheikh-Ahmad, 2009, p.1).

In fact, what expected by using composite materials is to provide different physical, mechanical or chemical properties by the constituents, having these special features alone. When analyzing the internal structure of composite materials, which is highly heterogeneous character at macro level, it is possible to distinguish the body compounds. The different characteristics of structural components integrate into one formation. It is therefore impossible to observe the characteristics, all of which composite material possess, in a single component.

2.2 Historical Development of Composite Materials

In nature, composite materials have been in existent for millions of years. Wood, bamboo and bone are just a few examples of the natural occurring composite materials. Man has learned to fabricate composite materials relatively recently. Perhaps, one of the first evidence of a man-made composite material is the mud-blocks reinforced with straws. The composite material fabrication technology has since progressed from straw based mud-blocks to man-made fiber reinforced composite materials (Choo, 1990, p.2).

In the 20th century, modern composites were used in the 1930s when glass fibers reinforced resins. Boats and aircraft were built out of these glass composites,

commonly called fiber-glass. Since the 1970s, application of composites has widely increased due to development of new fibers such as carbon, boron, and aramids, and new composite systems with matrices made of metals and ceramics (Kaw, 2006, p.1,2).
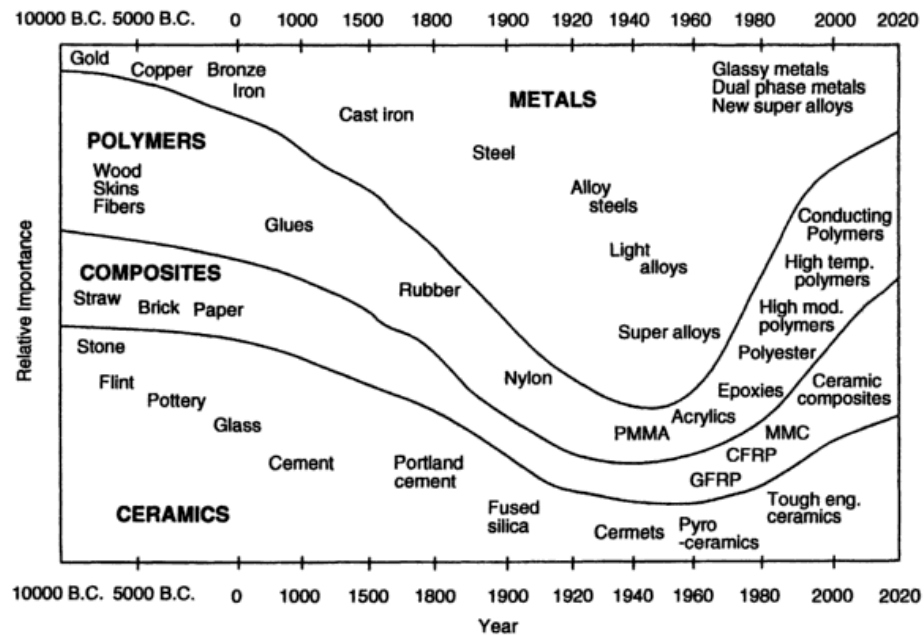
Figure 2.1 Relative importance of material development through history (Staab, 1999)

The structural materials most commonly used in design can be categorized in four primary groups: metals, polymers, composites and ceramics. These materials have been used to various degrees since the beginning of time. Their relative importance to various societies throughout history has fluctuated (Figure 2.1). The relative importance of each group of materials is not associated with any specific unit of measure (net tonnage, etc.). As with many advances throughout history, advances in material technology (from both manufacturing and analysis viewpoints) typically have their origins in military applications. Subsequently, this technology filters into the general population and alters many aspects of society. This has been most recently seen in the marked increase in relative importance of structural materials such as composites starting around 1960, when the race for space dominated many aspects of research and development. Similarly, the Strategic Defense Initiative

(SDI) program in the 1980s prompted increased research activities in the development of new material systems (Staab, 1999, p.2).

2.3 The Major Characteristics of Composites and Comparison with Conventional Materials

An obvious advantage that the fiber reinforced composite materials have over the conventional engineering materials such as copper, steel, aluminum, titanium, etc., is the high specific strength and modulus as seen in Table 2.1. The definition of specific strength is the ratio of the material strength to the material density and the specific modulus is defined as the material Young's modulus per unit material density. High specific strength and specific modulus have important applications on the engineering applications of composite materials. It means that the composite materials are strong and stiff and yet light in weight. Such characteristic are very desirable in the aeronautical and aerospace industry. The weight savings realized by fabricating structural components out of composite materials is directly translated into fuel savings which in turn makes the operation of aeroplane and space vehicle more economical (Choo, 1990, p.2). A comparative representation of the performance of typical structural composites from the point of view of specific properties is shown in Figure 2.2.

Figure 2.2 Performance map of structural composites (Daniel & Ishai, 1994)

Table 2.1 Specific Modulus and Specific Strength of Typical Fibers, Composites, and Bulk Metals (Kaw, 2006)

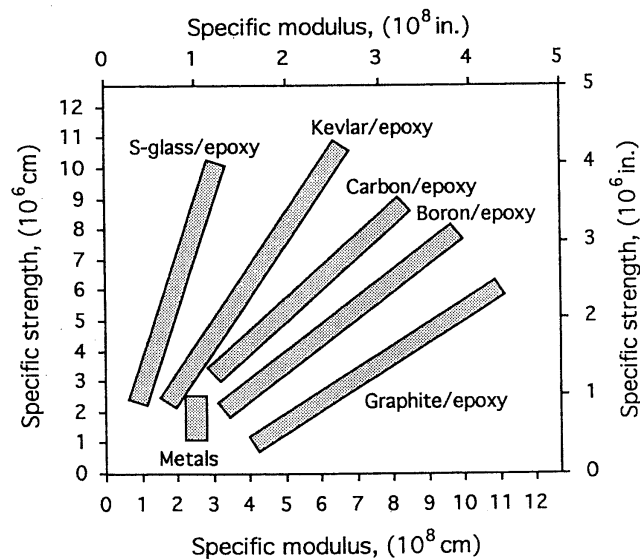| Material Units	Specific Gravity	Young's modulus (Gpa)	Ultimate strength (Mpa)	Specific modulus (Gpa-m³/kg)	Specific Strength (Mpa-m³/kg)
System of Units: SI					
Graphite fiber	1.8	230.00	2067.00	0.1278	1.148
Aramid fiber	1.4	124.00	1379.00	0.08857	0.9850
Glass fiber	2.5	85.00	1550.00	0.0340	0.6200
Unidirectional graphite/epoxy	1.6	181.00	1500.00	0.1131	0.9377
Unidirectional glass/epoxy	1.8	38.60	1062.00	0.02144	0.5900
Cross-ply graphite/epoxy	1.6	95.98	373.00	0.06000	0.2331
Cross-ply glass/epoxy	1.8	23.58	88.25	0.01310	0.0490
Quasi-isotropic graphite/epoxy	1.6	69.64	276.48	0.04353	0.1728
Quasi-isotropic glass/epoxy	1.8	18.96	73.08	0.01053	0.0406
Steel	7.8	206.84	648.01	0.02652	0.08309
Aluminum	2.6	68.95	275.80	0.02652	0.1061

Specific gravitiy of a material is the ratio between its density and density of water.

Besides strength, stiffness and lightweight, some additional outstanding improvements in material properties can be achieved by using composite materials. Those are, corrosion resistance, abrasion resistance, fatigue life, temperature-dependent behavior, thermal insulation, thermal and electrical conductivity, acoustic insulation etc.

As well as these advantages, some disadvantages may also be encountered when working with composite materials. High costs of production, difficulties in processing, repairing and in obtaining the required surface quality, lack of recycling property and low elongation values before fracture are main drawbacks representing limits when employing composites in structures. In addition, mechanical characterization of a composite structure is more complex than that of a metal structure. Properties of composites depend on both the fiber orientation and the lay-up sequence in the laminate because of anisotropic nature of fiber-reinforced composites, unlike metals. The other challenge is the impracticability of nondestructive inspection techniques, such as eddy currents and X-ray which give satisfying results in metal parts. Ultrasound, laser and acoustic emission techniques are more convenient to inspect flaws and crack initiation in composite structures. The mentioned drawbacks forces researchers to develop manufacture processes which is controlled by the real-time monitoring tools. In order to obtain high quality products,

optimum process parameters should be estimated by using a mathematical model, which is appropriate to the certain manufacturing process.

2.4 Classifications of Composite Materials

2.4.1 Classifications by the Geometry of the Reinforcement

The second constituent is referred to as the reinforcing phase, or reinforcement, as it enhances or reinforces the mechanical properties of the matrix. In most cases the reinforcement is harder, stronger and stiffer than the matrix, although there are some exceptions; for example, ductile metal reinforcement in a ceramic matrix and rubberlike reinforcement in a brittle polymer matrix. At least one of the dimensions of the reinforcement is small, say less than 500 µm and sometimes only of the order of a micron. The geometry of the reinforcing phase is one of the major parameters in determining the effectiveness of the reinforcement; in other words, the mechanical properties of composites are a function of the shape and dimensions of the reinforcement. We usually describe the reinforcement as being either fibrous or particulate (Matthews & Rawlings, 1999, p.5).

2.4.1.1 Fibrous Composite Materials

Fibrous Composite Materials are composed of fibers embedded in matrix material. Such a composite is considered to be a discontinuous fiber or short fiber composite if its properties vary with fiber length. On the other hand, when the length of the fiber is such that, any further increase in length does not further increase, the elastic modulus of the composite, the composite is considered to be continuous fiber reinforced.

Discontinuous or short-fiber composites contain short fibers or whiskers as the reinforcing phase (Figure 2.3). These short fibers, which can be fairly long compared with the diameter, can be either all oriented along one direction or randomly oriented. In the first instance the composite material tents to be markedly anisotropic

or, more specifically, orthotropic, whereas in the second it can be regarded as quasi-isotropic.

Continuous fiber composites are reinforced by long continuous fibers and are the most efficient from the point of view of stiffness and strength (Figure 2.3). The continuous fibers can be all parallel (unidirectional continuous fiber composite), can be oriented at right angles to each other (crossply or woven fabric continuous fiber composite), or can be oriented along several directions (multidirectional continuous fiber composite). In the latter case, for a certain number of fiber directions and distribution of fibers, the composite can be characterized as a quasi-isotropic material (Daniel & Ishai, 1994, p.20).
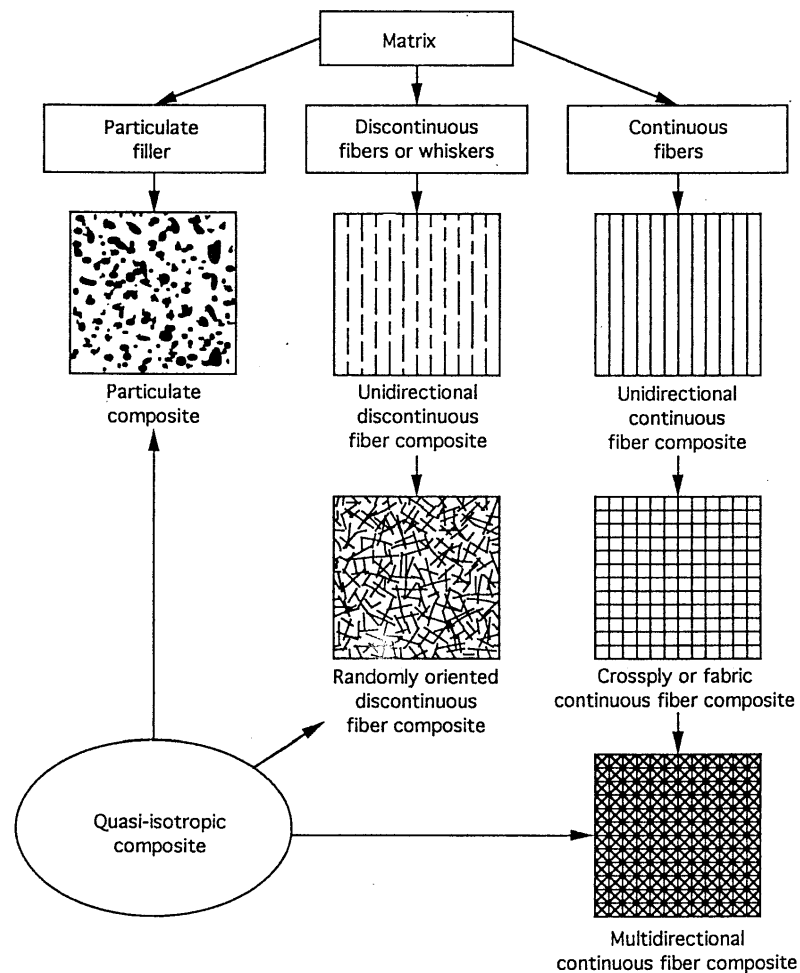
Figure 2.3 Classification of composite materials by the geometry of the reinforcement (Daniel & Ishai, 1994)

A fibrous reinforcement is characterized by its length being much greater than its cross-sectional dimension. Nevertheless, the ratio of length to the cross-sectional dimension, known as the aspect ratio, can vary considerably. In single-layer composites long fibers with high aspect ratios give what are called continuous fiber reinforced composites, whereas discontinuous fiber composites are fabricated using short fibers of low aspect ratio. The orientation of the discontinuous fibers may be random or preferred. The frequently encountered preferred orientation in the case of a continuous fiber composite is termed unidirectional and the corresponding random situation can be approximated to by bidirectional woven reinforcement (Matthews & Rawlings, 1999, p.5)

2.4.1.2 Particulate Composite Materials

Particulate composites consist of particles of various sizes and shapes randomly dispersed within the matrix (Daniel & Ishai, 1994, p.20). Particulate reinforcements have dimensions that are approximately equal in all dimensions. The shape of the reinforcing particles may be spherical, cubic, platelet, or any regular or irregular geometry. The arrangement of the particulate reinforcement may be random or with a preferred orientation, and this characteristics is also used as a part of classification scheme. In the majority of particulate reinforced composites the orientation of the particles is considered, for practical purposes, to be random (Matthews & Rawlings, 1999, p.5).

Particulate composites may nonmetallic particles in a nonmetallic matrix (concrete, glass reinforced with mica flakes, brittle polymers reinforced with rubberlike particles); metallic particles in nonmetallic matrices (aluminum, particles in polyurethane rubber used in rocked propellants); metallic particles in metallic matrices (lead particles in copper alloys to improve machinability); and non metallic particles in metallic matrices (silicon carbide particles in aluminum, SiC(p)Al) (Daniel & Ishai, 1994, p.20).

2.4.2 Classifications by the Type of Matrix

It has been stated before, that composites consist of two or more distinctly different materials. In most cases, the composite is made of matrix and reinforcement materials that are mixed in certain proportions. The matrix material may be made from metals, ceramics, or polymers. It may be pure, or mixed with other materials (additives) to enhance its properties. The reinforcement may also be treated to enhance bonding to the matrix (Sheikh & Ahmad, 2009, p.7).

2.4.2.1 Polymer Matrix Composites

The most common advanced composites are polymer matrix composites (PMCs) consisting of a polymer (e.g., epoxy, polyester, urethane) reinforced by thin diameter fibers (e.g., graphite, aramids, boron). For instance, graphite/ epoxy composites are approximately five times stronger than steel on a weight for- weight basis. The reasons why they are the most common composites include their low cost, high strength, and simple manufacturing principles. The main drawbacks of PMCs include low operating temperatures, high coefficients of thermal and moisture expansion,* and low elastic properties in certain directions (Kaw, 2006, p.19). Some mechanical properties of polymer matrix composites are given in Table 2.2.

Glass, graphite, and Kevlar are the most common fibers used in polymer matrix composites because of the unique advantages, including high strength, low cost, high chemical resistance, and good insulating properties. On the other hand, low elastic modulus, poor adhesion to polymers, high specific gravity, sensitivity to abrasion, and low fatigue strength present obstacles in construction.

The main types are E-glass (also called "fiberglass") and S-glass. The "E" in E-glass stands for electrical inasmuch as it was designed for electrical applications. Nonetheless, it is used for many other purposes now, such as decorations and structural applications. The "S" in S-glass stands for higher content of silica. It retains its strength at high temperatures compared to E-glass and has higher fatigue

strength. It is used mainly for aerospace applications. Other types available commercially are C-glass ("C" stands for corrosion) used in chemical environments, such as storage tanks; R-glass used in structural applications such as construction; D-glass (dielectric) used for applications requiring low dielectric constants, such as radomes; and A-glass (appearance) used to improve surface appearance. Combination types such as E-CR glass ("E-CR" stands for electrical and corrosion resistance) and AR glass (alkali resistant) also exist (Kaw, 2006, p.19).

Table 2.2 Typical mechanical properties of polymer matrix composites and monoclinic materials (Kaw, 2006)

Property	Units	Graphite/ epoxy	Glass/ epoxy	Steel	Aluminum
System of Units: USCS					
Specific gravity	---	1.6	1.8	7.8	2.6
Young's modulus	Msi	26.25	5.598	30.0	10.0
Ultimate tensile stength	ksi	217.6	154.0	94.0	40.0
Coefficient of thermal expansion	μin./in./°F	0.01111	4.778	6.5	12.8
System of Units: SI					
Specific gravity	---	1.6	1.8	7.8	2.6
Young's modulus	GPa	181.0	38.6	206.8	68.95
Ultimate tensile stength	MPa	150.0	1062	648.1	275.8
Coefficient of thermal expansion	μn./m/°C	0.02	8.6	11.7	23

Graphite fibers are also very common in the applications of aircraft components, in terms of their high specific modulus and strength, low coefficient of thermal expansion and high fatigue strength. High cost, low impact resistance, and high electrical conductivity represent the disadvantages of graphite fibers in polymer matrix composites.

Aramid fibers are made of an aromatic organic compound, consisting of hydrogen, carbon, oxygen, and nitrogen. Aramid fibers are inexpensive, resistant to impact, low density, and high tensile strength, but high moisture uptake and sensitiveness to sunlight restrain its use in composites.

Epoxy, phenolics, acrylic, urethane, and polyamide are most commonly used binder materials in polymer matrix composites. Of these types of materials, epoxy is

one of the most preferred one, even though it is costlier than other polymer matrices. Its superior characteristics, such that high strength, low viscosity and low flow rates, which allow good wetting of fibers and prevent misalignment of fibers during processing, low volatility during cure, low shrink rates, which reduce the tendency of gaining large shear stresses of the bond between epoxy and its reinforcement, and its being available in more than 20 grades to meet specific property and processing requirements, makes this choice very sensible.

2.4.2.2 Metal Matrix Composites

Metal matrix composites (MMCs), as the name implies, have a metal matrix. Examples of matrices in such composites include aluminum, magnesium, and titanium. Typical fibers include carbon and silicon carbide. Metals are mainly reinforced to increase or decrease their properties to suit the needs of design. To illustrate, the elastic stiffness and strength of metals can be increased and large coefficients of thermal expansion and thermal and electric conductivities of metals can be reduced, by the addition of fibers such as silicon carbide.

Metal matrix composites are mainly used to provide advantages over monolithic metals such as steel and aluminum. These advantages include higher specific strength and modulus by reinforcing low density metals, such as aluminum and titanium; lower coefficients of thermal expansion by reinforcing with fibers with low coefficients of thermal expansion, such as graphite; and maintaining properties such as strength at high temperatures.

MMCs have several advantages over polymer matrix composites. These include higher elastic properties; higher service temperature; insensitivity to moisture; higher electric and thermal conductivities; and better wear, fatigue, and flaw resistances. The drawbacks of MMCs over PMCs include higher processing temperatures and higher densities (Kaw, 2006, p.40).

2.4.2.3 Ceramic Matrix Composites

Ceramic matrix composites (CMCs) have a ceramic matrix such as alumina calcium alumino silicate reinforced by fibers such as carbon or silicon carbide.

Advantages of CMCs include high strength, hardness, high service temperature limits for ceramics, chemical inertness, and low density. However, ceramics by themselves have low fracture toughness. Under tensile or impact loading, they fail catastrophically. Reinforcing ceramics with fibers, such as silicon carbide or carbon, increases their fracture toughness, because it causes gradual failure of the composite. This combination of a fiber and ceramic matrix makes CMCs more attractive for applications in which high mechanical properties and extreme service temperatures are desired (Kaw, 2006, p.45).

2.4.2.4 Carbon-Carbon Composites

Carbon–carbon composites use carbon fibers in a carbon matrix. These composites are used in very high-temperature environments of up to 6000°F (3315°C), and are 20 times stronger and 30% lighter than graphite fibers.

Carbon is brittle and flaw sensitive like ceramics. Reinforcement of a carbon matrix allows the composite to fail gradually and also gives advantages such as ability to withstand high temperatures, low creep at high temperatures, low density, good tensile and compressive strengths, high fatigue resistance, high thermal conductivity, and high coefficient of friction. Drawbacks include high cost, low shear strength, and susceptibility to oxidations at high temperatures (Kaw, 2006, p.46).

CHAPTER THREE
JOINING OF COMPOSITE STRUCTURES

3.1 Introduction

In practice, it is often unavoidable to apply joints to combine composite parts to each other or assemble them with other structural components.

Joining of composite materials poses a special challenge. How to achieve joint strength or other designed-in functionally specific properties anywhere close to those of the parent composite, since the integrity or continuity of the reinforcement across the joint is difficult or impossible to retain or re-establish. The irony here is that composite materials are usually selected for the exceptional properties they offer to improve performance. Joining is needed to produce the largest and/or most complex and/or most sophisticated structures. The performance of a structure or an assembly is critically dependent on the behavior of any joints it contains, and, as just stated, most contain joints. Hence, the very reason that composite materials may have been chosen in the first place may be lost if effective methods for joining cannot be found (Messler, 2004, p.653).

The most common requirements, affecting the joint design in composites is given in Figure 3.1. It should be kept in mind that, these requirements should be satisfied to be able to select the most suitable joint configuration. In general, fiber reinforced plastic (FRPs) structures can be assembled by using adhesively bonded and/or mechanically fastened joints. Welding or thermal bonding is also a viable option for thermoplastic polymer matrix composites.

Joints often occur in transitions between major composite parts and a metal feature or fitting. For instance, such a situation is represented in aircraft by articulated fittings on control surfaces as well as on wing and tail components, which require the ability to pivot the element during various stages of operation. Tubular elements such as power shafting often use metal end fittings for connection to power sources or for

articulation where changes in direction are required. In addition, assembly of the structure from its constituent parts will involve either bonded or mechanically fastened joints or both (Peters, 1998, p.610).
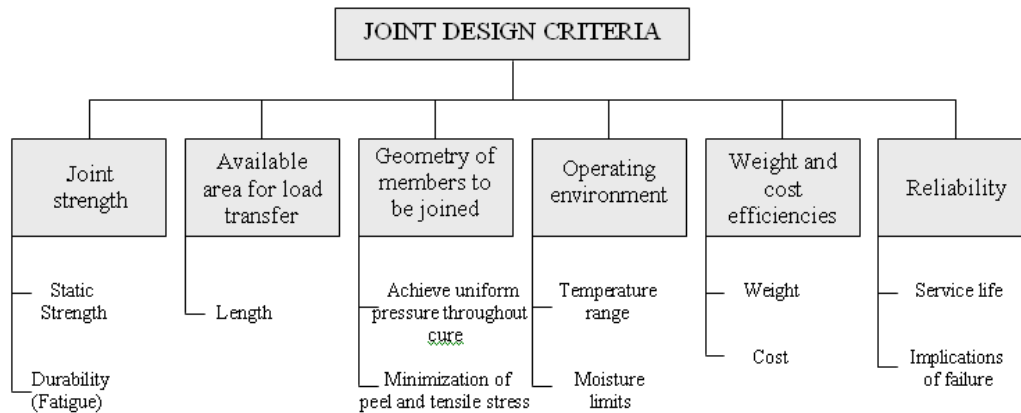

Figure 3.1 The most common requirement of the joint design

Table 3.1 A comparison of the advantages and disadvantages of adhesively bonded and bolted composite joints (Baker, Dutton, & Kelly, 2004)

Advantages	Disadvantages
Bonded Joints	
▪ Small stress concentration in adherents ▪ Stiff connection ▪ Excellent fatigue properties ▪ No fretting problems ▪ Sealed against corrosion ▪ Smooth surface contour ▪ Relatively lightweight ▪ Damage tolerant	▪ Limits to thickness that can be joined with simple joint configuration ▪ Inspection other than for gross flaws difficult ▪ Prone to environmental degradation ▪ Sensitive to peel and through-thickness stresses ▪ Residual stress problems when joining to metals ▪ Cannot be disassembled ▪ May require costly tooling and facilities ▪ Requires high degree of quality control ▪ May be of environmental concern
Bolted Joints	
▪ Positive connection, low initial risk ▪ Can be disassembled ▪ No thickness limitations ▪ Simple joint configuration ▪ Simple manufacturing process ▪ Simple inspection procedure ▪ Not environmentally sensitive ▪ Provides through-thickness reinforcement; not sensitive to peel stresses	▪ Considerable stress concentration ▪ Prone to fatigue cracking in metallic component ▪ Hole formation can damage composite ▪ Composite's relatively poor bearing properties ▪ Prone to fretting in metal ▪ Prone to corrosion in metal ▪ May require extensive shimming

In design process, the behavior of joints for certain individual material, geometric, and environmental conditions must be taken into account. As shown in Figure 3.1, load transfer from one joint member to the other is typically affected by the type of load, the environmental conditions, and the materials being joined. Notwithstanding adhesive bonding is the principal method and offer much greater joining efficiency, mechanically fastened composite joints are used in specific applications, in case adhesive bonding is not appropriate or optimum. In terms of being a clue for choosing the right joint type, the advantages and disadvantages of adhesively bonded and mechanically fastened joints are given in Table 3.1.

3.2 Adhesive Bonding

Having uniform load distribution in contact areas, little weight penalty with thin bond lines, smooth external surfaces for improved aerodynamic and hydrodynamic flow, adhesively bonding is still the principal method for joining composites.

As stated previously, adhesive joints are capable of high structural efficiency and constitute a resource for structural weight saving because of the potential for elimination of stress concentrations which cannot be achieved with mechanically fastened joints. However, due to lack of reliable inspection methods and a requirement for close dimensional tolerances in fabrication, aircraft designers have generally avoided bonded construction in primary structure (Peters, 1998, p.610).

In a structural adhesive joint, the load in one component must be transferred through the adhesive layer to another component. The efficiency with which this can be done depends on the joint design, the adhesive characteristics and the adhesive/substrate interface. In order to transfer the load through adhesive, the substrates (or adherend) are overlapped to place the adhesive in shear. Figure 3.2 shows some typical joint designs for adhesively bonded joints (Campbell, 2004, p.245).

A) Single Lap Joint
Good

B) Tapered Single Lap Joint
Very Good

C) Single Strap Joint
Fair

D) Double Lap Joint
Very Good

E) Double Strap Joint
Very Good

F) Tapered Double Strap Joint
Excellent

G) Scarf Joint
Excellent

H) Step Lap Joint
(Cocured Only)
Excellent
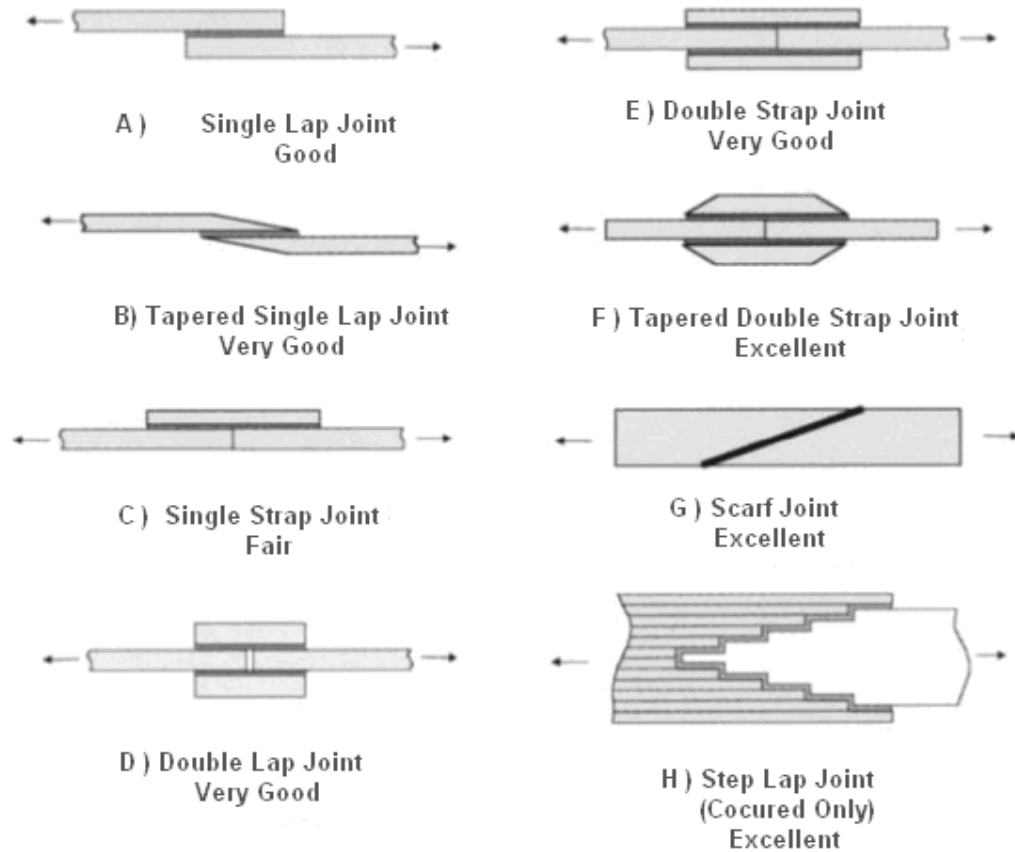
Figure 3.2 Typical adhesively bonded joint configurations (Campbell, 2011)

Obtaining adequate mechanical results from adhesively bonded joint requires an appropriate preference of adhesive material. The adhesives most often used for bonding polymer-matrix composites are synthetic polymeric adhesives that are generally similar to the matrix of the composite, or mutually compatible with the matrices of mating composites. Thus, thermosetting polymer adhesives are generally used for adhesive-bonding thermosetting-matrix composites (e.g., epoxy-glass), while thermoplastic polymer adhesives are generally used with thermoplastic-matrix composites (e.g., polyetheretherketone (PEEK) graphite). Solvent cementing can also be used for bonding thermoplastic-matrix composites, just as it can be used for bonding monolithic thermoplastics (Messler, 2004, P.665).

Figure 3.3 The four basic types of adhesive loading. Tension and shear are acceptable loading methods, provided the bond area is sufficient. Cleavage and peel are to be avoided.

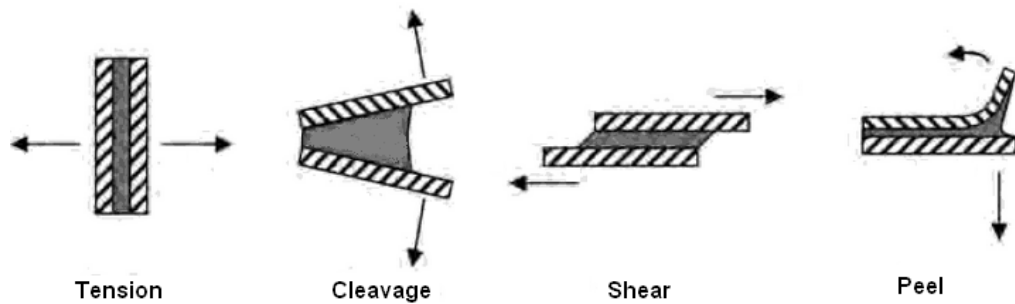The joint design must ensure that the adhesive is loaded in shear as much as possible. Cleavage and peel loading (Figure 3.3) should be avoided when using adhesives. Some further considerations for designing adhesively bonded joints are:

- The adhesive must be compatible with the adherents and be able to retain its required strength when exposed to in-service stresses and environmental factors.

- The joint should be designed to ensure a failure in one of the adherents rather than a failure within the adhesive bond line.

- Thermal expansion of dissimilar materials must be considered. Because of the large thermal expansion difference between carbon composite and aluminum, adhesively bonded joints between these two materials have been known to fail during cool down from elevated temperature cures as a result of the thermal stresses induced by their differential expansion coefficients.

- Proper joint design should be used, avoiding peel or cleavage loading whenever possible. If peel forces can not be avoided, a lower-modulus (non brittle) adhesive having high peel strength should be used.

- Tapered ends should be used on lap joints to feather out the edge-of-joint stresses. The fillet at the end of the exposed joint should not be removed.

- Selection tests for structural adhesives should include durability testing for heat, humidity, (and/or fluids), and stress, simultaneously (Campbell, 2011, p.250).

Bonded joints must be carefully designed by conducting adhesive joint tests. Tests should be done on the actual joints that will be used in production. Environmental conditions (temperature, moisture and any solvents) that the joint was exposed also

must be carried out. All test conditions must be carefully controlled including the surface preparation, the adhesive and the bonding cycle. The failure modes for all tests specimens should be examined. Some acceptable and unacceptable failure modes are shown in Figure 3.4. If the specimen exhibits an adhesive failure at the adherent-adhesive interface rather than a cohesive failure within the adhesive, it may be an indication of a surface preparation problem that will result in decreased joint durability (Campbell, 2004, p.251).
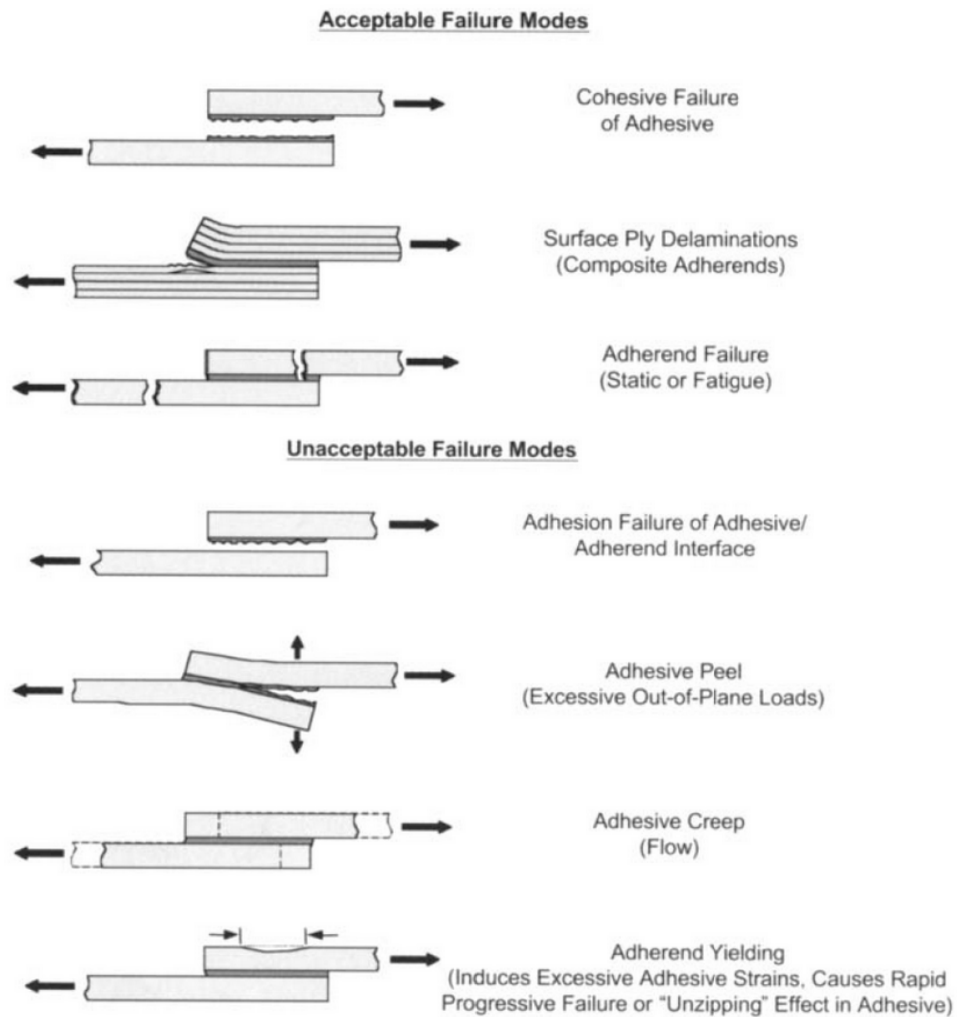

Figure 3.4 Typical failure modes of bonded joints (Campbell, 2011)

3.3 Mechanical Fastening

In many applications, joining composite plates by using mechanically fasteners such as, bolts, pins, rivets etc. cannot be avoided because of requirements for disassembly of the joint for replacement of damaged structure or to achieve access to underlying structure.

Adhesive joints tend to lack structural redundancy and are highly sensitive to manufacturing deficiencies including poor bonding technique, poor fit of mating parts and sensitivity of the adhesive to temperature and environmental effects such as moisture. Assurance of bond quality has been a continuing problem in adhesive joints. While non-destructive evaluation techniques (ultrasonic and X-ray inspection) may reveal gaps in the bond, there is no present technique, which can guarantee that a bond, which appears to be intact does, in fact, have adequate load transfer capability. Thus mechanically fastened joints tend to be preferred over bonded construction in highly critical and safety related applications such as primary aircraft structural components, especially in large commercial transports, since assurance of the required level of structural integrity is easier to be guaranteed in mechanically fastened assemblies. As a rule, bonded joints prove to be more efficient for lightly loaded/non-flight critical aircraft structures whereas mechanically fastened joints are more efficient for highly loaded structures. Bonded construction tends to be more prevalent in smaller aircraft components (Peters, 1998, p.611).

In mechanical fastening, load transfer is accomplished by compression (bearing) on the faces of holes passing through the joint members by shear (and, less desirably, bending) of the fasteners. Some of the load is also transferred through friction on the face of the joint element if the clamping forces imposed by the fasteners are sufficient. However, in spite of the fact that high clamping forces (bolt-tightening torque) are very important to develop high-friction forces to maximize bearing strength, it may not be possible to maintain these levels of clamping force during prolonged service, for example, due to wear under service loading conditions.

Now that high through-thickness reinforcement is provided by the fasteners, peel failure of the composite is generally not a problem. Nonetheless, problems can arise resulting from the relatively low bearing and transverse strengths of the composite compared with those of metals. Bearing failure results in hole elongation, allowing bending and subsequent fatigue of the bolt or substructure. Alternatively, the fastener head may pull through the composite.
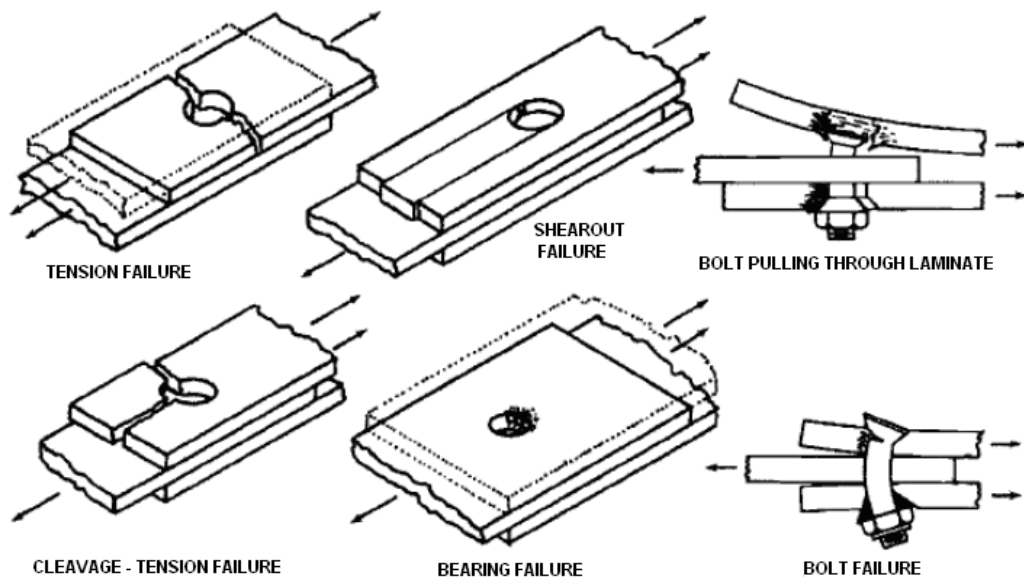
Figure 3.5 Schematic illustrations of the main failure modes in mechanical joints in composites (Jones, 1999)

Figure 3.5 illustrates the failure modes of a composite joint. They are, briefly, *tension failure*, caused by tangential or compressive stresses at the hole edge, *bearing failure* mode, governed by compressive stresses acting on the hole surface, *shear-out failure*, caused by shear stresses acting in shear-out planes on the hole boundary in the principal load direction, *bolt failure mode,* resulted from high shear stresses acting in the bolt shank.

In addition, mixed-mode failures can occur, including *cleavage tension*, essentially mixed tension / shear; *bolt-head pulling through the laminate*, a problem particularly with deeply countersunk holes; and bolt failure due to bearing failure.

The type of failure that occurs depends on the ratio of the effective width to the diameter of the fastener hole *w/d*, and the ratio of the edge distance to the diameter *e/d*. The variation of failure load with *w/d* and *e/d* for a quasi isotropic laminate is indicated in Figure 3.6. For large *w/d* and *e/d,* the joint fails in bearing, and the failure load is independent of *w/d* or *e/d*. With reduced *w/d* tension failure of the net section will occur with the joint strength dropping to zero when *w/d* = 1. If the edge distance *e* is reduced, shear failure occurs with the strength of the joint dropping to zero when *e/d* =0.5 (Baker, Dutton, & Kelly, 2004, p.338).
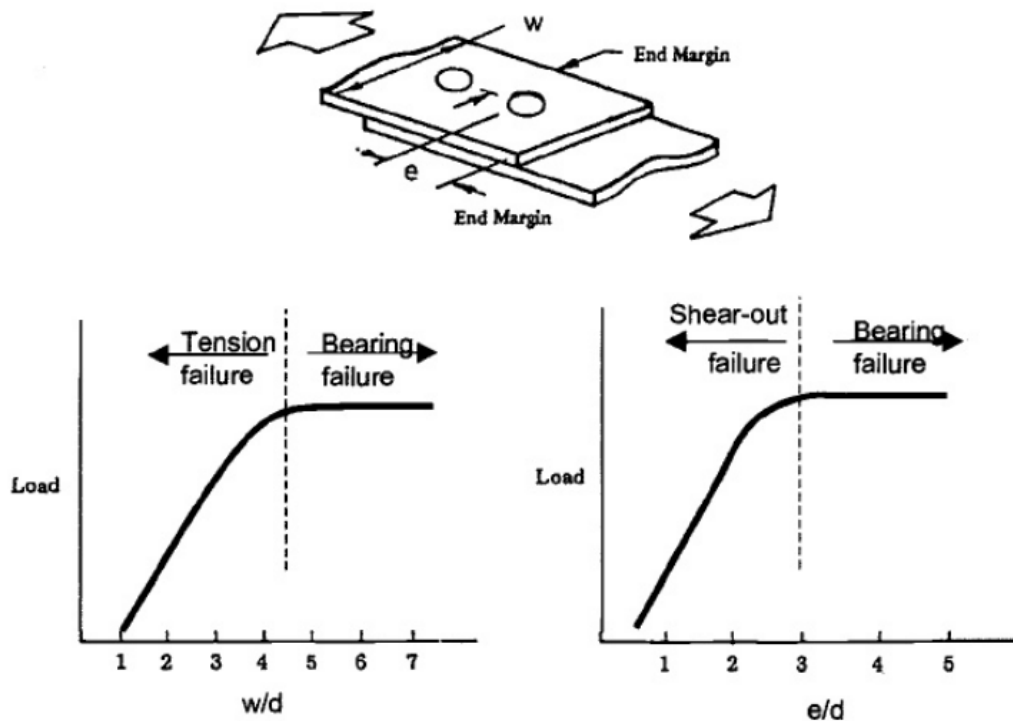
Figure 3.6 Transition between failure modes with specimen width (rivet pitch) and edge distance (Baker, Dutton, & Kelly, 2004)

The allowable stresses in each of these modes are a function of:

- Geometry of the joint, including thickness.
- Hole size, spacing, and bearing area, allowing for countersink.
- Fastener loading, single or double shear; that is, loading symmetrical, as in a double-lap joint, or unsymmetrical, as in a single-lap joint.
- Fastener fit tolerance.
- Clamping area and pressure, allowing for any countersink.

- Fiber orientation and ply sequence.
- Moisture content and service temperature.
- Nature of stressing: tension, compression, shear; cyclic variation of stressing; any secondary bending, resulting in out-of-plane loading. Stresses due to thermal expansion mismatch in metal-to-composite joints may also have an effect, but these are rarely considered in mechanical joints.

The ply configuration in most bolted joints is usually chosen to be close to quasi-isotropic, based on 0°, ± 45 °, and 90° fibers. The non-zero fibers are needed to carry load around the hole to prevent shear or cleavage-type failures, whereas the 0° fibers carry the primary bearing loads and tension. The desired failure mode is usually net tension or compression; however, in some situations (the softer or less catastrophic) bearing failure may be preferred. If stiff (highly orthotropic) laminates are required for a particular application, a higher proportion of 0° fibers may be used and further measures may be required to increase hole strength (Baker, Dutton, & Kelly, 2004, p.340).

3.4 Hybrid (bolted/bonded) Joining

A joint bonded with a structural adhesive is usually much stiffer than a similar joint joined by mechanical fastening; even when the mechanical joint is optimally designed and interference fit fasteners are used. Thus it is not possible to design a joint in which the load is effectively shared between the bonded and fastened regions. It was shown that for an optimally designed step-lap joint the bolts transmit only around one percent of the total load. However, fastening and bonding can be beneficially used together for several reasons:

- Fasteners provide an alternate in-plane load path as well as through-thickness reinforcement and therefore can contain the spread of damage in thick-section composite-bonded joints where failure (for example, due to an overload or to the development of local bond or inter laminar flaws) would occur by disbonding of the adhesive layer or by delamination of the composite.

- Fasteners can be used at the end of a lap joint to reduce peel stresses. However, this is a somewhat hazardous application because the fastener holes, unless very carefully sealed, allow environmental ingress into the bond interface in the most critical region.

- Fasteners can be used both as a jigging aid and to apply pressure during adhesive bonding of composite components; generally, this approach would be effective only with paste adhesives.

- Bonding can be used to alleviate local stresses in the metallic component in a mechanically fastened joint, markedly improving fatigue and static strength properties. For the reasons mentioned, the bond line carries most of the load, and the fasteners become effective only after bond failure. This approach is extensively used with riveting in the metallic longitudinal fuselage splice region in commercial aircraft. With composite construction, this approach is more likely to be used for rework of areas found to be prone to damage (Baker, Dutton, & Kelly, 2004, p.340).

CHAPTER FOUR
STRESS ANALYSIS IN COMPOSITES

4.1 Introduction

A lamina can be defined as a thin plane layer of unidirectional fibers or woven fabric in a matrix. It is generally of a thickness on the order of 0.125 mm. Even though several layers of fibers actually exist in the same lamina, the modeled lamina has only a single fiber per layer (Figure 4.1). A laminate is constructed by stacking a number of such lamina in the direction of the lamina thickness (Figure 4.2). Mechanical structures made of these laminates, such as a leaf spring suspension system in an automobile, are subjected to various loads, such as bending and twisting (Kaw, 2006, p.61). Laminated composite materials have different responses to the applied loads in different directions. Therefore, the behavior of each individual lamina must be predicted to analyze the whole body of composite structure.
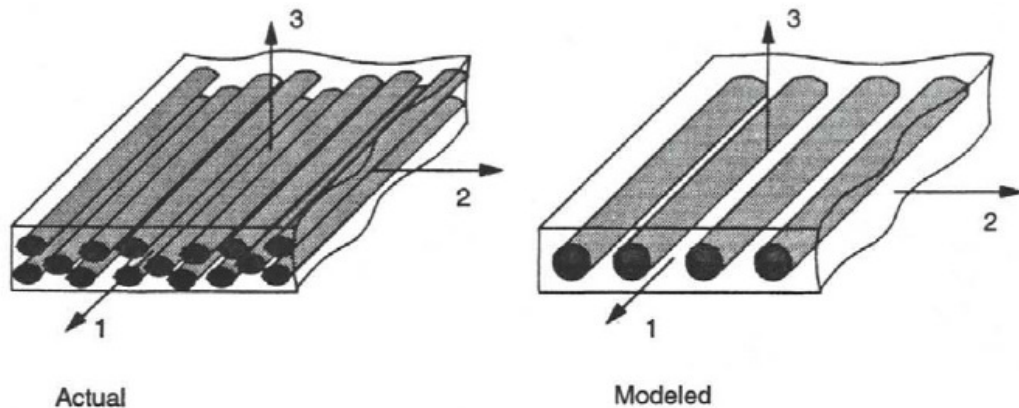

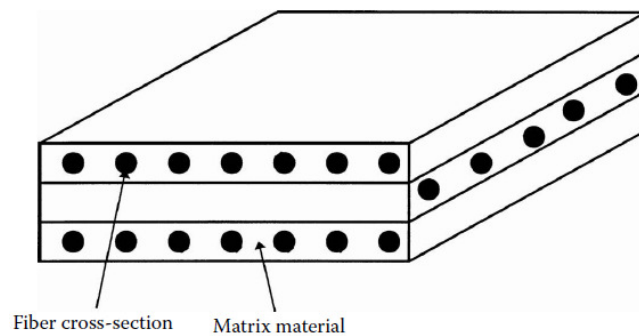Figure 4.1 Schematic illustration of actual and modeled lamina (Staab, 1999)

Figure 4.2 Typical laminate made of three laminas

The lamina has principal axes and is characterized as an orthotropic material (Figure 4.1). Axis 1 is the longitudinal fiber direction, Axis 2 is the transverse direction in the plane of the lamina, and, Axis 3 is normal to the plane of the lamina. If two or more unidirectional laminas are stacked together at various orientations, they constitute a composite laminate.

Stress analysis in composites is performed at two different levels, named as micromechanics and macromechanics. In micromechanics, fiber diameter, particle size, or matrix interstices between reinforcement are observed and the interactions of the constituents are studied on the microscopic scale. Stress, strain and deformation analysis in the constituents, including matrix and fiber, and their interface also are dealt in micromechanics. Micromechanics is an important scale when studying the properties, such as fracture toughness, strength, and fatigue life which are strongly affected by local characteristics, as they can not be integrated or averaged.

Macromechanics is concerned with the average stiffness and strength properties of the unidirectional lamina, which is considered to be a quasi homogenous anisotropic material. The whole elastic or elastic-plastic behavior of composite laminates should be studied at macroscopic level. None of the particular local failure mechanism is referenced, while expressing failure criteria on the basis of average stresses and overall lamina strengths.

At laminate level, the macromechanical analysis is applied in the form of lamination theory dealing with overall behavior as a function of lamina properties and stacking sequence. Finally, at the component or structure level, methods such as finite element analysis coupled with lamination theory give the overall behavior of the structure as well as the state of stress in each lamina (Daniel & Ishai, 1994, p.25).

4.2 Macromechanical Behavior of a Lamina

4.2.1 Stress-Strain Relations for Anisotropic Materials

The deformations caused by an arbitrary combination of stresses can be predicted by using Generalized Hook's Low. It also reveals that, if a member is exposed a force (which produce a stress in dimension of application) in one direction, strains in other directions does not equal to zero. Like an elastic band, when you pull the material by any of the planes, the other planes move to inward to fill in the space and it becomes thinner. Therefore, strain is produced without stress in other directions, too. The Generalized Hook's Low is a convenient tool to simplify stress-strain relations for materials having increased symmetries, and reduce three dimensional formulations to plane stress and plane strain case. In the most general case, the Generalized Hook's Low, defining stress-strain relation can be written in indicial notation as

$$\sigma_{ij} = C_{ijkl}\varepsilon_{kl}$$

$$i,j,k,l = 1,2,3 \tag{4.1}$$

$$\varepsilon_{ij} = S_{ijkl}\sigma_{kl}$$

where σ_{ij} are stress components as shown in Figure 4.3, ε_{kl} are the strain components, C_{ijkl} is the stiffness matrix, and S_{ijkl} is the compliance matrix. As seen the compliance matrix S_{ijkl} is the inverse of the stiffness matrix C_{ijkl}. In general, 81 elastic constants wholly characterize the material. Because of the symmetry in the stress and strain tensors, the number of elastic constants reduces to 36.
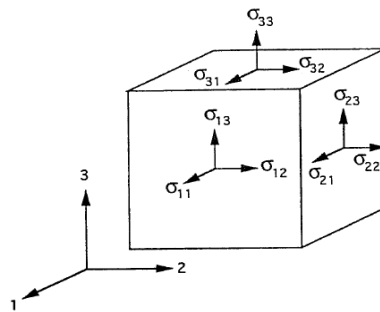
Figure 4.3 State of stress at a point of continuum

$$\sigma_{ij} = \sigma_{ji}, \ S_{ij} = S_{ji} \tag{4.2}$$

The stress-strain relations for anisotropic materials can be written in contracted form as follows,

$$\begin{bmatrix} \sigma_1 \\ \sigma_2 \\ \sigma_3 \\ \tau_{23} \\ \tau_{31} \\ \tau_{12} \end{bmatrix} = \begin{bmatrix} C_{11} & C_{12} & C_{13} & C_{14} & C_{15} & C_{16} \\ C_{21} & C_{22} & C_{23} & C_{24} & C_{25} & C_{26} \\ C_{31} & C_{32} & C_{33} & C_{34} & C_{35} & C_{36} \\ C_{41} & C_{42} & C_{43} & C_{44} & C_{45} & C_{46} \\ C_{51} & C_{52} & C_{53} & C_{54} & C_{55} & C_{56} \\ C_{61} & C_{62} & C_{63} & C_{64} & C_{65} & C_{66} \end{bmatrix} \begin{bmatrix} \varepsilon_1 \\ \varepsilon_2 \\ \varepsilon_3 \\ \gamma_{23} \\ \gamma_{31} \\ \gamma_{12} \end{bmatrix} \quad \text{or} \ \sigma_i = C_{ij}\varepsilon_j \tag{4.3}$$

$$i, j = 1,\ldots,6$$

$$\begin{bmatrix} \varepsilon_1 \\ \varepsilon_2 \\ \varepsilon_3 \\ \gamma_{23} \\ \gamma_{31} \\ \gamma_{12} \end{bmatrix} = \begin{bmatrix} S_{11} & S_{12} & S_{13} & S_{14} & S_{15} & S_{16} \\ S_{21} & S_{22} & S_{23} & S_{24} & S_{25} & S_{26} \\ S_{31} & S_{32} & S_{33} & S_{34} & S_{35} & S_{36} \\ S_{41} & S_{42} & S_{43} & S_{44} & S_{45} & S_{46} \\ S_{51} & S_{52} & S_{53} & S_{54} & S_{55} & S_{56} \\ S_{61} & S_{62} & S_{63} & S_{64} & S_{65} & S_{66} \end{bmatrix} \begin{bmatrix} \sigma_1 \\ \sigma_2 \\ \sigma_3 \\ \tau_{23} \\ \tau_{31} \\ \tau_{12} \end{bmatrix} \quad \text{or} \ \varepsilon_i = S_{ij}\sigma_j \tag{4.4}$$

For elastic materials, the important characteristics of strain energy should be also considered. Consider a stress component σ_i produced an infinitesimal strain $d\varepsilon_i$. The strain energy in the body per unit volume is:

$$dW = \sigma_i.d\varepsilon_i \tag{4.5}$$

Because of stress-strain relationship in Equation (4.3) the strain energy becomes,

$$dW = C_{ij}\varepsilon_j.d\varepsilon_i \tag{4.6}$$

$$W = \frac{1}{2}C_{ij}\varepsilon_i\varepsilon_j \tag{4.7}$$

Now, by partial differentiation of Equation (4.7),

$$\frac{d^2W}{d\varepsilon_i d\varepsilon_j} = C_{ij} \tag{4.8}$$

and,

$$\frac{d^2W}{d\varepsilon_j d\varepsilon_i} = C_{ji} \tag{4.9}$$

Because the order of differentiation does not matter, so

$$C_{ij} = C_{ji} \tag{4.10}$$

Thus, the stiffness matrix is deduced to be symmetric and the number of independent constants is reduced from 36 to 21. This means that the compliance matrix $[S]$ in Equation (4.4) also has only 21 independent constants because of symmetry.

$$S_{ij} = S_{ji} \tag{4.11}$$

4.2.1.1 Anisotropic Material

After the reduction of material constants from 36 to 21, the stress strain relations are described,

$$\begin{bmatrix} \sigma_1 \\ \sigma_2 \\ \sigma_3 \\ \tau_{23} \\ \tau_{31} \\ \tau_{12} \end{bmatrix} = \begin{bmatrix} C_{11} & C_{12} & C_{13} & C_{14} & C_{15} & C_{16} \\ & C_{22} & C_{23} & C_{24} & C_{25} & C_{26} \\ & & C_{33} & C_{34} & C_{35} & C_{36} \\ & & & C_{44} & C_{45} & C_{46} \\ & \text{Sym.} & & & C_{55} & C_{56} \\ & & & & & C_{66} \end{bmatrix} \begin{bmatrix} \varepsilon_1 \\ \varepsilon_2 \\ \varepsilon_3 \\ \gamma_{23} \\ \gamma_{31} \\ \gamma_{12} \end{bmatrix} \tag{4.12}$$

$$\begin{bmatrix} \varepsilon_1 \\ \varepsilon_2 \\ \varepsilon_3 \\ \gamma_{23} \\ \gamma_{31} \\ \gamma_{12} \end{bmatrix} = \begin{bmatrix} S_{11} & S_{12} & S_{13} & S_{14} & S_{15} & S_{16} \\ & S_{22} & S_{23} & S_{24} & S_{25} & S_{26} \\ & & S_{33} & S_{34} & S_{35} & S_{36} \\ & & & S_{44} & S_{45} & S_{46} \\ & \text{Sym.} & & & S_{55} & S_{56} \\ & & & & & S_{66} \end{bmatrix} \begin{bmatrix} \sigma_1 \\ \sigma_2 \\ \sigma_3 \\ \tau_{23} \\ \tau_{31} \\ \tau_{12} \end{bmatrix} \tag{4.13}$$

Equation (4.12) and (4.13) are referred to as characterizing anisotropic materials. Anisotropic materials, (or called alternatively triclinic materials) have no planes of symmetry for material properties. Even if the material is assumed to be homogenous, to find the 21 elastic constant, analytic and experimental studies are needed.

Fortunately, many natural or synthetic materials possess material symmetries, which reduce the number of independent elastic constants.

4.2.1.2 Monoclinic Material

If there is one plane of material property symmetry, such a material is called monoclinic material. For example, elastic body whose properties are symmetric with respect to the $x_1 - x_2$ plane is illustrated in Figure 4.4.

Directional Cosines

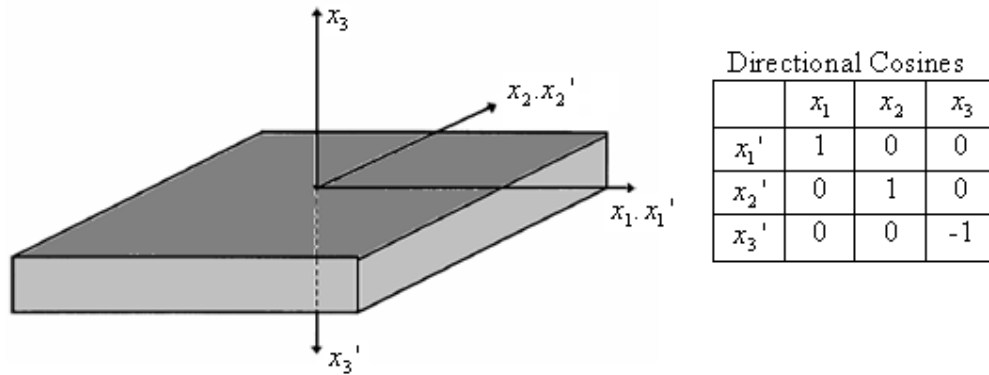|	x_1	x_2	x_3
x_1'	1	0	0
x_2'	0	1	0
x_3'	0	0	-1

Figure 4.4   One plane of symmetry

The stresses and strains of the new coordinate system are related to the original one by the following relations,

$$\sigma_{kl}' = t_{ki}.t_{lj}.\sigma_{ij} \quad \text{and} \quad \varepsilon_{kl}' = t_{ki}.t_{lj}.\varepsilon_{ij} \tag{4.14}$$

where, t_{ij} are the direction cosines associated with the transformation coordinate system. The stress and strain transformations to the symmetrical coordinate system are as follows,

$$
\begin{aligned}
\sigma_{11}' &= \sigma_1 = t_{11}.t_{11}.\sigma_{11} = 1.1.\sigma_1 = \sigma_1 \\
\sigma_{22}' &= \sigma_2 = t_{22}.t_{22}.\sigma_{22} = 1.1.\sigma_2 = \sigma_2 \\
\sigma_{33}' &= \sigma_3 = t_{33}.t_{33}.\sigma_{33} = (-1).(-1).\sigma_2 = \sigma_2 \\
\sigma_{23}' &= \sigma_4 = t_{22}.t_{33}.\sigma_{23} = 1.(-1).\sigma_4 = -\sigma_4 \\
\sigma_{31}' &= \sigma_5 = t_{33}.t_{11}.\sigma_{31} = (-1).1.\sigma_5 = -\sigma_5 \\
\sigma_{12}' &= \sigma_6 = t_{11}.t_{22}.\sigma_{12} = 1.1.\sigma_6 = \sigma_6
\end{aligned}
\tag{4.15}
$$

$$\varepsilon_{11}' = \varepsilon_1 = t_{11}.t_{11}.\varepsilon_{11} = 1.1.\varepsilon_1 = \varepsilon_1$$
$$\varepsilon_{22}' = \varepsilon_2 = t_{22}.t_{22}.\varepsilon_{22} = 1.1.\varepsilon_2 = \varepsilon_2$$
$$\varepsilon_{33}' = \varepsilon_3 = t_{33}.t_{33}.\varepsilon_{33} = (-1).(-1).\varepsilon_2 = \varepsilon_2 \qquad (4.16)$$
$$\varepsilon_{23}' = \varepsilon_4 = t_{22}.t_{33}.\varepsilon_{23} = 1.(-1).\sigma.\varepsilon_4 = -\varepsilon_4$$
$$\varepsilon_{31}' = \varepsilon_5 = t_{33}.t_{11}.\varepsilon_{31} = (-1).1.\varepsilon_5 = -\varepsilon_5$$
$$\varepsilon_{12}' = \varepsilon_6 = t_{11}.t_{22}.\varepsilon_{12} = 1.1.\varepsilon_6 = \varepsilon_6$$

According to Equation (4.3) σ_4 and σ_4' can be written as,

$$\sigma_4 = C_{41}\varepsilon_1 + C_{42}\varepsilon_1 + C_{43}\varepsilon_3 + C_{44}\varepsilon_4 + C_{45}\varepsilon_5 + C_{46}\varepsilon_6 \qquad (4.17)$$

$$\sigma_4' = C_{41}\varepsilon_1' + C_{42}\varepsilon_1' + C_{43}\varepsilon_3' + C_{44}\varepsilon_4' + C_{45}\varepsilon_5' + C_{46}\varepsilon_6' \qquad (4.18)$$

After summation Equation (4.17) and (4.18), it can be concluded that $C_{41} = C_{42} = C_{43} = C_{46} = 0$ and σ_5 and σ_5' can be written as,

$$\sigma_5 = C_{51}\varepsilon_1 + C_{52}\varepsilon_1 + C_{53}\varepsilon_3 + C_{54}\varepsilon_4 + C_{55}\varepsilon_5 + C_{56}\varepsilon_6 \qquad (4.19)$$

$$\sigma_5' = C_{51}\varepsilon_1' + C_{52}\varepsilon_1' + C_{53}\varepsilon_3' + C_{54}\varepsilon_4' + C_{55}\varepsilon_5' + C_{56}\varepsilon_6' \qquad (4.20)$$

Similarly, the summation Equation (4.19) and (4.20) gives that $C_{51} = C_{52} = C_{53} = C_{56} = 0$

For the material, having only one plane of symmetry the elastic constants are reduced to 13. Thus, stress-strain relations in a monoclinic material is,

$$
\begin{bmatrix} \sigma_1 \\ \sigma_2 \\ \sigma_3 \\ \tau_{23} \\ \tau_{31} \\ \tau_{12} \end{bmatrix} =
\begin{bmatrix}
C_{11} & C_{12} & C_{13} & 0 & 0 & C_{16} \\
 & C_{22} & C_{23} & 0 & 0 & C_{26} \\
 & & C_{33} & 0 & 0 & C_{36} \\
 & & & C_{44} & C_{45} & 0 \\
 & Sym. & & & C_{55} & 0 \\
 & & & & & C_{66}
\end{bmatrix}
\begin{bmatrix} \varepsilon_1 \\ \varepsilon_2 \\ \varepsilon_3 \\ \gamma_{23} \\ \gamma_{31} \\ \gamma_{12} \end{bmatrix} \qquad (4.21)
$$

$$
\begin{bmatrix} \varepsilon_1 \\ \varepsilon_2 \\ \varepsilon_3 \\ \gamma_{23} \\ \gamma_{31} \\ \gamma_{12} \end{bmatrix} = \begin{bmatrix} S_{11} & S_{12} & S_{13} & 0 & 0 & S_{16} \\ & S_{22} & S_{23} & 0 & 0 & S_{26} \\ & & S_{33} & 0 & 0 & S_{36} \\ & & & S_{44} & S_{45} & 0 \\ & \text{Sym.} & & & S_{55} & 0 \\ & & & & & S_{66} \end{bmatrix} \begin{bmatrix} \sigma_1 \\ \sigma_2 \\ \sigma_3 \\ \tau_{23} \\ \tau_{31} \\ \tau_{12} \end{bmatrix} \tag{4.22}
$$

4.2.1.3 Orthotropic Material

In addition to the symmetry plane, if there are two orthogonal planes of symmetry, so the material has three mutually perpendicular planes of material property symmetry, it is called orthotropic or orthogonally anisotropic. In such a case, there are four more constants are equal to zero ($C_{16} = C_{26} = C_{36} = C_{45} = 0$). Namely, for orthotropic elastic bodies, such as most composite materials nine elastic constants exist in three dimensional cases. Thus, stress-strain relations for orthotropic materials are shaped like this:

$$
\begin{bmatrix} \sigma_1 \\ \sigma_2 \\ \sigma_3 \\ \tau_{23} \\ \tau_{31} \\ \tau_{12} \end{bmatrix} = \begin{bmatrix} C_{11} & C_{12} & C_{13} & 0 & 0 & 0 \\ & C_{22} & C_{23} & 0 & 0 & 0 \\ & & C_{33} & 0 & 0 & 0 \\ & & & C_{44} & 0 & 0 \\ & \text{Sym.} & & & C_{55} & 0 \\ & & & & & C_{66} \end{bmatrix} \begin{bmatrix} \varepsilon_1 \\ \varepsilon_2 \\ \varepsilon_3 \\ \gamma_{23} \\ \gamma_{31} \\ \gamma_{12} \end{bmatrix} \tag{4.23}
$$

$$
\begin{bmatrix} \varepsilon_1 \\ \varepsilon_2 \\ \varepsilon_3 \\ \gamma_{23} \\ \gamma_{31} \\ \gamma_{12} \end{bmatrix} = \begin{bmatrix} S_{11} & S_{12} & S_{13} & 0 & 0 & 0 \\ & S_{22} & S_{23} & 0 & 0 & 0 \\ & & S_{33} & 0 & 0 & 0 \\ & & & S_{44} & 0 & 0 \\ & \text{Sym.} & & & S_{55} & 0 \\ & & & & & S_{66} \end{bmatrix} \begin{bmatrix} \sigma_1 \\ \sigma_2 \\ \sigma_3 \\ \tau_{23} \\ \tau_{31} \\ \tau_{12} \end{bmatrix} \tag{4.24}
$$

A wooden bar, rolled steel, and a lamina of continuous fiber composite are good examples for the orthotropic bodies.

4.2.1.4 Transversely Isotropic Material

Consider a material; at every point of which there is one plane, that the material properties are equal in all directions. In that case, the nine independent elastic constants reduced to five and the material is called Transversely Isotropic. The stress-strain relationship is

$$
\begin{bmatrix} \sigma_1 \\ \sigma_2 \\ \sigma_3 \\ \tau_{23} \\ \tau_{31} \\ \tau_{12} \end{bmatrix} = \begin{bmatrix} C_{11} & C_{12} & C_{13} & 0 & 0 & 0 \\ & C_{11} & C_{13} & 0 & 0 & 0 \\ & & C_{33} & 0 & 0 & 0 \\ & & & C_{44} & 0 & 0 \\ & \textit{Sym.} & & & C_{44} & 0 \\ & & & & & \dfrac{(C_{11}-C_{12})}{2} \end{bmatrix} \begin{bmatrix} \varepsilon_1 \\ \varepsilon_2 \\ \varepsilon_3 \\ \gamma_{23} \\ \gamma_{31} \\ \gamma_{12} \end{bmatrix}
\tag{4.25}
$$

$$
\begin{bmatrix} \varepsilon_1 \\ \varepsilon_2 \\ \varepsilon_3 \\ \gamma_{23} \\ \gamma_{31} \\ \gamma_{12} \end{bmatrix} = \begin{bmatrix} S_{11} & S_{12} & S_{13} & 0 & 0 & 0 \\ & S_{11} & S_{13} & 0 & 0 & 0 \\ & & S_{33} & 0 & 0 & 0 \\ & & & S_{44} & 0 & 0 \\ & \textit{Sym.} & & & S_{44} & 0 \\ & & & & & \dfrac{(S_{11}-S_{12})}{2} \end{bmatrix} \begin{bmatrix} \sigma_1 \\ \sigma_2 \\ \sigma_3 \\ \tau_{23} \\ \tau_{31} \\ \tau_{12} \end{bmatrix}
\tag{4.26}
$$

4.2.1.5 Isotropic Material

If there is infinite number of symmetry planes in material, it means that material properties do not change depending on the direction. This material is named as Isotropic Material, with only two independent material constants in its stiffness matrix:

$$
\begin{bmatrix} \sigma_1 \\ \sigma_2 \\ \sigma_3 \\ \tau_{23} \\ \tau_{31} \\ \tau_{12} \end{bmatrix} = \begin{bmatrix} C_{11} & C_{12} & C_{12} & 0 & 0 & 0 \\ & C_{11} & C_{12} & 0 & 0 & 0 \\ & & C_{11} & 0 & 0 & 0 \\ & & & \dfrac{(C_{11}-C_{12})}{2} & 0 & 0 \\ & & & & \dfrac{(C_{11}-C_{12})}{2} & 0 \\ & Sym. & & & & \dfrac{(C_{11}-C_{12})}{2} \end{bmatrix} \begin{bmatrix} \varepsilon_1 \\ \varepsilon_2 \\ \varepsilon_3 \\ \gamma_{23} \\ \gamma_{31} \\ \gamma_{12} \end{bmatrix} \qquad (4.27)
$$

$$
\begin{bmatrix} \varepsilon_1 \\ \varepsilon_2 \\ \varepsilon_3 \\ \gamma_{23} \\ \gamma_{31} \\ \gamma_{12} \end{bmatrix} = \begin{bmatrix} S_{11} & S_{12} & S_{12} & 0 & 0 & 0 \\ & S_{11} & S_{12} & 0 & 0 & 0 \\ & & S_{11} & 0 & 0 & 0 \\ & & & \dfrac{(S_{11}-S_{12})}{2} & 0 & 0 \\ & & & & \dfrac{(S_{11}-S_{12})}{2} & 0 \\ & Sym. & & & & \dfrac{(S_{11}-S_{12})}{2} \end{bmatrix} \begin{bmatrix} \sigma_1 \\ \sigma_2 \\ \sigma_3 \\ \tau_{23} \\ \tau_{31} \\ \tau_{12} \end{bmatrix} \qquad (4.28)
$$

4.2.2 Engineering Constants for Orthotropic Materials

The mechanical constants, which describe the stress-strain relations, can be expressed in terms of engineering constants. The relations between them are obtained by using some basic imaginary experiments. Imagine that, an elastic orthotropic lamina is exposed longitudinal tension (σ_1), transverse in-plane tension (σ_2), transverse out-of-plane tension (σ_3), out-of-plane shears (τ_{32} & τ_{31}) and in-plane shear (τ_{12}) loads, separately. After superposing the relations for different loading types in the same material, the stress-strain relations for an orthotropic lamina became (Daniel & Ishai, 1994, P.66):

$$
\begin{bmatrix} \varepsilon_1 \\ \varepsilon_2 \\ \varepsilon_3 \\ \gamma_{23} \\ \gamma_{31} \\ \gamma_{12} \end{bmatrix} =
\begin{bmatrix}
\dfrac{1}{E_1} & -\dfrac{\gamma_{21}}{E_2} & -\dfrac{\gamma_{31}}{E_3} & 0 & 0 & 0 \\[2mm]
-\dfrac{\gamma_{12}}{E_1} & \dfrac{1}{E_2} & -\dfrac{\gamma_{32}}{E_3} & 0 & 0 & 0 \\[2mm]
-\dfrac{\gamma_{13}}{E_1} & -\dfrac{\gamma_{23}}{E_2} & \dfrac{1}{E_3} & 0 & 0 & 0 \\[2mm]
0 & 0 & 0 & \dfrac{1}{G_{23}} & 0 & 0 \\[2mm]
0 & 0 & 0 & 0 & \dfrac{1}{G_{13}} & 0 \\[2mm]
0 & 0 & 0 & 0 & 0 & \dfrac{1}{G_{12}}
\end{bmatrix}
\begin{bmatrix} \sigma_1 \\ \sigma_2 \\ \sigma_3 \\ \tau_{23} \\ \tau_{31} \\ \tau_{12} \end{bmatrix}
\qquad (4.29)
$$

As seen in Equation (4.29), it is easy to express the compliance matrix $[S]$ in terms of the engineering constants. However, the case is different for the stiffness matrix $[C]$; such that, converting the compliance matrix, the stress-strain relation is found as follows:

$$
\begin{bmatrix} \sigma_1 \\ \sigma_2 \\ \sigma_3 \\ \tau_{23} \\ \tau_{31} \\ \tau_{12} \end{bmatrix} =
\begin{bmatrix}
\dfrac{1-v_{23}v_{32}}{E_2 E_3 \Delta} & \dfrac{v_{12}+v_{13}v_{32}}{E_1 E_3 \Delta} & \dfrac{v_{31}+v_{21}v_{32}}{E_2 E_3 \Delta} & 0 & 0 & 0 \\[3mm]
\dfrac{v_{12}+v_{13}v_{32}}{E_1 E_3 \Delta} & \dfrac{1-v_{13}v_{31}}{E_1 E_3 \Delta} & \dfrac{v_{23}+v_{21}v_{13}}{E_1 E_2 \Delta} & 0 & 0 & 0 \\[3mm]
\dfrac{v_{31}+v_{21}v_{32}}{E_2 E_3 \Delta} & \dfrac{v_{23}+v_{21}v_{13}}{E_1 E_2 \Delta} & \dfrac{1-v_{12}v_{21}}{E_1 E_2 \Delta} & 0 & 0 & 0 \\[3mm]
0 & 0 & 0 & G_{23} & 0 & 0 \\[2mm]
0 & 0 & 0 & 0 & G_{13} & 0 \\[2mm]
0 & 0 & 0 & 0 & 0 & G_{12}
\end{bmatrix}
\begin{bmatrix} \varepsilon_1 \\ \varepsilon_2 \\ \varepsilon_3 \\ \gamma_{23} \\ \gamma_{31} \\ \gamma_{12} \end{bmatrix}
\qquad (4.30)
$$

in which Δ is defined as

$$
\Delta = \frac{1}{E_1 E_2 E_3}
\begin{vmatrix}
1 & -v_{21} & -v_{31} \\
-v_{12} & 1 & -v_{32} \\
-v_{13} & -v_{23} & 1
\end{vmatrix}
\qquad (4.31)
$$

4.2.3 Stress-Strain Relations for Thin Lamina

A thin lamina is considered to be a plane stress case, so the stress components σ_3, τ_{23}, and τ_{31} are equal to zero. Thus, the stress-strain relationship in Equation (4.29) is reduced to the following form,

$$\begin{bmatrix} \sigma_1 \\ \sigma_2 \\ \tau_{12} \end{bmatrix} = \begin{bmatrix} Q_{11} & Q_{12} & 0 \\ Q_{12} & Q_{22} & 0 \\ 0 & 0 & Q_{66} \end{bmatrix} \begin{bmatrix} \varepsilon_1 \\ \varepsilon_2 \\ \gamma_{12} \end{bmatrix} \tag{4.32}$$

$$\begin{bmatrix} \varepsilon_1 \\ \varepsilon_2 \\ \gamma_{12} \end{bmatrix} = \begin{bmatrix} S_{11} & S_{12} & 0 \\ S_{12} & S_{22} & 0 \\ 0 & 0 & S_{66} \end{bmatrix} \begin{bmatrix} \sigma_1 \\ \sigma_2 \\ \tau_{12} \end{bmatrix} \tag{4.33}$$

The relations is then can be written by using engineering constants,

$$\begin{bmatrix} \sigma_1 \\ \sigma_2 \\ \tau_{12} \end{bmatrix} = \begin{bmatrix} \dfrac{E_1}{1-v_{12}v_{21}} & \dfrac{v_{12}E_2}{1-v_{12}v_{21}} & 0 \\ \dfrac{v_{21}E_1}{1-v_{12}v_{21}} & \dfrac{E_2}{1-v_{12}v_{21}} & 0 \\ 0 & 0 & G_{12} \end{bmatrix} \begin{bmatrix} \varepsilon_1 \\ \varepsilon_2 \\ \gamma_{12} \end{bmatrix} \tag{4.34}$$

$$\begin{bmatrix} \varepsilon_1 \\ \varepsilon_2 \\ \gamma_{12} \end{bmatrix} = \begin{bmatrix} \dfrac{1}{E_1} & -\dfrac{v_{21}}{E_2} & 0 \\ -\dfrac{v_{12}}{E_1} & \dfrac{1}{E_2} & 0 \\ 0 & 0 & \dfrac{1}{G_{12}} \end{bmatrix} \begin{bmatrix} \sigma_1 \\ \sigma_2 \\ \tau_{12} \end{bmatrix} \tag{4.35}$$

4.2.4 Material Orientation in Two-Dimensional Lamina

Unidirectional composite laminas have very low transverse stiffness and strain properties. Therefore, some of the laminas in laminates were oriented in angled directions. Obtaining stress-strain relation in an angle lamina is essential (Kaw, 2006, p.110).

The local and the global coordinate systems are used to define the stress-strain equations of an angle lamina (Figure 4.5). In local coordinate system, direction 1 is the longitudinal direction, which is parallel to fibers and direction 2 is the transverse direction oriented perpendicular to the fiber direction. The global coordinate system is represented by x-y axes. The angle between the two coordinate systems is named as θ. Here is intended to establish the stress-strain relations in global coordinate system.
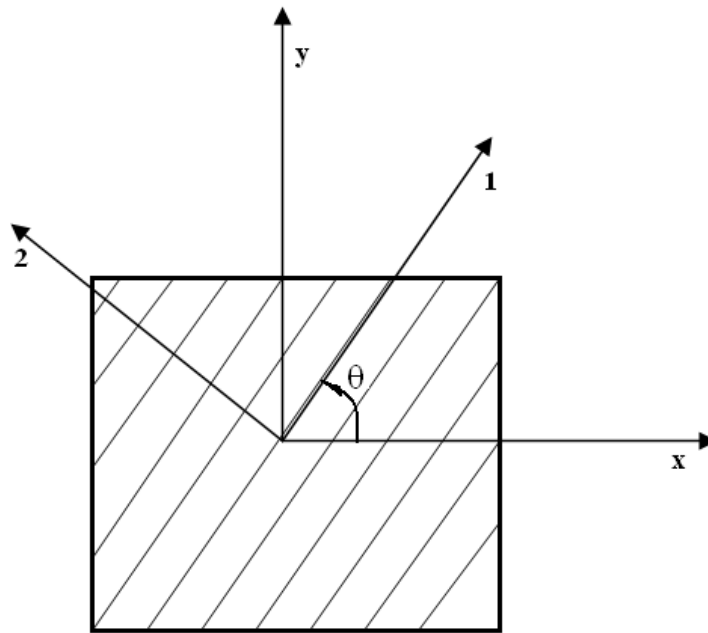

Figure 4.5 Local and global axes of an angle lamina

The stress and strain components in local coordinate system are converted into the global coordinate system by the transformation matrix $[T]$.

$$
\begin{bmatrix} \sigma_1 \\ \sigma_2 \\ \tau_{12} \end{bmatrix} = [T] \begin{bmatrix} \sigma_x \\ \sigma_y \\ \tau_{xy} \end{bmatrix} \quad \text{and} \quad \begin{bmatrix} \varepsilon_1 \\ \varepsilon_2 \\ \frac{1}{2}\gamma_{12} \end{bmatrix} = [T] \begin{bmatrix} \varepsilon_x \\ \varepsilon_y \\ \frac{1}{2}\gamma_{xy} \end{bmatrix} \tag{4.36}
$$

$$[T] = \begin{bmatrix} m^2 & n^2 & 2mn \\ n^2 & m^2 & -2mn \\ -mn & mn & m^2 - n^2 \end{bmatrix} \quad \text{and} \quad m = Cos\theta, \quad n = Sin\theta \qquad (4.37)$$

Putting Equation (4.32) and (4.33), in the inverse form of Equation (4.36) yields,

$$\begin{bmatrix} \sigma_x \\ \sigma_y \\ \tau_{xy} \end{bmatrix} = [T]^{-1}[Q] \begin{bmatrix} \varepsilon_1 \\ \varepsilon_2 \\ \gamma_{12} \end{bmatrix} = [T]^{-1} \begin{bmatrix} Q_{11} & Q_{11} & 0 \\ Q_{11} & Q_{11} & 0 \\ 0 & 0 & 2Q_{66} \end{bmatrix} \begin{bmatrix} \varepsilon_1 \\ \varepsilon_2 \\ \frac{1}{2}\gamma_{12} \end{bmatrix}$$

$$\qquad (4.38)$$

$$\begin{bmatrix} \sigma_x \\ \sigma_y \\ \tau_{xy} \end{bmatrix} = [T]^{-1} \begin{bmatrix} Q_{11} & Q_{11} & 0 \\ Q_{11} & Q_{11} & 0 \\ 0 & 0 & 2Q_{66} \end{bmatrix} [T] \begin{bmatrix} \varepsilon_x \\ \varepsilon_y \\ \frac{1}{2}\gamma_{xy} \end{bmatrix} = [T]^{-1}[Q][R][T][R]^{-1} \begin{bmatrix} \varepsilon_x \\ \varepsilon_y \\ \gamma_{xy} \end{bmatrix}$$

where $[R]$ is the Reuter matrix defined as,

$$[R] = \begin{bmatrix} 1 & 0 & 0 \\ 0 & 1 & 0 \\ 0 & 0 & 2 \end{bmatrix} \qquad (4.39)$$

The transformed reduced stiffness matrix $[\overline{Q}]$ is obtained by multiplying $[T]^{-1}, [Q], [R], [T], [R]^{-1}$.

$$\begin{bmatrix} \sigma_x \\ \sigma_y \\ \tau_{xy} \end{bmatrix} = \begin{bmatrix} \overline{Q}_{11} & \overline{Q}_{12} & \overline{Q}_{16} \\ \overline{Q}_{21} & \overline{Q}_{22} & \overline{Q}_{26} \\ \overline{Q}_{61} & \overline{Q}_{62} & \overline{Q}_{66} \end{bmatrix} \begin{bmatrix} \varepsilon_x \\ \varepsilon_y \\ \gamma_{xy} \end{bmatrix} \qquad (4.40)$$

$$\overline{Q}_{11} = Q_{11}m^4 + Q_{22}n^4 + 2(Q_{12} + 2Q_{66})m^2 n^2$$
$$\overline{Q}_{12} = (Q_{11} + Q_{22} - 4Q_{66})m^2 n^2 + Q_{12}(m^4 + n^2)$$
$$\overline{Q}_{22} = Q_{11}n^4 + Q_{22}m^4 + 2(Q_{12} + 2Q_{66})m^2 n^2$$
$$\overline{Q}_{16} = (Q_{11} - Q_{12} - 2Q_{66})m^3 n - (Q_{22} - Q_{12} - 2Q_{66})n^3 m$$
$$\overline{Q}_{26} = (Q_{11} - Q_{12} - 2Q_{66})m.n^3 - (Q_{22} - Q_{12} - 2Q_{66})m^3 n$$
$$\overline{Q}_{66} = (Q_{11} + Q_{22} - 2Q_{12} - 2Q_{66})m^2 n^2 + Q_{66}(m^4 + n^4)$$

$$\qquad (4.41)$$

4.2.5 Elastic Properties of multidirectional laminates

4.2.5.1 Basic Assumptions

The stress-strain relations for a single lamina were explained in the previous sections. Nevertheless, a real composite material consists of more than one lamina, oriented in different directions. A unidirectional lamina neither has enough thickness to take realistic loads nor is convenient to carry multidirectional loads because of its low transverse mechanical properties. Building a laminate by stacking layers at different angles satisfies the loading and stiffness requirements, although it increases the cost and weight (Daniel & Ishai, 1994, p.142), (Kaw, 2006, p.320).

It is obvious that, the whole behavior of composite plate is a function of properties of each individual lamina. The following assumptions are required to develop the equations according to classical lamination theory.

- Each lamina is orthotropic.
- Each lamina is homogeneous.
- A line straight and perpendicular to the middle surface remains straight and perpendicular to the middle surface during deformation $(\gamma_{xz} = \gamma_{xz} = 0)$.
- The laminate is thin and is loaded only in its plane (plane stress) $(\sigma_z = \tau_{xz} = \tau_{yz} = 0)$.
- Displacements are continuous and small throughout the laminate $(|u|, |v|, |w| << |h|)$, where h is the laminate thickness.
- Each lamina is elastic.
- No slip occurs between the lamina interfaces.

4.2.5.2 Strain Displacement Relations

Figure 4.6 illustrates a section view of a plate normal to the y-axis in the global coordinate system (x, y, z) before and after deformation. The reference plane ($x - y$) is equal in distance from top and bottom surfaces, that is also z = 0. $u_0, v_0,$ and w_0

are the displacements at the middle plane and u, v and w are the displacement components at any point in x, y and z directions, respectively.
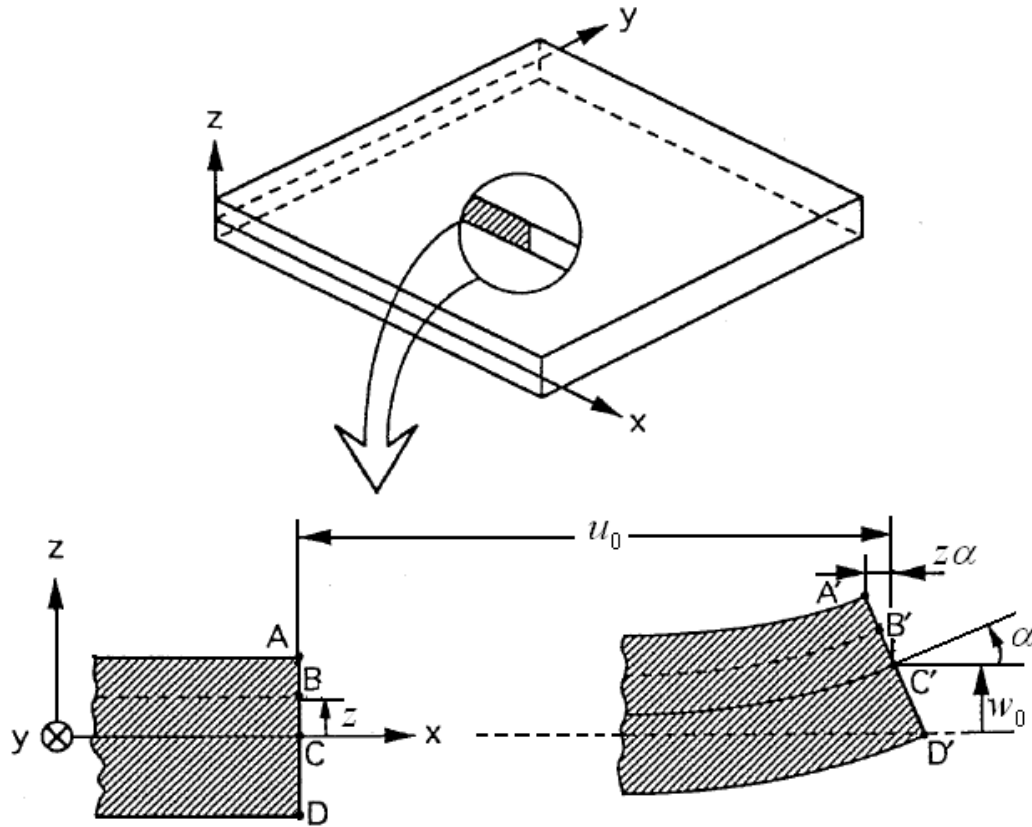

Figure 4.6 Laminate section before (ABCD) and after (A'B'C'D') (Daniel, & Ishai, 1994)

The middle plane displacements u_0, v_0 and out-of-plane displacement w are only the function of x and y.

$$u_0 = u_0(x, y)$$
$$v_0 = v_0(x, y) \qquad (4.42)$$
$$w = f(x, y)$$

At any point the two displacements u and v in $x - y$ plane is dependent on the axial location of the point and the slope of the laminate middle plane with the x and y directions.

$$u = u_0 - z\alpha \qquad \text{and} \qquad \alpha = \frac{\partial w_0}{\partial x} \qquad (4.43)$$

The displacement in x direction is then,

$$u = u_0 - z\frac{\partial w_0}{\partial x} \qquad (4.44)$$

Similarly, other displacement component can be written in the same manner.

$$v = v_0 - z\frac{\partial w_0}{\partial y}$$
(4.45)

The strain components at any point are expressed,

$$\varepsilon_x = \frac{\partial u}{\partial x} = \frac{\partial u_0}{\partial x} - z\frac{\partial^2 w_0}{\partial x^2}$$
(4.46)

$$\varepsilon_x = \frac{\partial v}{\partial y} = \frac{\partial v_0}{\partial y} - z\frac{\partial^2 w_0}{\partial y^2}$$
(4.47)

$$\gamma_{xy} = \frac{\partial u}{\partial y} + \frac{\partial v}{\partial x} = \frac{\partial u_0}{\partial y} + \frac{\partial v_0}{\partial x} - 2z\frac{\partial^2 w_0}{\partial x\partial y}$$
(4.48)

Equations (4.46), (4.47), and (4.47) can be combined in matrix form,

$$\begin{bmatrix} \varepsilon_x \\ \varepsilon_y \\ \gamma_{xy} \end{bmatrix} = \begin{bmatrix} \dfrac{\partial u_0}{\partial x} \\ \dfrac{\partial v_0}{\partial y} \\ \dfrac{\partial u_0}{\partial y} + \dfrac{\partial v_0}{\partial x} \end{bmatrix} + z.\begin{bmatrix} -\dfrac{\partial^2 w_0}{\partial x^2} \\ -\dfrac{\partial^2 w_0}{\partial y^2} \\ -2\dfrac{\partial^2 w_0}{\partial x\partial y} \end{bmatrix}$$
(4.49)

Strains at any point can be written in terms of reference plane strains and laminate curvatures,

$$\begin{bmatrix} \varepsilon_x \\ \varepsilon_y \\ \gamma_{xy} \end{bmatrix} = \begin{bmatrix} \varepsilon_x{}^0 \\ \varepsilon_y{}^0 \\ \gamma_{xy}{}^0 \end{bmatrix} + z\begin{bmatrix} K_x \\ K_y \\ K_{xy} \end{bmatrix}$$
(4.50)

Equation (4.50) shows the linear relationship of strains in a laminate to the curvatures of the laminate. It also indicates that the strains are independent of the $x-y$ coordinates (Kaw, 2006, p.324).

4.2.5.3 Strain and Stress Relations in a Laminate

In case the strains at any point through the laminate thickness are known, the stresses of each lamina in the global coordinate system can be calculated according to Equation (4.40). The transformed reduced stiffness matrix, $[\overline{Q}]$, corresponds the layer at that point. It can be derived from Equation (4.40) and (4.50),

$$\begin{bmatrix} \sigma_x \\ \sigma_y \\ \tau_{xy} \end{bmatrix} = \begin{bmatrix} \overline{Q}_{11} & \overline{Q}_{12} & \overline{Q}_{16} \\ \overline{Q}_{21} & \overline{Q}_{22} & \overline{Q}_{26} \\ \overline{Q}_{61} & \overline{Q}_{62} & \overline{Q}_{66} \end{bmatrix} \cdot \begin{bmatrix} \varepsilon_x^{\,0} \\ \varepsilon_y^{\,0} \\ \gamma_{xy}^{\,0} \end{bmatrix} + z \cdot \begin{bmatrix} \overline{Q}_{11} & \overline{Q}_{12} & \overline{Q}_{16} \\ \overline{Q}_{21} & \overline{Q}_{22} & \overline{Q}_{26} \\ \overline{Q}_{61} & \overline{Q}_{62} & \overline{Q}_{66} \end{bmatrix} \begin{bmatrix} K_x \\ K_y \\ K_{xy} \end{bmatrix} \qquad (4.51)$$

Unlike a linear variation of strain through the thickness of laminate, stress variations in each lamina changes because transformed reduces stiffness matrix $[\overline{Q}]$ for each lamina is different.
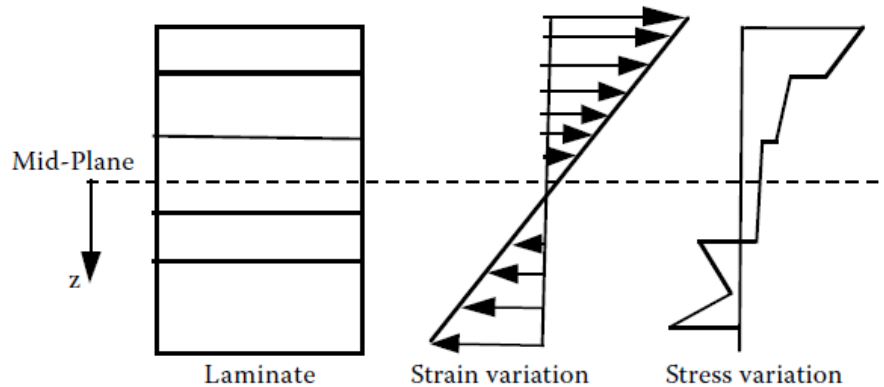

Figure 4.7 Strain and stress variations through thickness of a laminate

4.2.5.4 Force and Moment Resultants

Consider a laminate manufactured by using N layers as shown in Figure 4.8. The thickness of the laminate is "t". The resulting forces and moments acting in a laminate can be found by integrating the stresses in each lamina through thickness.

$$N_x = \int\limits_{\frac{-t}{2}}^{\frac{t}{2}} \sigma_x \, dz \qquad\qquad M_x = \int\limits_{\frac{-t}{2}}^{\frac{t}{2}} \sigma_x . z . dz \qquad\qquad (4.52)$$
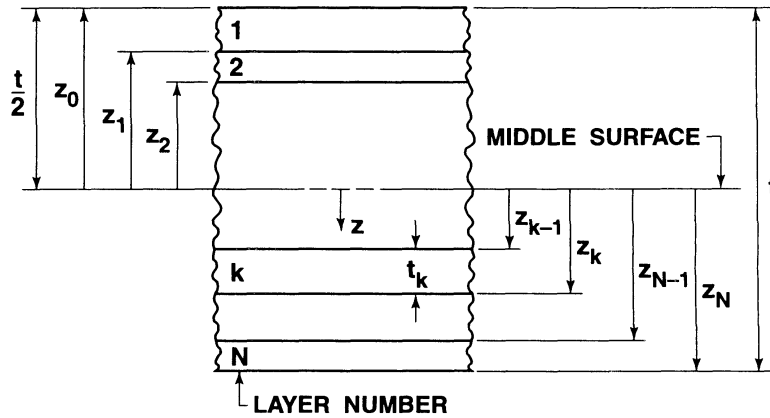

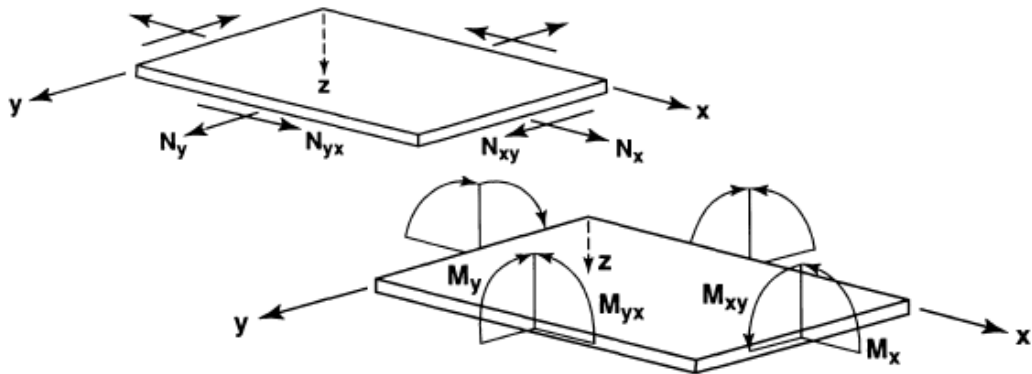Figure 4.8 Coordinate locations of layers in a laminate

Figure 4.9 Force and moment resultants of a flat laminate

The normal force N_x and the bending moment M_x per unit width of the laminate, illustrated in Figure 4.9 is calculated with the Equation (4.52) , but the whole collection of force and moment resultants can be defined as,

$$\begin{bmatrix} N_x \\ N_y \\ N_{xy} \end{bmatrix} = \int\limits_{\frac{-t}{2}}^{\frac{t}{2}} \begin{bmatrix} \sigma_x \\ \sigma_y \\ \tau_{xy} \end{bmatrix} dz = \sum_{k=1}^{N} \int\limits_{z_{k-1}}^{z_k} \begin{bmatrix} \sigma_x \\ \sigma_y \\ \tau_{xy} \end{bmatrix}_k dz \qquad\qquad (4.53)$$

$$\begin{bmatrix} M_x \\ M_y \\ M_{xy} \end{bmatrix} = \int_{-\frac{t}{2}}^{\frac{t}{2}} \begin{bmatrix} \sigma_x \\ \sigma_y \\ \tau_{xy} \end{bmatrix} .z.dz = \sum_{k=1}^{N} \int_{Z_{k-1}}^{Z_k} \begin{bmatrix} \sigma_x \\ \sigma_y \\ \tau_{xy} \end{bmatrix}_k z.dz \qquad (4.54)$$

Substituting Equation (4.51) in Equation (4.53) and (4.54) resultant forces and moments is expressed by the middle plane strains and curvatures,

$$\begin{bmatrix} N_x \\ N_y \\ N_{xy} \end{bmatrix} = \sum_{k=1}^{N} \int_{Z_{k-1}}^{Z_k} \begin{bmatrix} \overline{Q}_{11} & \overline{Q}_{12} & \overline{Q}_{16} \\ \overline{Q}_{21} & \overline{Q}_{22} & \overline{Q}_{26} \\ \overline{Q}_{61} & \overline{Q}_{62} & \overline{Q}_{66} \end{bmatrix}_k \cdot \begin{bmatrix} \varepsilon_x^0 \\ \varepsilon_y^0 \\ \gamma_{xy}^0 \end{bmatrix} dz + \sum_{k=1}^{N} \int_{Z_{k-1}}^{Z_k} \begin{bmatrix} \overline{Q}_{11} & \overline{Q}_{12} & \overline{Q}_{16} \\ \overline{Q}_{21} & \overline{Q}_{22} & \overline{Q}_{26} \\ \overline{Q}_{61} & \overline{Q}_{62} & \overline{Q}_{66} \end{bmatrix}_k \begin{bmatrix} K_x \\ K_y \\ K_{xy} \end{bmatrix} zdz \quad (4.55)$$

$$\begin{bmatrix} M_x \\ M_y \\ M_{xy} \end{bmatrix} = \sum_{k=1}^{N} \int_{Z_{k-1}}^{Z_k} \begin{bmatrix} \overline{Q}_{11} & \overline{Q}_{12} & \overline{Q}_{16} \\ \overline{Q}_{21} & \overline{Q}_{22} & \overline{Q}_{26} \\ \overline{Q}_{61} & \overline{Q}_{62} & \overline{Q}_{66} \end{bmatrix}_k \cdot \begin{bmatrix} \varepsilon_x^0 \\ \varepsilon_y^0 \\ \gamma_{xy}^0 \end{bmatrix} zdz$$

$$+ \sum_{k=1}^{N} \int_{Z_{k-1}}^{Z_k} \begin{bmatrix} \overline{Q}_{11} & \overline{Q}_{12} & \overline{Q}_{16} \\ \overline{Q}_{21} & \overline{Q}_{22} & \overline{Q}_{26} \\ \overline{Q}_{61} & \overline{Q}_{62} & \overline{Q}_{66} \end{bmatrix}_k \begin{bmatrix} K_x \\ K_y \\ K_{xy} \end{bmatrix} z^2 dz \qquad (4.56)$$

As seen in Equation (4.55) and (4.56) strains and curvatures are not dependent on the z coordinate in middle plane. Additionally, transformed reduced stiffness matrix $[\overline{Q}]$ does not vary in the laminas. For that reason resultant force and moment Equations can be written like this,

$$\begin{bmatrix} N_x \\ N_y \\ N_{xy} \end{bmatrix} = \left\{ \sum_{k=1}^{N} \begin{bmatrix} \overline{Q}_{11} & \overline{Q}_{12} & \overline{Q}_{16} \\ \overline{Q}_{21} & \overline{Q}_{22} & \overline{Q}_{26} \\ \overline{Q}_{61} & \overline{Q}_{62} & \overline{Q}_{66} \end{bmatrix}_k \int_{Z_{k-1}}^{Z_k} dz \right\} \begin{bmatrix} \varepsilon_x^0 \\ \varepsilon_y^0 \\ \gamma_{xy}^0 \end{bmatrix}$$

$$+ \left\{ \sum_{k=1}^{N} \begin{bmatrix} \overline{Q}_{11} & \overline{Q}_{12} & \overline{Q}_{16} \\ \overline{Q}_{21} & \overline{Q}_{22} & \overline{Q}_{26} \\ \overline{Q}_{61} & \overline{Q}_{62} & \overline{Q}_{66} \end{bmatrix}_k \int_{Z_{k-1}}^{Z_k} zdz \right\} \begin{bmatrix} K_x \\ K_y \\ K_{xy} \end{bmatrix} \qquad (4.57)$$

$$
\begin{bmatrix} M_x \\ M_y \\ M_{xy} \end{bmatrix} = \left\{ \sum_{k=1}^{N} \begin{bmatrix} \overline{Q}_{11} & \overline{Q}_{12} & \overline{Q}_{16} \\ \overline{Q}_{21} & \overline{Q}_{22} & \overline{Q}_{26} \\ \overline{Q}_{61} & \overline{Q}_{62} & \overline{Q}_{66} \end{bmatrix}_k \int_{z_{k-1}}^{z_k} z \, dz \right\} \begin{bmatrix} \varepsilon_x^{\,0} \\ \varepsilon_y^{\,0} \\ \gamma_{xy}^{\,0} \end{bmatrix}
$$

$$
+ \left\{ \sum_{k=1}^{N} \begin{bmatrix} \overline{Q}_{11} & \overline{Q}_{12} & \overline{Q}_{16} \\ \overline{Q}_{21} & \overline{Q}_{22} & \overline{Q}_{26} \\ \overline{Q}_{61} & \overline{Q}_{62} & \overline{Q}_{66} \end{bmatrix}_k \int_{z_{k-1}}^{z_k} z^2 \, dz \right\} \begin{bmatrix} K_x \\ K_y \\ K_{xy} \end{bmatrix} \qquad (4.58)
$$

Based on the information $\int_{z_{k-1}}^{z_k} dz = (t_k - t_{k-1})$, $\int_{z_{k-1}}^{z_k} z.dz = \dfrac{1}{2}(t_k^{\,2} - t_{k-1}^{\,2})$, and

$\int_{z_{k-1}}^{z_k} z^2.dz = \dfrac{1}{3}(t_k^{\,3} - t_{k-1}^{\,3})$ Equations (4.57) and (4.58) transform

$$
\begin{bmatrix} N_x \\ N_y \\ N_{xy} \end{bmatrix} = \begin{bmatrix} A_{11} & A_{12} & A_{16} \\ A_{12} & A_{22} & A_{26} \\ A_{16} & A_{26} & A_{66} \end{bmatrix} \begin{bmatrix} \varepsilon_x^{\,0} \\ \varepsilon_y^{\,0} \\ \gamma_{xy}^{\,0} \end{bmatrix} + \begin{bmatrix} B_{11} & B_{12} & B_{16} \\ B_{12} & B_{22} & B_{26} \\ B_{16} & B_{26} & B_{66} \end{bmatrix} \begin{bmatrix} K_x \\ K_y \\ K_{xy} \end{bmatrix} \qquad (4.59)
$$

$$
\begin{bmatrix} M_x \\ M_y \\ M_{xy} \end{bmatrix} = \begin{bmatrix} B_{11} & B_{12} & B_{16} \\ B_{12} & B_{22} & B_{26} \\ B_{16} & B_{26} & B_{66} \end{bmatrix} \begin{bmatrix} \varepsilon_x^{\,0} \\ \varepsilon_y^{\,0} \\ \gamma_{xy}^{\,0} \end{bmatrix} + \begin{bmatrix} D_{11} & D_{12} & D_{16} \\ D_{12} & D_{22} & D_{26} \\ D_{16} & D_{26} & D_{66} \end{bmatrix} \begin{bmatrix} K_x \\ K_y \\ K_{xy} \end{bmatrix} \qquad (4.60)
$$

Where, the matrixes, $[A]$, $[B]$ and $[D]$ are extensional, coupling and bending stiffness matrixes, respectively. $[A]$ relates in-plane loads to in-plane strains; $[B]$ relates in-plane loads to curvatures and moments to in plane strains; and $[D]$ relates moments to curvatures. The components of these matrixes are,

$$
A_{ij} = \sum_{k=1}^{N} \left[\left(\overline{Q}_{ij} \right) \right]_k (t_k - t_{k-1}), \qquad i = 1,2,6; \quad j = 1,2,6 \qquad (4.61)
$$

$$
B_{ij} = \frac{1}{2} \sum_{k=1}^{N} \left[\left(\overline{Q}_{ij} \right) \right]_k (t_k^{\,2} - t_{k-1}^{\,2}), \quad i = 1,2,6; \quad j = 1,2,6 \qquad (4.62)
$$

$$
D_{ij} = \frac{1}{3} \sum_{k=1}^{N} \left[\left(\overline{Q}_{ij} \right) \right]_k (t_k^{\,3} - t_{k-1}^{\,3}), \quad i = 1,2,6; \quad j = 1,2,6 \qquad (4.63)
$$

If the equations are combined into a general expression, which converts reference plane strain and curvatures into in-plane forces and moments, the final form of the expression becomes,

$$
\begin{bmatrix} N_x \\ N_y \\ N_{xy} \\ M_x \\ M_y \\ M_{xy} \end{bmatrix} = \begin{bmatrix} A_{11} & A_{12} & A_{16} & B_{11} & B_{12} & B_{16} \\ A_{12} & A_{22} & A_{26} & B_{12} & B_{22} & B_{26} \\ A_{16} & A_{26} & A_{66} & B_{16} & B_{26} & B_{66} \\ B_{11} & B_{12} & B_{16} & D_{11} & D_{12} & D_{16} \\ B_{12} & B_{22} & B_{26} & D_{12} & D_{22} & D_{26} \\ B_{16} & B_{26} & B_{66} & D_{16} & D_{26} & D_{66} \end{bmatrix} \begin{bmatrix} \varepsilon_x^{\,0} \\ \varepsilon_y^{\,0} \\ \gamma_{xy}^{\,0} \\ K_x \\ K_y \\ K_{xy} \end{bmatrix}
\tag{4.64}
$$

4.3 Micromechanical Behavior of a Lamina

The elastic behavior of a lamina can be either examined experimentally or estimated mathematically. These properties vary depending on the properties and proportions of fibers and matrix materials. The basic goal of micromechanics is to find out the relationship between properties of composite material and its constituents mathematically, as illustrated in Figure 4.10 (Jones, 1999, p.121).
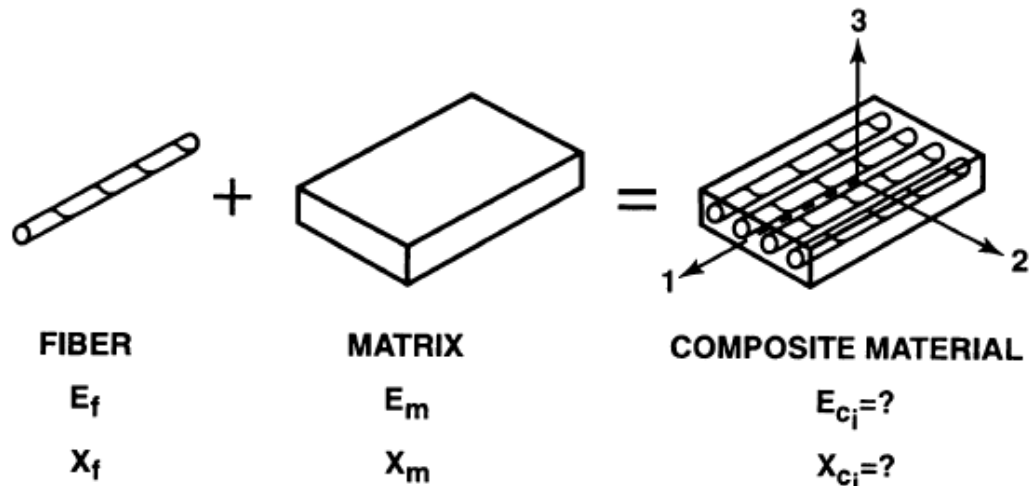

Figure 4.10 Basic goal of micromechanics

The stiffnesses and compliances of composites are calculated by the aid of fiber and matrix properties ($C_{ij} = C_{ij}(E_f, \nu_f, V_f, E_m, \nu_m, V_m)$). Here the definitions, $E_f =$ Young's modulus for an isotropic fiber, $\nu_f =$ Poisson's ratio for an isotropic fiber, and $V_f =$ Volume of fibers / Total volume of composite material, are analogous to

that of matrix material with subscript "m". The determination of composite material strengths via the strengths of constituents is also another objective of micromechanical analysis. For example the composite strengths in functional form are, $X_i = X_i(X_{if}, V_f, X_{im}, V_m)$, where $X_i = X, Y, S = $ Composite material strengths, $X_{if} = X_f, Y_f, S_f = $ Fiber strengths, and $V_f = $ Volume of fibers / Total volume of composite. These definitions are analogous to that of matrix materials.

4.3.1 The prediction of E_1

Consider a microscopically heterogeneous element is subjected a tensional stress in fiber direction (Figure 4.11). In that case, the longitudinal strain (ε_1) both for fiber and matrix material would be the same,

$$\varepsilon_1 = \frac{\Delta_L}{L} \tag{4.65}$$

In elastic region, the stresses in fiber direction are,

$$\sigma_f = E_f \varepsilon_1 \qquad \sigma_m = E_m \varepsilon_1 \tag{4.66}$$

The total load carried by the matrix and fiber is,

$$P = \sigma_1 A = \sigma_f A_f + \sigma_m A_m \tag{4.67}$$

where A is the cross-sectional area, on which σ_1 is acting, A_f and A_m are the cross-sectional areas of fiber and matrix respectively.
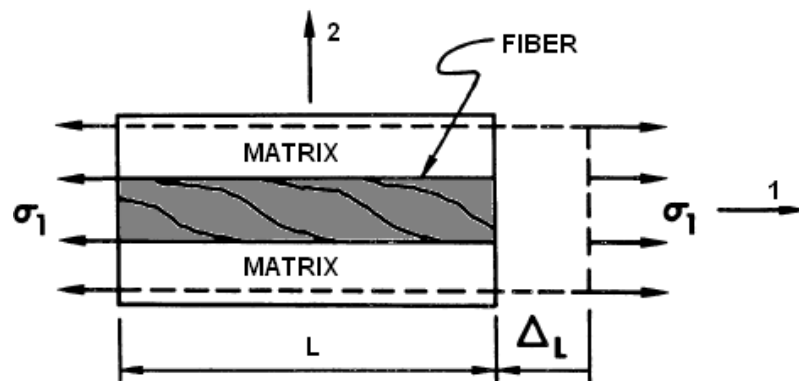

Figure 4.11 Element loaded in direction 1

The stress in fiber direction is,

$$\sigma_1 = E_1 \varepsilon_1 \tag{4.68}$$

Thus, the young's modulus in fiber direction is derived,

$$E_1 = E_f \frac{A_f}{A} + E_m \frac{A_m}{A} \tag{4.69}$$

Fiber and matrix volume fractions are just related to the areas,

$$V_f = \frac{A_f}{A} \qquad V_m = \frac{A_m}{A} \tag{4.70}$$

$$E_1 = E_f V_f + E_m V_m \tag{4.71}$$

4.3.2 The prediction of E₂

The young's modulus in transverse direction to fibers is characterized by E_2. It is assumed that both fiber and matrix are subjected the same stress level σ_2. Under transverse loading condition however, it is not possible to approximate or assume strains in direction 1 and 2 (Figure 4.12).
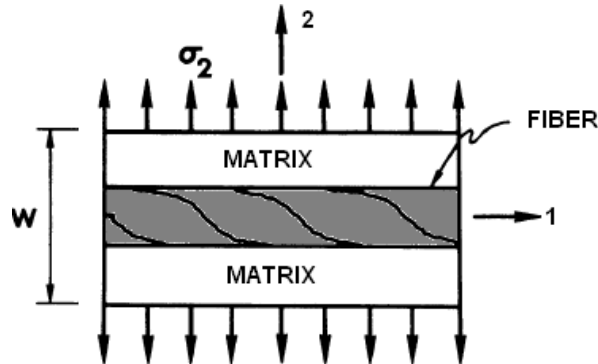
Figure 4.12 Element loaded in direction 2

The strains in fiber and matrix materials are found from the stress σ_2.

$$\varepsilon_f = \frac{\sigma_2}{E_f} \qquad \varepsilon_m = \frac{\sigma_2}{E_m} \tag{4.72}$$

The total transverse deformation is the summation of fiber and matrix deformations,

$$\Delta W = \varepsilon_2 W = V_f W \varepsilon_f + V_m W \varepsilon_m \quad \text{or} \quad \varepsilon_2 = V_f \varepsilon_f + V_m \varepsilon_m \tag{4.73}$$

Combining Equations (4.72) and (4.73) gives,

$$\varepsilon_2 = V_f \frac{\sigma_2}{E_f} + V_m \frac{\sigma_2}{E_m} \tag{4.74}$$

According to the stress-strain relation at macroscopic level,

$$\sigma_2 = E_2 \varepsilon_2 = E_2 \left[V_f \frac{\sigma_2}{E_f} + V_m \frac{\sigma_2}{E_m} \right] \tag{4.75}$$

E_2 is then expressed in terms of fiber and matrix properties,

$$E_2 = \frac{E_f E_m}{V_m E_f + V_f E_m} \tag{4.76}$$

4.3.3 The prediction of V_{12}

Just like the approach, through which E_1 obtained the major Poisson's ratio is also derived by applying a stress σ_1 in fiber direction. When $\sigma_1 = \sigma$ and the other stresses are equal to zero, the Poisson's ratio V_{12} is defined (Figure 4.13),

$$v_{12} = -\frac{\varepsilon_2}{\varepsilon_1} \tag{4.77}$$
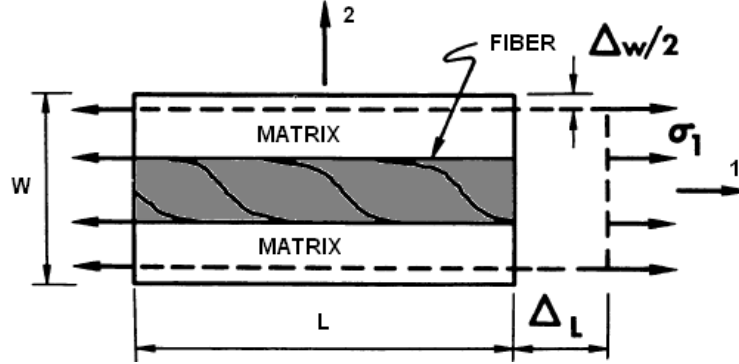
Figure 4.13 Element loaded in direction 1

Fiber and matrix strains are assumed to be identical and equal to ε_1. On the other hand, the deformation in transverse direction Δ_W is defined as macroscopically,

$$\Delta_W = -W\varepsilon_2 = W v_{12} \varepsilon_1 \tag{4.78}$$

Δ_W is also expressed by its microscopic components, fiber and matrix deformations.

$$\Delta_W = \Delta_{mW} + \Delta_{fW} \tag{4.79}$$

Transverse deformations in fiber and matrix are defined approximately,

$$\Delta_{mW} = WV_m \nu_m \varepsilon_1 \qquad \Delta_{fW} = WV_f \nu_f \varepsilon_1 \qquad (4.80)$$

Putting Equation (4.78), (4.79), and (4.80) into one expression and eliminating $\varepsilon_1 W$ gives,

$$\nu_{12} = \nu_m V_m + \nu_f V_f \qquad (4.81)$$

4.3.4 The prediction of G_{12}

While determining G_{12} in micromechanics, the shear stresses acting on fiber and matrix materials are assumed to be the same. But the shear deformations can not be the same and expressed basically,

$$\gamma_m = \frac{\tau}{G_m} \qquad \gamma_f = \frac{\tau}{G_f} \qquad (4.82)$$

The non linearity of the stress-strain behavior in shear loading is ignored and the relation is presumed linear for convenience,

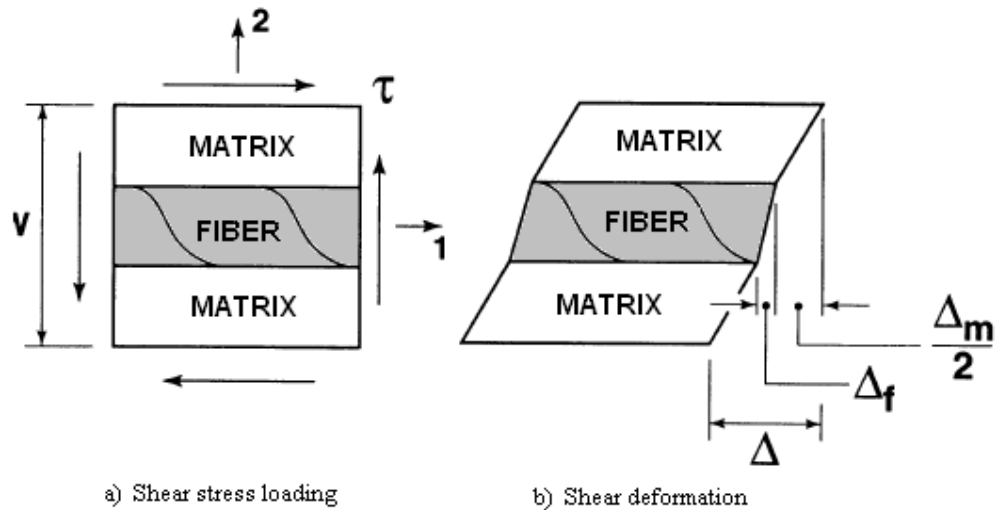a) Shear stress loading   b) Shear deformation

Figure 4.14 Element loaded in shear

The total shear deformation in macroscopic scale is,

$$\Delta = \gamma.W \qquad (4.83)$$

Fiber and matrix deformations in microscopic scale are,

$$\Delta_m = V_m W \gamma_m \qquad \Delta_f = V_f W \gamma_f \qquad (4.84)$$

Because the total deformation is the sum of fiber and matrix components ($\Delta = \Delta_m + \Delta_f$), and eliminating W yields,

$$\gamma = V_m \gamma_m + V_f \gamma_f \tag{4.85}$$

Total deformation can be written basically,

$$\gamma = \frac{\tau}{G_{12}} \tag{4.86}$$

When Equation (4.85) is rewritten combining Equation (4.86)

$$\frac{\tau}{G_{12}} = V_m \frac{\tau}{G_m} + V_f \frac{\tau}{G_f} \tag{4.87}$$

As obtained expression for transverse young's modulus E_2, the shear modulus is given finally,

$$G_{12} = \frac{G_m G_f}{V_m G_f + V_f G_m} \tag{4.88}$$

CHAPTER FIVE
FAILURE ANALYSIS IN COMPOSITES

5.1 Introduction

The general nature of failure for orthotropic materials is more complicated than for an isotropic material. A Mohr's circle analysis would show a principal angle different from that of an isotropic material, indicating that analysis techniques valid for isotropic materials are not adequate for composites. A lamina is stronger in the fiber direction than in the transverse direction, so the largest stress on the lamina may not be the one that causes failure.

Failure of a unidirectional laminate begins on the microscopic level. Microscopic failures can become macroscopic and result in catastrophic failure. Initial microscopic failures can be represented by local failure modes, such as:

- Fiber failure: breakage, micro buckling, dewetting.
- Bulk matrix failure: voids, crazing.
- Interface/flaw dominated failures: crack propagation and edge delamination (Staab, 1999, p.142).

Most of the experiments, conducted to obtain the material strength are based on unidirectional state of stresses. In real structures however, two or three dimensional stresses may be simultaneously acting on the material. It is physically impossible to obtain strength properties at all possible orientations. Therefore, methods, which calculate the characteristics at any orientation, using the material characteristics in principal directions must be determined (Jones, 1999, p.102).

For composite structures, the strength of the laminate is dependent on each individual lamina. In order to compare the state of stress to failure criteria in the lamina, failure theories were developed. Basically, all of the theories are related to the normal and shear strengths of unidirectional lamina.

For isotropic materials, failure theories generally based on principal normal stresses and maximum shear stresses. In a lamina however, failure theories are originated from the stresses in the material or in the local coordinates thanks to its orthotropic nature and varying properties at different angles.

Unidirectional laminas have two material axes; those are fiber direction and perpendicular to fiber direction. Therefore, four normal strength parameters exist concerning unidirectional lamina, so that one tension and one compression strength for each two local axes should be specified. Additionally, the shear strength appears to be fifth parameter in unidirectional laminas, although the shear stresses do not affect the shear strengths of a unidirectional lamina. The five strength parameters of a unidirectional lamina are listed below (Kaw, 2006, p.138).

X_t: Ultimate longitudinal tensile strength (in direction 1),

X_c: Ultimate longitudinal compressive strength (in direction 1),

Y_t : Ultimate transverse tensile strength (in direction 2),

Y_c : Ultimate transverse compressive strength (in direction 2), and

S : Ultimate in-plane shear strength (in plane 12).

$$\sigma_1 = \sigma_x . Cos^2\theta$$
$$\sigma_2 = \sigma_x . Sin^2\theta$$
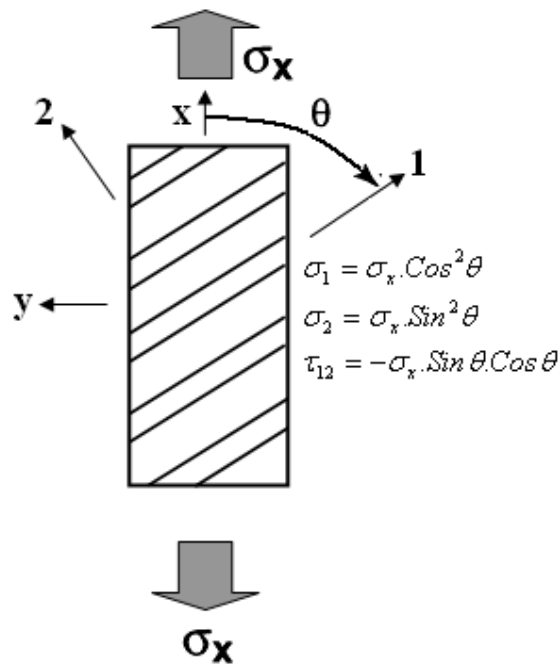$$\tau_{12} = -\sigma_x . Sin\,\theta . Cos\,\theta$$

Figure 5.1 Biaxial stresses generated by off-axis uniaxial loading

By an off-axis loading on a unidirectional lamina, biaxial stresses will be generated to explain each failure criteria as illustrated in Figure 5.1. An off-axis stress, σ_x which is at the angle of θ to the fiber direction produces biaxial stresses in principal material directions. During examining the failure theories, the material is going to be regarded as homogenous, although it is orthotropic structure (Jones, 1999, p.105).

5.2 Failure Criteria of a Lamina

5.2.1 Maximum Stress Failure Criterion

In the maximum stress failure criterion, failure occurs whenever normal and shear stress component in the principal material coordinates is equal or exceeds the correspondent strengths. The criterion can be written for tensile, compressive and shear stresses as follows,

$$\sigma_1 < X_t \qquad \sigma_2 < Y_t \qquad \sigma_1 > X_c \qquad \sigma_2 > Y_c \qquad |\tau_{12}| < S \qquad (5.1)$$

As seen, the sign of the shear stress has no effect on the shear strength. If any of the inequality conditions in Equation (5.1) are not satisfied, the material would fail by the associated failure mechanism. There are actually five failure sub criteria exist and there is no interaction between them.

In order to evaluate the state of stress and failure in a material according to maximum stress criterion, the stresses in the principal material coordinates must be primarily determined. In a uniaxial loading type in Figure 5.1, biaxial stress components are obtained by stress transformations.

$$\sigma_1 = \sigma_x Cos^2\theta \qquad \sigma_2 = \sigma_x Sin^2\theta \qquad \tau_{12} = -\sigma_x Sin\theta.Cos\theta \qquad (5.2)$$

Then, by putting the expressions σ_1, σ_2, and τ_{12} in Equation (5.2) to Equation (5.1), the maximum uniaxial stress must be the smallest of

$$\frac{X_c}{Cos^2\theta} < \sigma_x < \frac{X_t}{Cos^2\theta} \qquad \frac{Y_c}{Sin^2\theta} < \sigma_x < \frac{Y_t}{Sin^2\theta} \qquad |\sigma_x| < \left|\frac{S}{Sin\theta.Cos\theta}\right| \qquad (5.3)$$

5.2.2 Maximum Strain Failure Criterion

In this criterion, the strains in the material principal directions are limited just as the stresses in the maximum stress criterion. Failure occurs if one or more of the following conditions are not satisfied.

$$\varepsilon_1 < X_{\varepsilon_t} \qquad \varepsilon_2 < Y_{\varepsilon_t} \qquad \varepsilon_1 > X_{\varepsilon_c} \qquad \varepsilon_2 > Y_{\varepsilon_c} \qquad |\gamma_{12}| < S_\varepsilon \qquad (5.4)$$

where,

X_{ε_t} $\left(X_{\varepsilon_c}\right)$: maximum tensile (compressive) normal strain in the direction 1

Y_{ε_t} $\left(Y_{\varepsilon_c}\right)$: maximum tensile (compressive) normal strain in the direction 2

S_ε : maximum shear strain in the material coordinates 1-2

Similar to that with the shear strength, the sign of the shear strain does not affect the maximum shear strain. Initially, the strains in principal directions, ε_1, ε_2, and γ_{12} must be obtained by transforming the strains in global coordinate system, before applying this failure criterion.

As studied in maximum failure criterion, a uniaxial load is applied on a unidirectional lamina at an angle of θ to the longitudinal fiber direction. First allowable strains are going to be found and then allowable stresses can be calculated through them.

The two dimensional strain-stress relations in material coordinate system are,

$$\varepsilon_1 = \frac{1}{E_1}\left(\sigma_1 - \nu_{12}\sigma_2\right)$$

$$\varepsilon_2 = \frac{1}{E_2}\left(\sigma_2 - \nu_{21}\sigma_1\right) \qquad (5.5)$$

$$\gamma_{12} = \frac{\tau_{12}}{G_{12}}$$

Substituting the stress transformation expressions in Equation (5.2) to Equation (5.5),

$$\varepsilon_1 = \frac{1}{E_1}\left(Cos^2\theta - v_{12}Sin^2\theta\right)\sigma_x$$

$$\varepsilon_2 = \frac{1}{E_2}\left(Sin^2\theta - v_{21}Cos^2\theta\right)\sigma_x \tag{5.6}$$

$$\gamma_{12} = -\frac{1}{G_{12}}\left(Sin\theta.Cos\theta\right)\sigma_x$$

Maximum strains are written in terms of ultimate strengths in linear elastic behavior,

$$X_{\varepsilon_t} = \frac{X_t}{E_1} \qquad Y_{\varepsilon_t} = \frac{Y_t}{E_2} \qquad X_{\varepsilon_c} = \frac{X_c}{E_1} \qquad Y_{\varepsilon_c} = \frac{Y_c}{E_2} \qquad S_\varepsilon = \frac{S}{G_{12}} \tag{5.7}$$

Finally, the maximum strain criterion can be constituted in the following form,

$$\frac{X_c}{Cos^2\theta - v_{12}Sin^2\theta} < \sigma_x < \frac{X_t}{Cos^2\theta - v_{12}Sin^2\theta}$$

$$\frac{Y_c}{Sin^2\theta - v_{21}Cos^2\theta} < \sigma_x < \frac{Y_t}{Sin^2\theta - v_{21}Cos^2\theta} \tag{5.8}$$

$$|\sigma_x| < \left|\frac{S}{Sin\theta.Cos\theta}\right|$$

A prominent situation is that the maximum stress criterion, Equation (5.3) and the maximum strain criterion, Equation (5.8) seem to be similar except for the terms of Poisson's ratio. Predictions, made according these two criteria for glass-epoxy composites have given pronounced differences from the experimental results. Thus, it is recognized that neither the maximum stress nor maximum strain criterion is appropriate for e-glass-epoxy composite materials.

5.2.3 Tsai-Hill Failure Criterion

This is a yield criterion, predicting failure boundaries for orthotropic materials. Tsai-Hill criterion is described in general form,

$$(G+H)\sigma_1^2 + (F+H)\sigma_2^2 + (F+G)\sigma_3^2 - 2H\sigma_1\sigma_2 - 2G\sigma_1\sigma_3 - 2F\sigma_2\sigma_3$$
$$+ 2L\tau_{23}^2 + 2M\tau_{13}^2 + 2N\tau_{12}^2 = 1 \tag{5.9}$$

This is a related and modified form of von Mises distortional energy yield criterion for anisotropic materials. In the Equation (5.9), the

parameters F, G, H, L, M, and N are failure strength parameters which are related to the material strengths, X, Y, and S. If the only stress acting on the body is S, then the equation becomes,

$$2N = \frac{1}{S^2} \tag{5.10}$$

If σ_1 is the only stress, then

$$G + H = \frac{1}{X^2} \tag{5.11}$$

If σ_2 is the only stress, then

$$F + H = \frac{1}{Y^2} \tag{5.12}$$

Similarly, if σ_3 act in the direction 3, then

$$F + G = \frac{1}{Z^2} \tag{5.13}$$

Equation (5.11) + Equation (5.13) - Equation (5.12) is equal to

$$2G = \frac{1}{X^2} + \frac{1}{Z^2} - \frac{1}{Y^2} \tag{5.14}$$

Equation (5.12) + Equation (5.13) - Equation (5.11) is equal to

$$2F = \frac{1}{Y^2} + \frac{1}{Z^2} - \frac{1}{X^2} \tag{5.15}$$

Equation (5.11) + Equation (5.12) - Equation (5.13) is equal to

$$2H = \frac{1}{X^2} + \frac{1}{Y^2} - \frac{1}{Z^2} \tag{5.16}$$

In plane strain case, intended for a unidirectional lamina, $\sigma_3 = \tau_{13} = \tau_{23} = 0$. In addition to that, for such a lamina, depicted in Figure 5.2 it is obvious that $Y = Z$ because of the geometrical symmetry. The failure criterion in Equation (5.9) can be written for unidirectional lamina

$$\frac{\sigma_1^2}{X^2} - \frac{\sigma_1 \sigma_2}{X^2} + \frac{\sigma_2^2}{Y^2} + \frac{\tau_{12}^2}{S^2} = 1 \tag{5.17}$$

The signs of σ_1 and σ_2 determine whether the values will be X_t or X_c and Y_t or Y_c. If it is an off-axis case, the stress transformation equations (Equation (5.2)) is combined with the Equation (5.17)

$$\frac{Cos^4\theta}{X^2}+\left[\frac{1}{S^2}-\frac{1}{X^2}\right].Cos^2\theta.Sin^2\theta+\frac{Sin^4\theta}{Y^2}=\frac{1}{\sigma_x^{\ 2}} \tag{5.18}$$
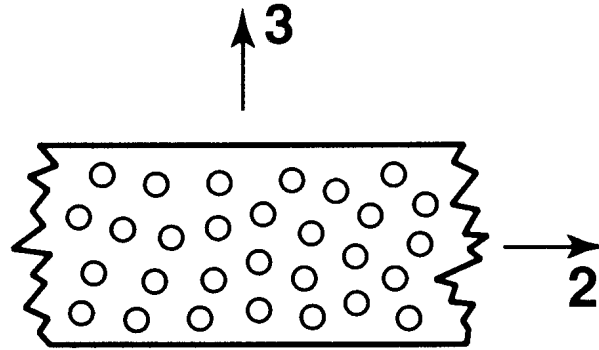
Figure 5.2 Cross-section of a unidirectional lamina (1 is the fiber direction)

Experimental results for E-glass-epoxy exhibits a good agreement with numerical solutions in Tsai-Hill failure criterion. It is found to be an appropriate failure criterion for E-glass-epoxy composite laminas in two dimensional stress fields although depending on their ductile or brittle nature, maximum stress and maximum strain can be better for other type of composite materials. It can be also said that the Tsai-Hill is an important criterion for the materials, whose properties are the same in tension and compression.

5.2.4 Hoffman Failure Criterion

In addition to the Tsai-Hill's equation some terms were added to take into account the disparities between tension and compression strengths.

$$\begin{aligned}
& C_1(\sigma_2-\sigma_3)^2+C_2(\sigma_3-\sigma_1)^2+C_3(\sigma_1-\sigma_2)^2 \\
& +C_4\sigma_1+C_5\sigma_2+C_6\sigma_3+C_7\tau_{23}^{\ 2}+C_8\tau_{31}^{\ 2}+C_9\tau_{12}^{\ 2}=1
\end{aligned} \tag{5.19}$$

The 9 coefficients ($C_1...C_9$) are determined by the principal material strengths ($X_t,X_c,Y_t,Y_c,Z_t,Z_c,S_{23},S_{31},$ and S_{12}). The Hoffman criterion is more simplified in plane stress case, where $\sigma_3=\tau_{23}=\tau_{31}=0$ and because of the isotropy in transverse direction the equities, $Z_t=Y_t$, $Z_c=Y_c$, and $S_{31}=S_{12}$ are also exist. Thus, the failure criterion is degraded from Equation (5.19) to,

$$-\frac{\sigma_1^2}{X_cX_t}+\frac{\sigma_1\sigma_2}{X_cX_t}-\frac{\sigma_2^2}{Y_tY_t}+\frac{X_c+X_t}{X_cX_t}\sigma_1+\frac{Y_c+Y_t}{Y_cY_t}\sigma_2+\frac{\tau_{12}^2}{S_{12}^2}=1 \qquad (5.20)$$

The Hoffman criterion becomes the same as Tsai-Hill criterion while studying the materials, of which the tension and compression strengths are equal ($X_c=-X_t=-X$ and $Y_c=-Y_t=-Y$). This criterion is a convenient tool if it is the case of materials with different tension and compression strengths. Experiments with the glass-epoxy, graphite-epoxy, and baron-epoxy materials have given compatible failure data with the Hoffmann criterion according to Jones (1999).

5.2.5 Tsai-Wu Tensor Failure Criterion

This criterion is based on the postulation by Tsai and Wu, which gives a strength definition, representing the interaction between stresses in different directions. If a six dimensional state of stress exist in material then the criterion is defined in indicial notation as

$$F_i\sigma_i+F_{ij}\sigma_i\sigma_j=1 \qquad i,j=1,\ldots,6 \qquad (5.21)$$

F_i and F_{ij} are representing the second and fourth rank strength tensors, and stress notations, σ_4,σ_5 and σ_6 are τ_{23},τ_{31} and τ_{12}, respectively. In the plane stress case of an orthotropic lamina, the equation is reduced to a less complex form.

$$F_1\sigma_1+F_2\sigma_2+F_6\sigma_6+F_{11}\sigma_1^2+F_{22}\sigma_2^2+F_{66}\sigma_6^2+2F_{12}\sigma_1\sigma_2=1 \qquad (5.22)$$

Looking at the Equation (5.22) in detail, the linear stress terms are for representation of different tensile and compressive properties, whereas the quadratic stress terms characterize the ellipsoidal contour in stress space. The normal stress interactions between direction 1 and 2 is taken into account by using an independent parameter F_{12}.

The parameters in the stress tensor can be defined in terms of the material tension, compression and shear properties. If only tensile load is applied to the body

$$F_1X_t+F_{11}X_t^2=1 \qquad (5.23)$$

Similarly, under pure compression,

$$F_1 X_c + F_{11} X_c{}^2 = 1 \tag{5.24}$$

Upon the joint solution of Equations (5.23) and (5.24)

$$F_1 = \frac{1}{X_t} + \frac{1}{X_c} \qquad F_{11} = -\frac{1}{X_t X_c} \tag{5.25}$$

In similar way,

$$F_2 = \frac{1}{Y_t} + \frac{1}{Y_c} \qquad F_{22} = -\frac{1}{Y_t Y_c} \tag{5.26}$$

If thinking of the shear strength being independent of the shear stress signs in principal coordinates, that means,

$$F_6 = 0 \qquad F_{66} = \frac{1}{S^2} \tag{5.27}$$

For materials with the same tensile and compressive properties ($X_t = -X_c$ and $Y_t = -Y_c$)

$$F_1 = 0 \qquad F_{11} = \frac{1}{X^2} \qquad F_2 = 0 \qquad F_{22} = \frac{1}{Y^2} \tag{5.28}$$

These equations result in the failure criterion to reduce to the following form,

$$\frac{\sigma_1{}^2}{X^2} + 2F_{12}\sigma_1\sigma_2 + \frac{\sigma_2{}^2}{Y^2} + \frac{\tau_{12}{}^2}{S^2} = 1 \tag{5.29}$$

Equation (5.29) seems to be similar to Equation (5.17) in Tsai-Hill criterion except for the term F_{12} which is instead $-\dfrac{1}{X^2}$. As F_{12} is the common product of σ_1 and σ_2, it is impossible to obtain F_{12} from uniaxial tests. Consider a biaxial loading only in principal directions with a magnitude of $\sigma_1 = \sigma_2 = \sigma$. From Equation (5.22)

$$(F_1 + F_2)\sigma + (F_{11} + F_{22} + 2F_{12})\sigma^2 = 1 \tag{5.30}$$

Finally, F_{12} is derived from substituting the definitions of F_1, F_2, F_{11} and F_{22} into Equation (5.30).

$$F_{12} = \frac{1}{2\sigma^2}\left[1 - \left[\frac{1}{X_t} + \frac{1}{X_c} + \frac{1}{Y_t} + \frac{1}{Y_c}\right]\sigma + \left[\frac{1}{X_t X_c} + \frac{1}{Y_t Y_c}\right]\sigma^2\right] \tag{5.31}$$

In addition to the tensile biaxial failure stress σ, the definition of F_{12} is dependent on several material strengths. Owing to the difficulties of performing biaxial tension

tests, Tsai and Wu suggested a 45° off-axis tests or shear tests for determining F_{12}. It was also reported that slight variations in fiber orientation can fully disrupt the determination of F_{12}. The off-axis tests have given poor results. Another test method proposed to determine F_{12} is to restrict deformations in transverse direction of applied load but nonetheless to find the exact value of F_{12} remains still unclear (Staab, 1999, p.161).

CHAPTER SIX
DETERMINATION OF BASIC MATERIAL PROPERTIES

6.1 Introduction
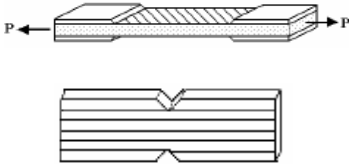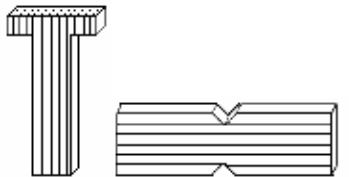
Designing composite structures requires an accurate knowledge about mechanical properties of composite material. Mechanical tests that are used to derive mechanical properties of conventional metallic materials are not applicable for composite materials because of anisotropy, coupling effects and different possible failure modes. Therefore, appropriate test methods were developed and these were evolved into standards, adopted by the American Society for Testing and Materials (ASTM).

Researches in composite materials always entail basic material properties of unidirectional laminated composite plates derived from quasi-static experimental study. The data collected from these tests are used to reveal strength and stiffness characteristics of the material. For an orthotropic lamina, those are nine independent constants, each of which is a specific value defining mechanical response. The strength and stiffness characteristics are listed in Table 6.1 (Gibson, 1994).

Table 6.1 The strength and stiffness characteristics of an orthotropic laminate

Strength characteristics		Stiffness characteristics	
X	Axial or longitudinal strength in direction 1.	E_1, E_2	Longitudinal and transverse Young modulus
Y	Transverse strength in direction 2.	v_{12}	Poisson's ratio
S	Shear strength in plane 1, 2.	G_{12}	Shear modulus

Table 6.2 ASTM test standards and specimen geometries in determining mechanical characteristics (Okutan, 2001)

Determinable properties	Symbol and Unit	ASTM test method	Specimen geometry
Axial or longitudinal modulus Axial Poisson's ratio Longitudinal tensile strength	E_1 (MPa) ν_{12} (-) X_t (MPa)	ASTM 3039-76	
Transverse modulus Transverse Poisson's ratio Transverse tensile strength	E_2 (MPa) ν_{21} (-) Y_t (MPa)	ASTM 3039-76	
Shear modulus	G_{12} (MPa)	ASTM 3518-76 ASTM D 7078-05 ASTM D 5379	
Shear strength	S (MPa)	ASTM D 5379 ASTM D 7078-05	
Longitudinal compressive strength	X_c (MPa)	ASTM 3410-75	
Transverse compressive strength	Y_c (MPa)	ASTM 3410	

6.2 Test Procedures

In order to assess mechanical responses of a unidirectional lamina, the following assumptions are needed, in tensile, compressive and shear loading conditions. These descriptions provide a simplified approach in fiber-matrix interactions (Mallick, 1993).

- Fibers are uniformly distributed throughout the matrix.
- Perfect bonding exists between fibers and matrix.
- The matrix is free of voids.
- Applied loads are either parallel to or normal to the fiber direction.
- The lamina is initially in a stress-free state (i.e., no residual stresses are present)
- Both fibers and matrix behave as linearly elastic materials.

6.2.1 Determination of the Tensile Properties

Tensile properties of a unidirectional lamina are Young's modulus in longitudinal and transverse directions (E_1, E_2), Poisson's ratio (v_{12}, v_{21}), longitudinal and transverse tensile strengths (X_t, Y_t). Static tensile tests were applied to the test specimens having orientations of $[0^0]_6$ and $[90^0]_6$ according to the ASTM D3039-76 standard test method. Test specimens were manufactured as straight sided and with a constant cross section. As illustrated in Figure 6.1, the specimens have 250 mm length, 13 mm width and a measured thickness of 1.7 mm.
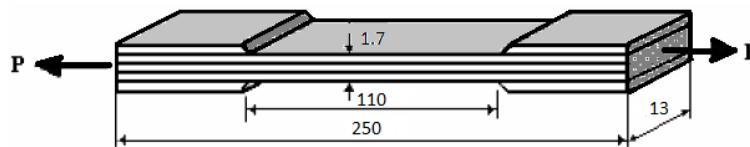

Figure 6.1 Test specimen geometry and dimensions for longitudinal tensile loading

Tests were carried out in the Shimadzu AG-100, 100 KN loading capacity testing machine, at 0.5 mm/min test speed. A uniaxial tensile loading was applied to the specimens and the load was raised up step by step until final failure occurred. During experiments, the longitudinal elongation was measured simultaneously by the aid of

a video extensometer with two digital cameras connected to the data acquisition system of the test machine. The Young's modulus in fiber direction (E_1), and the axial strength (X_t) were calculated by using the following conventional equations,

$$\sigma_1 = \frac{P}{A}, \qquad E_1 = \frac{\sigma_1}{\varepsilon_1} = \frac{P}{\varepsilon_1 A}, \qquad X_t = \frac{P_{ult}}{A} \tag{6.1}$$

On the other hand, the Young's modulus in transverse direction (E_2) and the transverse tensile strength (Y_t) are found by loading $[90^0]_6$ test specimens in perpendicular to the fiber direction. The geometry and dimensions, which is compatible with the standard test method ASTM D3039-76 are given in Figure 6.2.
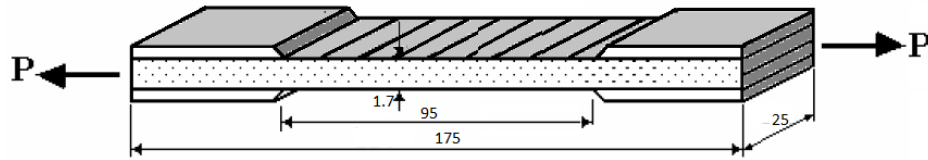
Figure 6.2 Test specimen geometry and dimensions for transverse tensile loading

The tensile test speed was 0.5 mm/min, and the load was increased step by step up to the occurrence of catastrophic failure. Filling the obtained data to Equation (6.2), the tensile properties in transverse direction can be calculated, easily.

$$\sigma_2 = \frac{P}{A}, \qquad E_2 = \frac{\sigma_2}{\varepsilon_2} = \frac{P}{\varepsilon_2 A}, \qquad Y_t = \frac{P_{ult}}{A} \tag{6.2}$$

6.2.2 Determination of the Compressive Properties

Notwithstanding the buckling effect exists in compression loading, selecting the convenient geometry and dimensions in accordance with ASTM D3410 and using test fixtures alleviate this effect, significantly. Test specimen geometry with dimensions and the test fixture is illustrated in Figure 6.3, schematically. The unidirectional laminated $[0°]_6$ test specimens with the dimensions of 140 mm long, 13 mm wide and 1.7 mm thick were prepared for longitudinal compressive tests and $[90°]_6$ test specimens with the dimensions of 140 mm long, 25 mm wide and 1.7 mm thick were prepared for transverse compressive tests. Having recorded the failure

loads by compression tests in fiber and perpendicular to fiber directions, longitudinal and transverse compressive strengths (X_c, Y_c) were calculated.
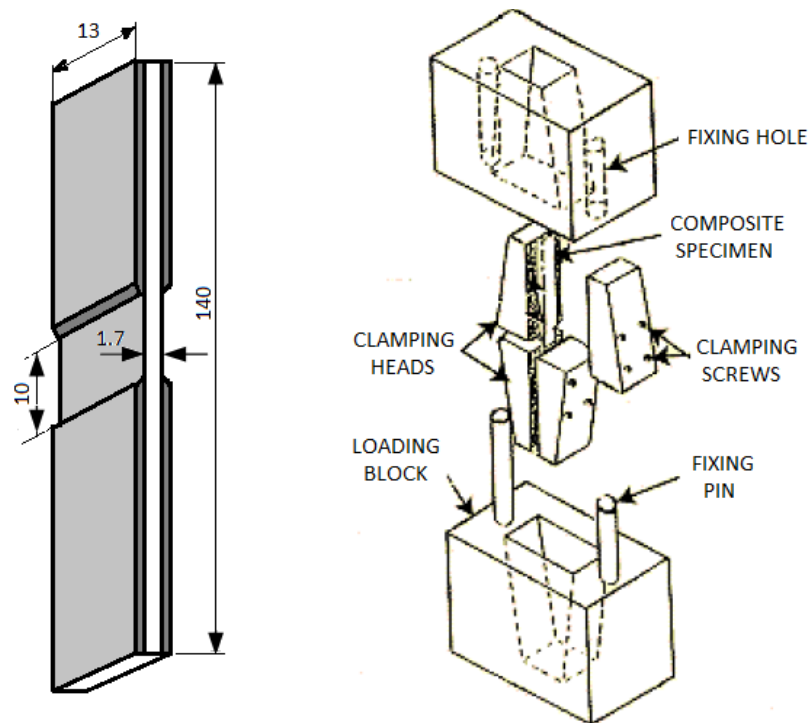

Figure 6.3 Test specimen geometry and dimensions for compressive loading and its test fixture

6.2.3 Determination of the Shear Properties

It is a very difficult task to obtain the mechanical shear properties of composites. This difficulty stems from the necessity of creating a pure and a constant magnitude shear stress in the gage section of specimen. Many test methods have been applied so far to assess the in-plane-shear properties of composites. The most common of these methods are listed below:

1. ±45 Shear test,
2. 10° Off-axis test,
3. Torsion tube,
4. Rail shear test,
5. Sandwich cross-beam test,
6. T-specimen shear,

7. Iosipescu shear test,

8. V-Notched rail shear test.

In the current study the v-notched rail shear test method was selected inasmuch as the V-notched rail shear test appears to be well-suited for measuring the in-plane shear modulus and shear strength of unidirectional and multidirectional composite laminates. This test method incorporates attractive features from both the Iosipescu V-notched shear test and the standard two-rail shear test. The V-notched specimen provides a larger gage section than the standard Iosipescu shear specimen and enhanced loading capability compared to other existing test methods (Adams et al., 2003).

The ASTM standard D 7078-05 approved by ASTM Committee in March of 2005 defines the v-notched rail shear test, which determines the shear strength and the shear stiffness of materials. The standard test fixture and specimen geometry are given in Figure 6.4. Specimens were prepared in $[0°]_6$ and $[90°]_6$ orientations to get shear strengths in fiber and perpendicular to the fiber direction.
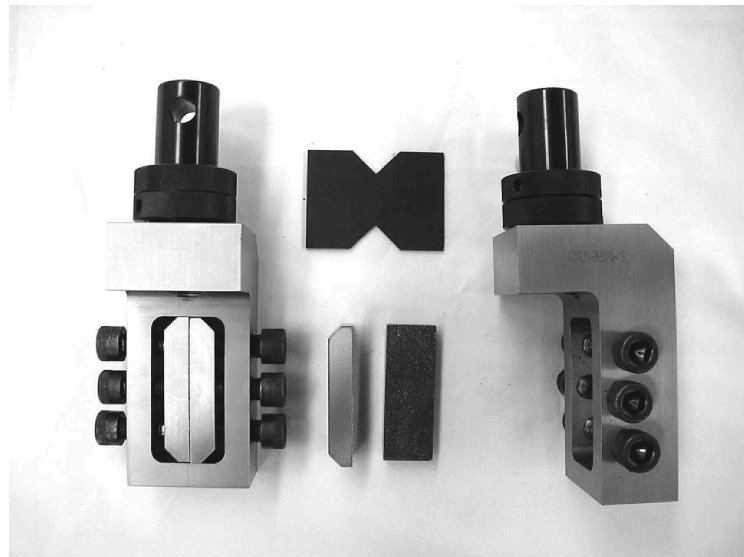

Figure 6.4 V-notched rail shear test fixture, shown with a standard v-notched specimen and one pair of grip plates removed (www.compositesworld.com)

The specimens for the present tests were produced according to the standard geometry and dimensions as illustrated in Figure 6.5. The test fixtures were mounted

on a SHIMADZU (100 kN) testing machine for loading specimens and in order to record strain values a digital strain meter TDS-530 was used. The strain gauges were installed on the specimen between the two notches at 45º as shown in Figure 6.6. When clamping specimens in grips, the two ends of them were embedded 25 mm inside the fixture, so only the notched part was left outside and between the grips. The specimens, on which strain gages stuck were loaded only in elastic region to get more accurate data, whereas the other specimens were tested until the final failure was detected.
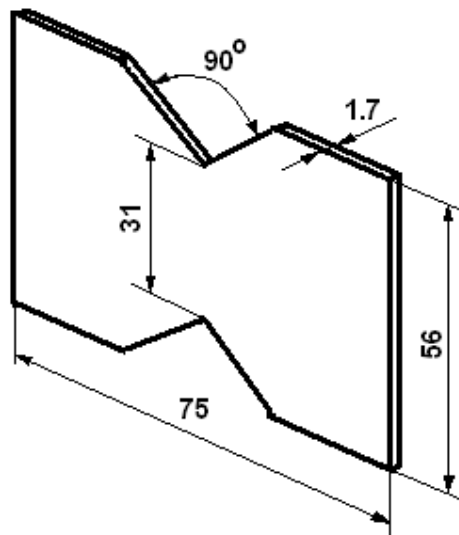
Figure 6.5 Dimensions (mm) of the V-notched rail shear test specimen
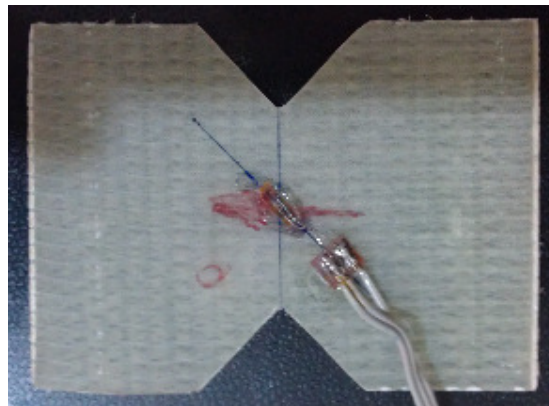
Figure 6.6 V-notched rail shear specimen with strain gage stuck on before testing

Shear properties were calculated by entering the test data to the following equations. Initially, in-plane shear strength (S) were calculated,

$$S = \frac{P_{max}}{w.t} \tag{6.3}$$

Where P_{max} is the maximum shear failure load, reached; w is the width of the narrowest point of the notch and t is the thickness of the plate.

6.3 Results of Mechanical Property Tests

In order to determine the longitudinal modulus E_1, transverse modulus E_2, longitudinal and transverse tensile strengths X_t and Y_t, longitudinal and transverse compressive strengths X_c and Y_c, rail-shear strength S and Poison's ratio v_{12}, a unidirectional glass fiber / epoxy composite plate was produced and a series of experiments were performed. Following repeated tests, average results obtained by tensile, compressive and rail-shear tests were calculated for each specimen having 0° and 90° fiber orientations (Table 6.3).

Table 6.3 Mechanical properties of the glass fiber / epoxy composite material

E_1(MPa)	E_2 (MPa)	v_{12}	X_t(MPa)	Y_t(MPa)	X_c(MPa)	Y_c(MPa)	S(MPa)
27200	12800	0.25	586.5	137.7	324.7	200.2	61.96

CHAPTER SEVEN
EXPERIMENTAL STUDY AND RESULTS 0F SINGLE LAP DOUBLE SERIAL FASTENER JOINTS AT ELEVATED TEMPERATURES

7.1 Introduction

Vast researches have been performed on mechanically fastened joints with different parameters such as material and geometrical properties together with a one or a combination of failure criterion to predict the failure load and failure mode on the strength of the joint by experimental, analytical and numerical means. Much of these previous studies on mechanically fastened composite joints have been carried out at room temperature except for a few of them, such as the work reported by Song et al.(2008), a study, aimed to investigate the bearing strength of a blind riveted single lap joint of a carbon/epoxy composite after heat exposure, but with the present study it was intended to investigate the failure behavior of bolted glass-epoxy composite material joints at elevated temperatures concurrent with the thermal exposure.

In this chapter, the results of an experimental failure analysis, which was carried out to determine the effects of thermal condition and tightening torque on the failure load and failure behavior of single lap double serial fastener glass fiber / epoxy composite joints were given. 40, 50, 60, 70, and 80 ºC temperatures were exposed to the specimens during tensile tests. Besides thermal effects, 0 and 6 Nm tightening torques were applied to observe how clamping forces affect the joint strength at high temperatures.

7.2 Explanation of the Problem

Consider a single shear, composite-to-composite, lap joint with 2 fasteners arranged in longitudinal direction, subjected to quasi-static loading in tension. Composite plates were prepared using glass fiber/epoxy with lay-up of [0/90/45/-45]s configuration. The laminate specimen was then cut into required dimensions,

(L=210mm, W=36mm and h was measured as 2mm). The geometrical features of specimens were prepared in accordance with ASTM D 5961/D 5961M – 01, the standard test method for bearing response of polymer matrix composite laminates (Figure 7.1). Two serial holes (D=6mm) were drilled along the centerline of the plates and doublers made of the same material (S=114mm, W=36mm) were stuck onto the specimens. Specimens were fastened to each other using rigid bolts with a nominal diameter of 6mm and the level of torque was either M=6 Nm or M=0Nm (finger tight) for all fasteners within the same joint (Figure 7.2).
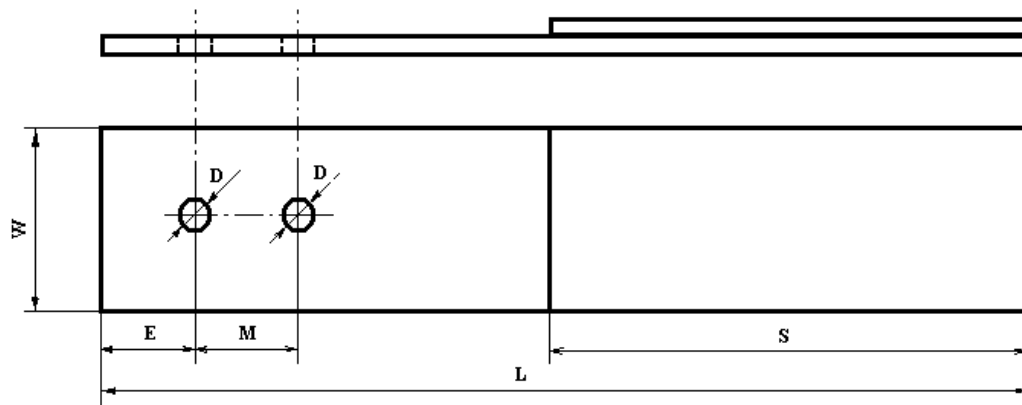
Figure 7.1 Composite specimen geometry for single lap double fastener bearing test
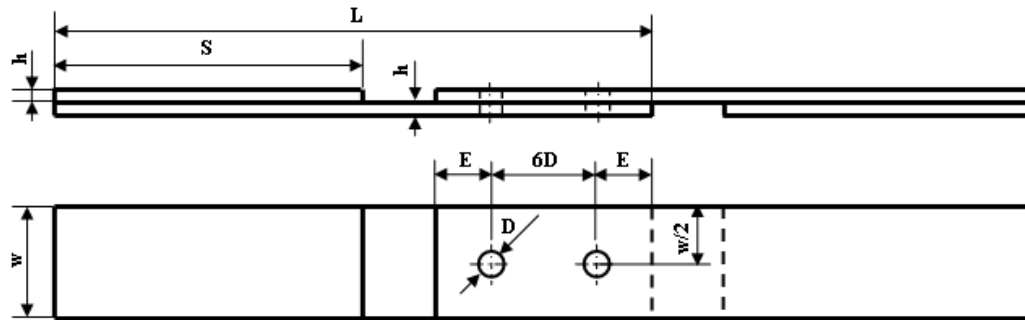
Figure 7.2 Joint of single shear double fastener composite test specimens

7.3 Material Production

The glass fiber / epoxy composite plate used in this study was manufactured using vacuum assisted resin infusion technique. Prior to the vacuum process, the glass-fiber

whose layer has the density of 300 g/m³ was laid on to the heater table according to specified orientations, [0/90/45/-45]s.

After preparing vacuum bag and evacuating the air by a vacuum pump, the mixture of Duratek DTE 1000 resin and Duratek DTS 1100 fast hardener was drawn into the component by vacuum and it was infused into the glass fiber until complete impregnation. It was cured under 0.1 MPa pressure at 120 ºC for 2 hours. The measured thickness of composite plate was 2 mm after production.

7.4 Thermal Test Chamber

In order to simulate environmental conditions and observe the behavior of composite joints at various temperatures, a thermal test chamber with a clamp resistance heater was designed (Figure 7.3). The chamber was isolated to obtain a stable temperature, and for setting the temperature to a fixed value, an adjustable thermostat was mounted inside it.
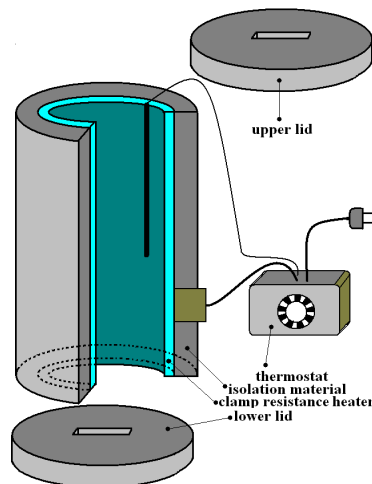

Figure 7.3 Thermal test chamber (1000 W)

The upper and lower ends of the chamber were also isolated by means of two lids. Rectangular clefts were cut on to the lids, so that upper and lower ends of the specimen could be passed through them. To avoid deviations in temperature, it was checked by measuring via a thermocouple device. During experiments, the sensors of

the measuring instrument were in contact with the fastener bolts where bearing failure usually occurs.

7.5 Testing Procedure

In order to examine the behavior of bolted joints in glass fiber / epoxy laminates at varying temperature levels under changing clamping forces, a series of experiments were performed. Specimens were tested at six different chamber temperatures (Room Temp.(~20ºC), 40-50-60-70-80 ºC) and the tightening torques of fastener bolts were M= 0 Nm (finger tight) and M= 6Nm. Tests were repeated for each thermal condition and toque level, after that average values of failure loads were recorded. All of the experiments were carried out in the Shimadzu AG-100, 100 kN loading capacity testing machine, at 1 mm/min test speed (Figure 7.4).

Figure 7.4 Set-up of thermal test chamber, thermostat and thermocouple

7.6 Results and Discussion

The failure loads of single shear double serial fastener glass fiber / epoxy composite joints exposed to high temperatures investigated experimentally. Figures 7.5 and 7.6 illustrate the effect of various temperatures on load/displacement curves in tensile tests of mechanically fastened joints, under M=0 Nm (finger tight) and M=6 Nm tightening torques, respectively. As seen in the figures, when the test

temperature increases, the composite matrix material softens to a large extent and it affects joint strength, namely the load-bearing capability of the composite gradually decreases. The non-linear part of deformation appears to be more dominant as the amount of plastic deformation is large and above 60 ℃ the whole load / displacement curve looks smoother. Nevertheless, slopes of the curves reduce dramatically, which means reducing load carried by joint for the same bolt-hole displacement rate. On the other hand, while at the peak values of bearing forces, bolt-hole displacements are formed to be between 12-14 mm for test temperatures smaller than 60 ℃, it reduces dramatically below 10 mm for higher temperature levels that approximates the glass transition temperature of the pure resin. High temperature levels cause resin damage and shorten residual bearing life of the composite joint.
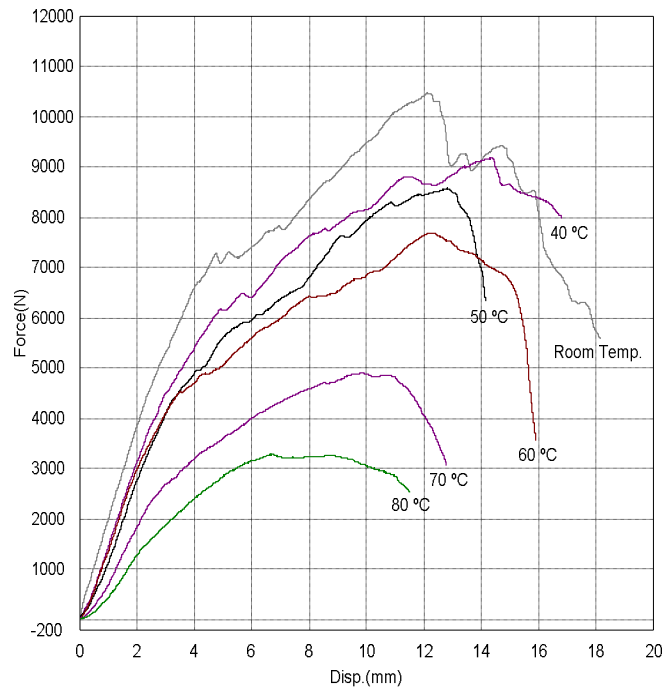

Figure 7.5 The effect of temperature on load/displacement curves in tensile tests of bolted glass fiber / epoxy composite joint under M= 0 Nm tightening torque.

In Figure 7.5, the curves are almost linear up to some point. Beyond that load, the joints exhibit intensively non-linear load-displacement curves. It is attributed to the bearing failure in front of the bolt and pulling-through of the fastener.
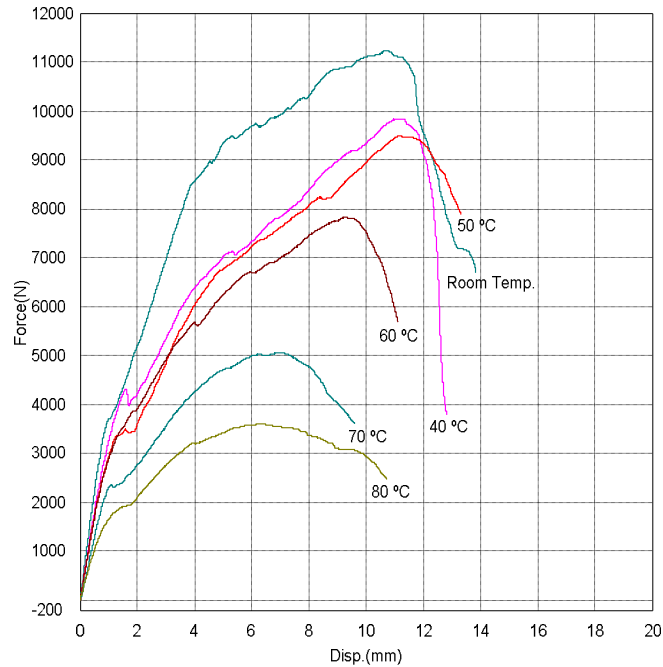
Figure 7.6 The effect of temperature on load/displacement curves in tensile tests of bolted glass fiber / epoxy composite joint under M= 6Nm tightening torque

For bolted joints, fixed under M= 6 Nm tightening torques (Figure 7.6), due to the clamping force generated by the fasteners, frictional forces develop between the plates. Initially, the load transfer is dominated by this friction when the level of applied load is low. When the load is increased to some point, friction forces are completely overcome and the composite plates start to slide relative to each other, causing the load to be picked up by bolts through contact between fastener and hole edges of the plates. The effect of clamping force, produced by tightening torque can be observed in load/displacement curves in Figure 7.6. The change in slopes of curves between 0-2 mm displacement levels is attributed to the frictional forces to be developed fully.

After exceeding frictional force, load pick-up is undertaken by fastener bolts and there is no significant difference between the slopes of curves relating to M= 0 Nm and M= 6 Nm torque levels at even elevated temperatures, as seen in Figure 7.7.
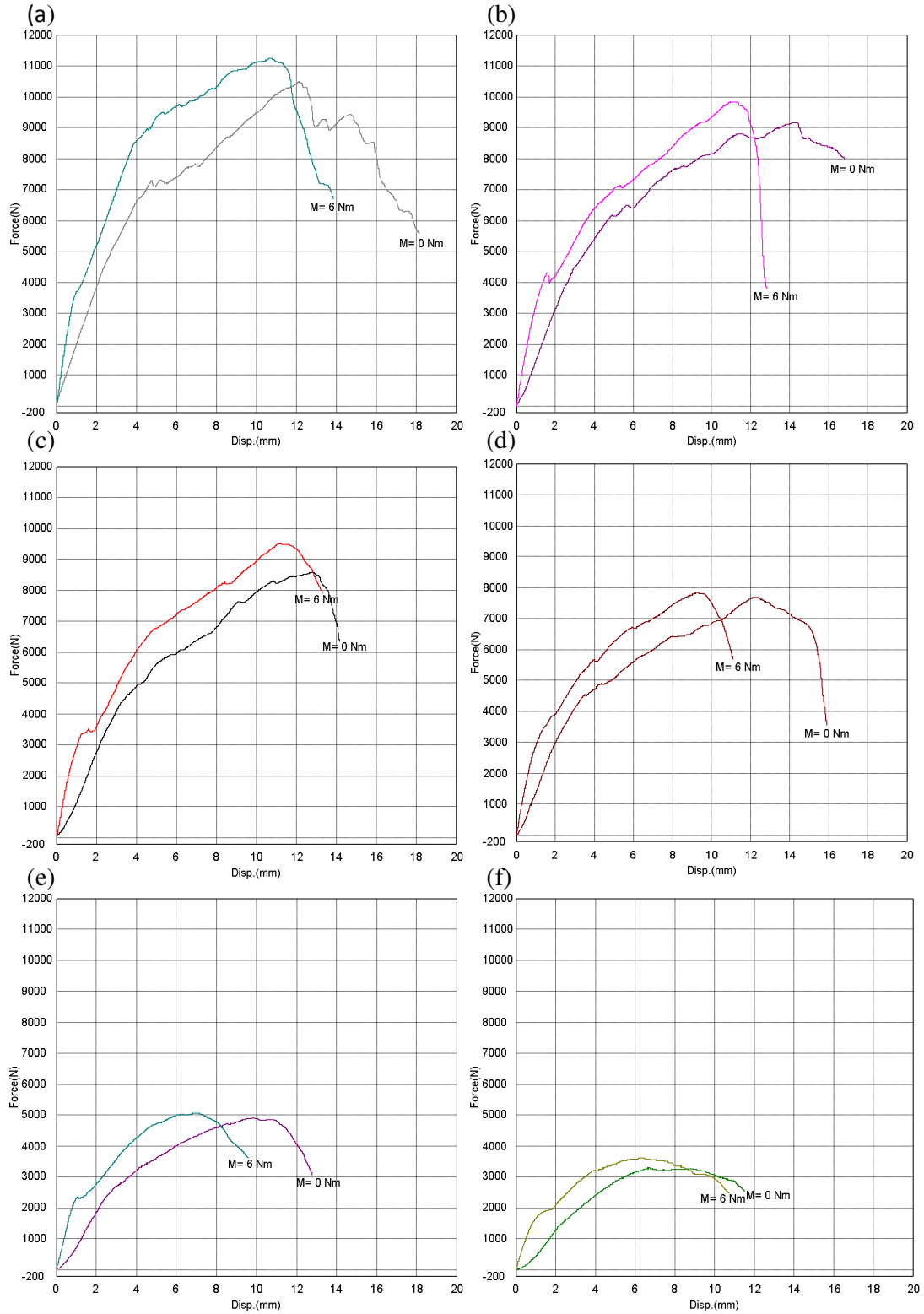
Figure 7.7 The effect of bolt tightening torques on load/displacement curves in tensile tests of bolted glass fiber / epoxy composite joint (a) Room Temp. (b) 40 °C, (c) 50 °C, (d) 60 °C (e) 70 °C, (f) 80 °C

Once the load is picked up by bolts, the geometrical (the edge distance-to-hole diameter ratio, (E/D), plate width-to-hole diameter ratio (W/D) etc.) and environmental (temperature, humidity etc.) parameters, which are the same in both specimens became important.

The obtained experimental data and some calculated statistical results (maximum and minimum values, range, mean values and standard deviations) are given Table 7.1 and Table 7.2 for M= 0 Nm and M= 6 Nm preloads, respectively . Under each temperature and preloading conditions, tests were repeated for three times and the data recorded. Data distribution and mean values of failure data were also depicted in Figures 7.8 and 7.10 by generating box plots at which the upper and lower edges of boxes represent the maximum and minimum failure loads experienced for each test condition and centers of the circular marks specify the location of mean values. Note that, some test values appear to be very close to the mean value, whereas some of them display bigger range and higher standard deviations. As a precise temperature control was provided during the test period, these fluctuations are attributed to some probable minor scale geometrical inequalities in specimens.

Table 7.1 Recorded and calculated test results of glass fiber / epoxy composite material joints, at various chamber temperatures under M= 0 Nm tightening torque

Temperature (C°)	20	40	50	60	70	80
Max. Value (N)	10538.30	9961.96	8656.61	7677.19	4899.38	3281.96
Min. Value (N)	10110.30	8940.87	8434.23	7209.86	4789.15	2952.04
Range (N)	428.00	1021.09	222.38	467.33	110.23	329.92
Mean Value (N)	10377.70	9358.82	8555.00	7443.53	4844.27	3117.00
Stnd. Deviation (N)	233.11	535.14	112.42	330.45	77.94	233.28

Table 7.2 Recorded and calculated test results of glass fiber / epoxy composite material joints, at various chamber temperatures under M= 6 Nm tightening torque.

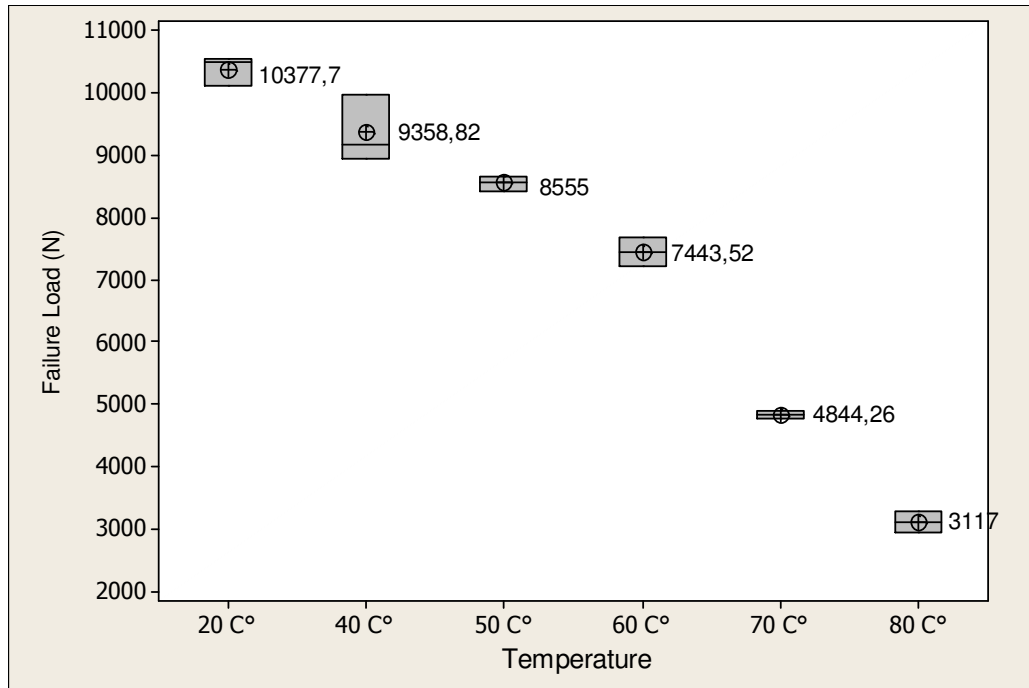| Temperature (C°)	20	40	50	60	70	80
Max. Value (N)	12180.00	9844.56	9856.56	7844.94	5212.47	4039.96
Min. Value (N)	11184.80	9562.24	9488.66	7781.78	5017.12	3077.48
Range (N)	995.20	282.32	367.90	63.16	195.35	962.48
Mean Value (N)	11533.50	9661.19	9612.15	7813.36	5095.39	3571.31
Stnd. Deviation (N)	560.43	158.97	211.67	44.66	103.29	481.73

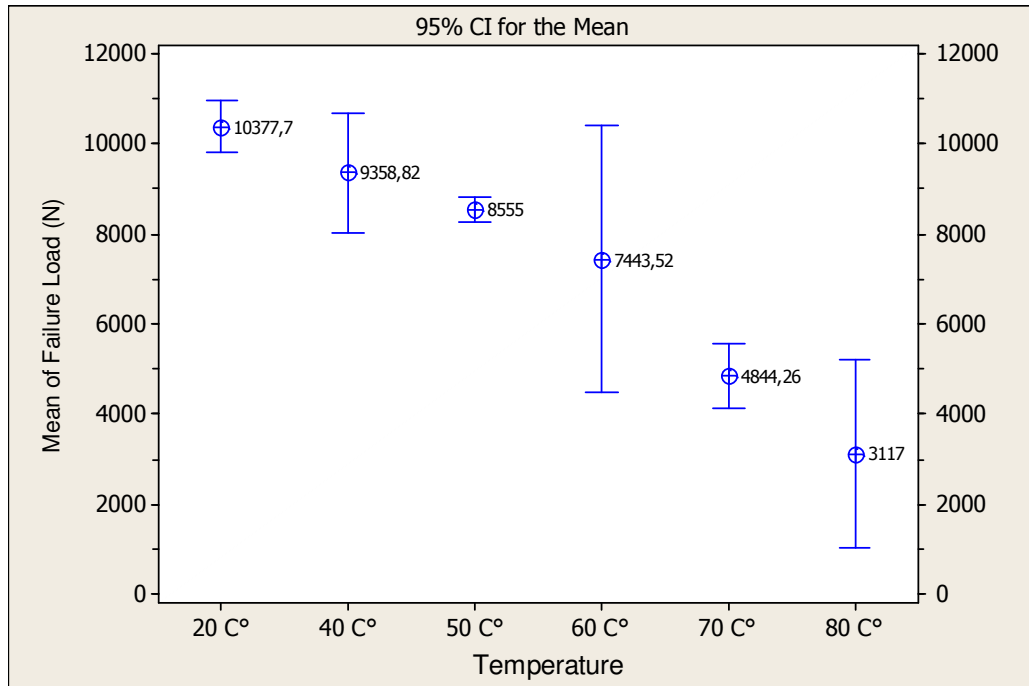Figure 7.8 Box plots of failure loads, occurring at different temperatures under M= 0 Nm

Figure 7.9 Confidence interval (CI) plots for mean values of failure loads, occurring at different temperatures under M= 0 Nm
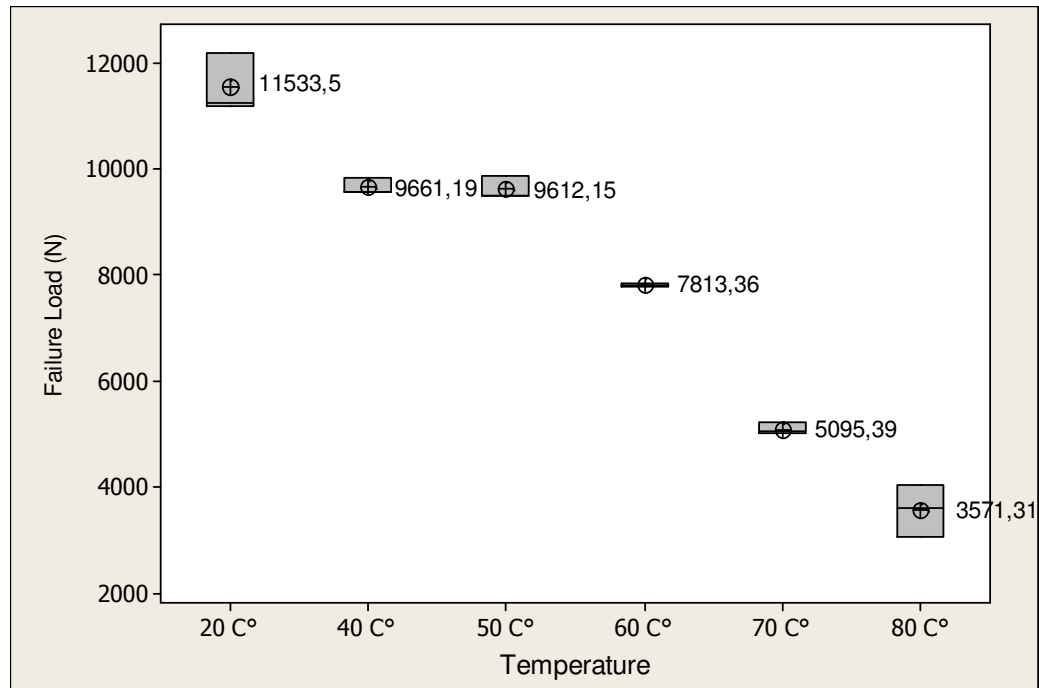
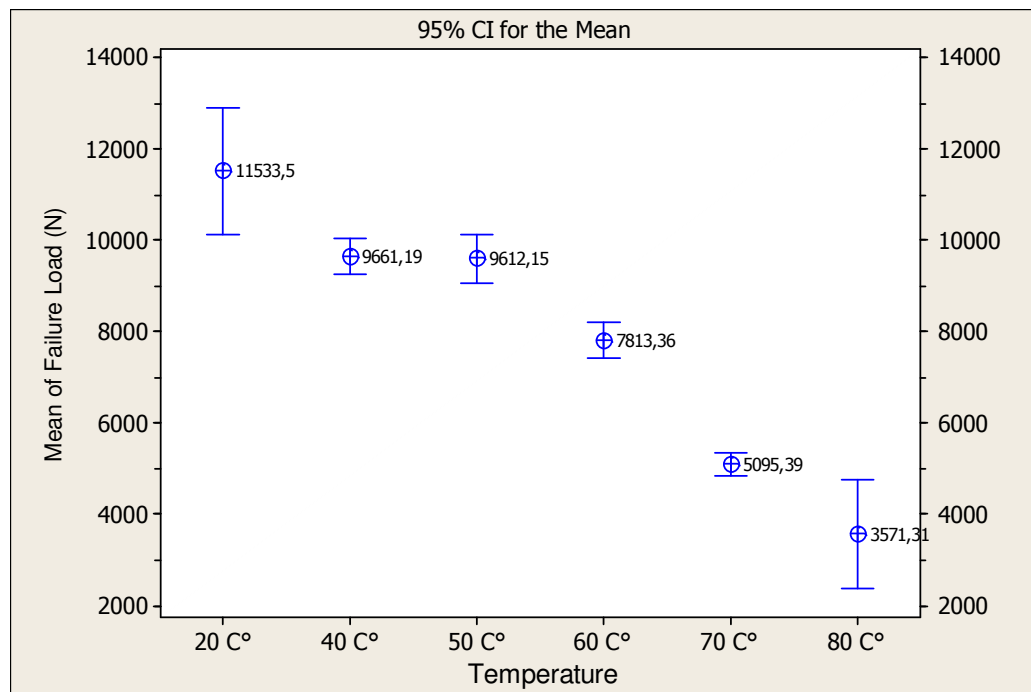Figure 7.10 Box plots of failure loads, occurring at different temperatures under M= 6 Nm

Figure 7.11 Confidence interval (CI) plots for mean values of failure loads, occurring at different temperatures under M= 6 Nm

While assessing the outstanding effects of the test parameters on the failure responses of bolted joints, the utilization of mean failure values of repeated test results was considered to be appropriate based on the Figures 7.9 and 7.11, which are the confidence interval plots of mean values for M= 0 Nm and M= 6 Nm tightening torques, respectively. The Figures illustrate mean values and confidence intervals of mean values, in which they are expected to happen with a confidence level of 95 percent according to the three performed test results. It was shown also, to what extent the mean values converge to the actual values and how credible they are. Of course, by increasing the number of experiments, it could be possible to minimize the size of the confidence intervals, thus it can be converged to the most accurate values. However, as regular decreases in failure results was observed and mean values of the ultimate loads follow a particular gradually descending curve, no additional repetition of tests was considered to be necessary.

In Table 7.1 and Table 7.2, failure loads are presented depending on varying chamber temperatures and tightening torques for glass fiber / epoxy composite bolted joints according to tension test results. The effect of temperature and tightening torque on bearing loads are also illustrated in Figure 7.12. As might be expected and can be observed in Figure 7.12, the load-carrying capacity of the joint is decreased by increasing temperature level. When the temperature has risen up, the internal energy increases and molecular movement of the material becomes easier. Joint is highly affected by this material degradation, thus failure occurs at lower stress levels. In comparison with the room temperature results, the reduction in failure loads between the chamber temperatures 40 ℃ and 80 ℃ varies from about 10 to 70 percent. Furthermore, the maximum decrease of failure loads occurs at 70 ℃ and 80 ℃ with the rate of nearly 55 % and 70 % respectively. This rapid fall is attributed to heat damage to the resin matrix.

The clamping force produced by tightening bolts plays an important role on bearing behavior of mechanically fastened composite joints. There is every appearance that, the influence of preload moment is effective not only at room temperature, but also at higher temperature grades, according the test results. M= 6

Nm torque level contributes to the joint strength approximately 5-15 % compared to the finger tightened ones.
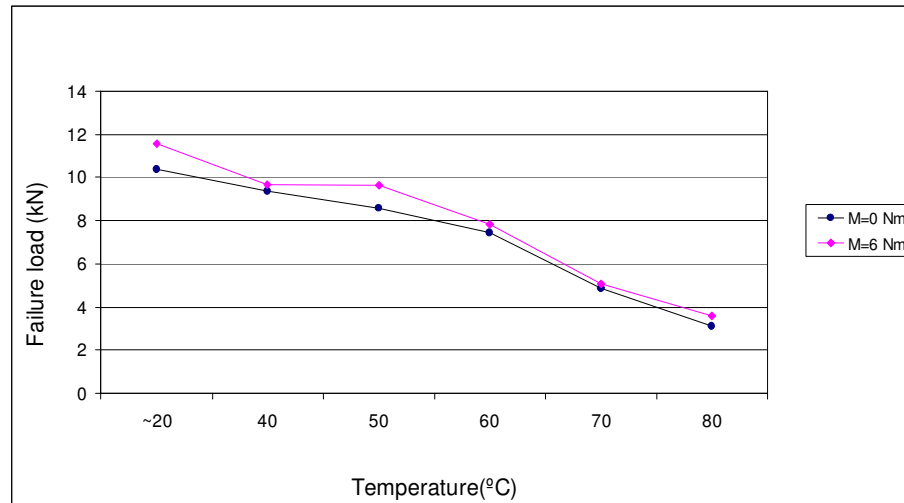

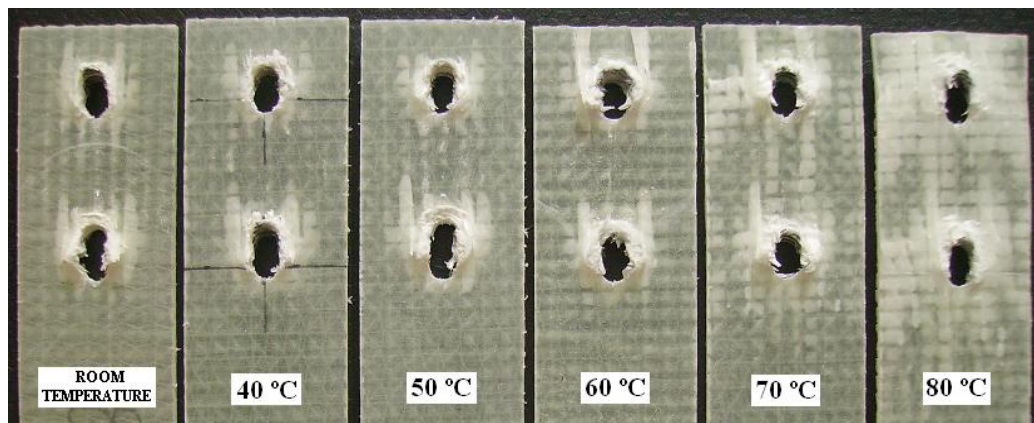Figure 7.12 The effect of temperature and tightening torque on failure load

Figure 7.13 Photo of deformed composite specimens at various temperature levels in tensile tests under M= 0 Nm tightening torque.

Generally speaking, there are three basic pinned joint failure modes related to composites: These are net-tension, shear-out and bearing. In practice, combinations of these failure modes are possible. Net-tension and shear-out modes are catastrophic and result from excessive tensile and shear stresses. Bearing mode is local failure and progressive, and related to compressive failure (Aktas, 2009), (Asi, 2010). In Figures 7.13 and 7.14, photos of deformed glass fiber / epoxy composite specimens exposed to six different temperature conditions during tensile loading tests are presented. As

it can be seen in the figures, the dominant failure type is bearing mode regardless of thermal and clamping force conditions. In addition to that, signs of delamination are observed in the specimens tested at the temperatures of 70 ℃ and 80℃.
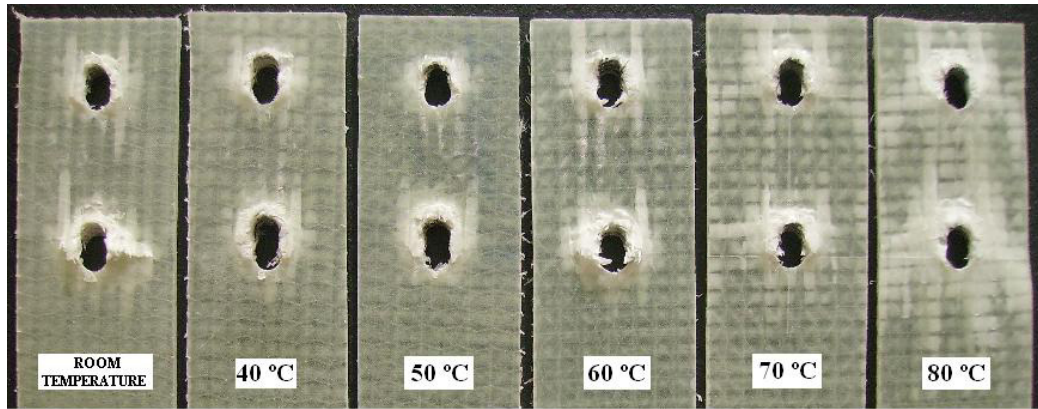

Figure 7.14. Photo of deformed composite specimens at various temperature levels in tensile tests under M= 6 Nm tightening torque.

CHAPTER EIGHT
EXPERIMENTAL STUDY AND RESULTS 0F SINGLE LAP DOUBLE SERIAL FASTENER JOINTS AT LOW TEMPERATURES

8.1 Introduction

According to the previous review, many authors were interested in the material and geometrical parameters influencing the failure behaviors of mechanically fastened composite joints. Nonetheless, a few of them have taken into account the environmental effects, particularly the temperature extremes that composite joints are exposed during operation. Among these studies, those associated with glass-fiber reinforced composites are even more limited.

The current section reports an experimental investigation on failure responses of single lap double serial fastener joints in glass fiber / epoxy composite laminates when subjected to low temperature environment. The results of experiments, implemented at five different low temperature levels ranging from 0 ºC to -40 ºC, were evaluated in comparison with room temperature tests.

8.2 Explanation of the Problem

Composite plates with lay-up of [0/90/45/-45]s configuration were prepared using glass fiber/epoxy. Each specimen has the dimensions of Length (L) = 210mm, Width (W) = 36mm and h (thickness measured) 2mm which are consistent with ASTM D 5961/D 5961M – 01, the standard test method for bearing response of polymer matrix composite laminates (Figure 8.1). A single shear, composite-to-composite, lap joint was formed using two fastener bolts arranged in longitudinal direction. Rigid bolts having a nominal diameter of 6mm were tightened under M=6 Nm or M=0Nm (finger tight) torque levels to observe clamping pressure effects in low temperature quasi-static tensile tests.
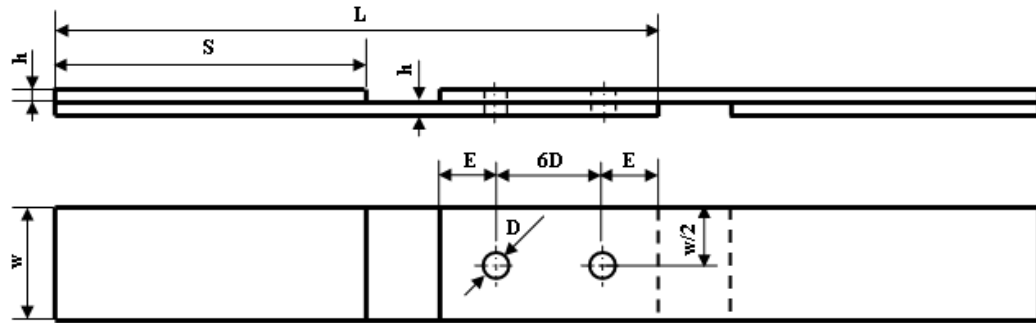
Figure 8.1 Joint of single shear double fastener composite test specimens.

8.3 Experimental Setup and the Cooling Process

To be able to simulate the low temperature conditions, a quick freezer spray (FREEZER BR, -50 ℃) was injected on to the joint zone where the stress concentrations result in the onset damage. The zone was also isolated to maintain the stability of the test temperature (Figure 8.2). The temperature of the material surface was measured simultaneously by means of a thermocouple device. Tests were started as soon as the required temperature level has been reached. During the experiment, the spray was injected continuously at some intervals, changing with the temperature level until the test ended, so that the heat losses could be compensated.

Figure 8.2 Set-up of low temperature test, thermocouple and insulation equipment

8.4 Testing Procedure

A set of experiments were conducted to examine the behavior of bolted joints in glass fiber / epoxy laminates at low temperatures under two different clamping forces. Six different temperature levels (-40, -30, -20, -10, 0 ℃ and ~20℃ (room temperature)) were exposed to the composite joints. When assembling specimen parts, tightening torques of fastener bolts were set to the values of M= 0 Nm (finger tight) and M= 6Nm. The torque was applied using a calibrated torque wrench. The experiments were carried out in Shimadzu AG-100, 100 KN testing machine, at 1 mm/min test speed. The tests were continued until the maximum failure load was reached and stopped when an instantaneous decrease was experienced in the tensile force.

8.5 Results and Discussion

The present study aimed to investigate the behavior of single lap double serial fastener glass fiber / epoxy composite joints in freezing environments, experimentally. Followed by the application at room temperature, static tensile tests were implemented to the specimens under low temperature exposure. Fastener bolts were tightened under the torque levels of M=0 Nm (finger tight) and M=6 Nm. Experiments were carried out at the temperatures ranging from room temperature down to -40 °C.

According to the results, the temperature was found to be effective on failure characteristics of bolted joints in composite laminates. In Figures 8.3 and 8.4, the load – displacement curves of tensile tests are shown that were implemented under M= 0 Nm and M= 6 Nm preload moments, respectively. In comparison with those at room temperature, an increase is observed in slopes of load – displacement curves depending on the exposed temperature level, so the stiffness of the joint increases with decreasing temperature. It also means that, the lower the temperature exposed, the higher load carrying capacity obtained for the same bolt-hole displacement rates.

The difference between slopes becomes more evident when the minimum test temperature was exposed to the test specimen.

Despite the fact that maximum failure loads varies depending on the temperature level, the failure displacements, at which the peak values of bearing forces are formed didn't change significantly when the temperature was decreased. As expected, there is a reduction in failure displacement when torque was applied to the fasteners. This occurrence is due to the increased effect of friction associated with the clamping force, which reduces the relative sliding of the composite laminates (Chishti et al., 2010). It can be seen clearly in Figures 8.3 and 8.4, in which the failure bolt-hole displacements appear to be between 13-15 mm and 11-13 mm, for M= 0 Nm and M= 6 Nm preload moments, respectively.

The load-displacement curves are linear up to a point. After that, the load-displacement curves deviate from linearity. The slopes of curves alter at more than one point (Okutan Baba, 2006). Following the first deflection, the curves follow a zigzag pattern and the load increases more slowly up to the maximum failure load. This behavior is called as bearing mode, which is the most desired failure mode due to its higher load carrying capacity. The matrix fracture, delamination between laminates, fiber breakages, fiber-matrix interface deformation, fiber buckling etc. are the main reasons for the zigzag formation of the curve (Asi, 2010).

All the specimens exhibited dominantly the bearing failure mode regardless of temperature and preload level. In the current experiments, no evidence was found that failure mode is directly affected by the environmental factors.

The load-displacement curves of joints tested under M= 6 Nm tightening torques were illustrated in Figure 8.4. Until the force level reaches up to specific point, the load transfer between plates is performed by the frictional forces generated by the clamping forces that are transmitted by the tightened bolts. The change in slopes of curves between 0-2 mm displacement levels is attributed to the frictional forces to be developed completely. In the subsequent section, once friction forces are fully

overcome, composite plates start to slide relative to each other, which leads the fasteners to pick up the carried load, through the contact between bolts and hole edges. The load transition from friction to the fasteners is getting more drastic at lower temperatures producing a zigzag line as seen in Figures 8.4a and 8.4b, due to the mutual adhesion between plate surfaces. After the load is picked up by fasteners, the geometrical (the edge distance-to-hole diameter ratio E/D, plate with-to-hole diameter ratio W/D etc.), material (stacking sequence etc.) and environmental (temperature, humidity etc.) parameters become of primary importance in determining the failure behavior of mechanically fastened composite joints. Whilst the maximum force, reached without sliding composite plates relatively, is about 3500 N at room temperature, it gets around to 5500 N at subzero degrees centigrade (Figure 8.4).

The temperature has an impact on the yield stress and ductility of the matrix. These effects are clearly observed in the final stage. At low temperatures, the matrix and each lamina become stiff and mechanically brittle. Thermal residual stresses increase as the temperature decreases. More importantly, the strength of the matrix generally increases with decreasing temperature (Hirano et al., 2007). In Table 8.1, failure loads are presented depending on varying temperatures and tightening torques for glass fiber / epoxy composite bolted joints according to test results. The decrease in temperature affects maximum bearing forces as an enhancer factor, as illustrated in Figure 8.6. When comparing with the room temperature data, the increase in failure loads between 0 °C and -40 °C varies from 4 to 22 percent and from 16 to 27 percent for M= 0 Nm and M= 6 Nm preload moments, respectively.

Table 8.1 Failure loads of glass fiber / epoxy composite material joints in tension tests at various temperatures and under different tightening torques

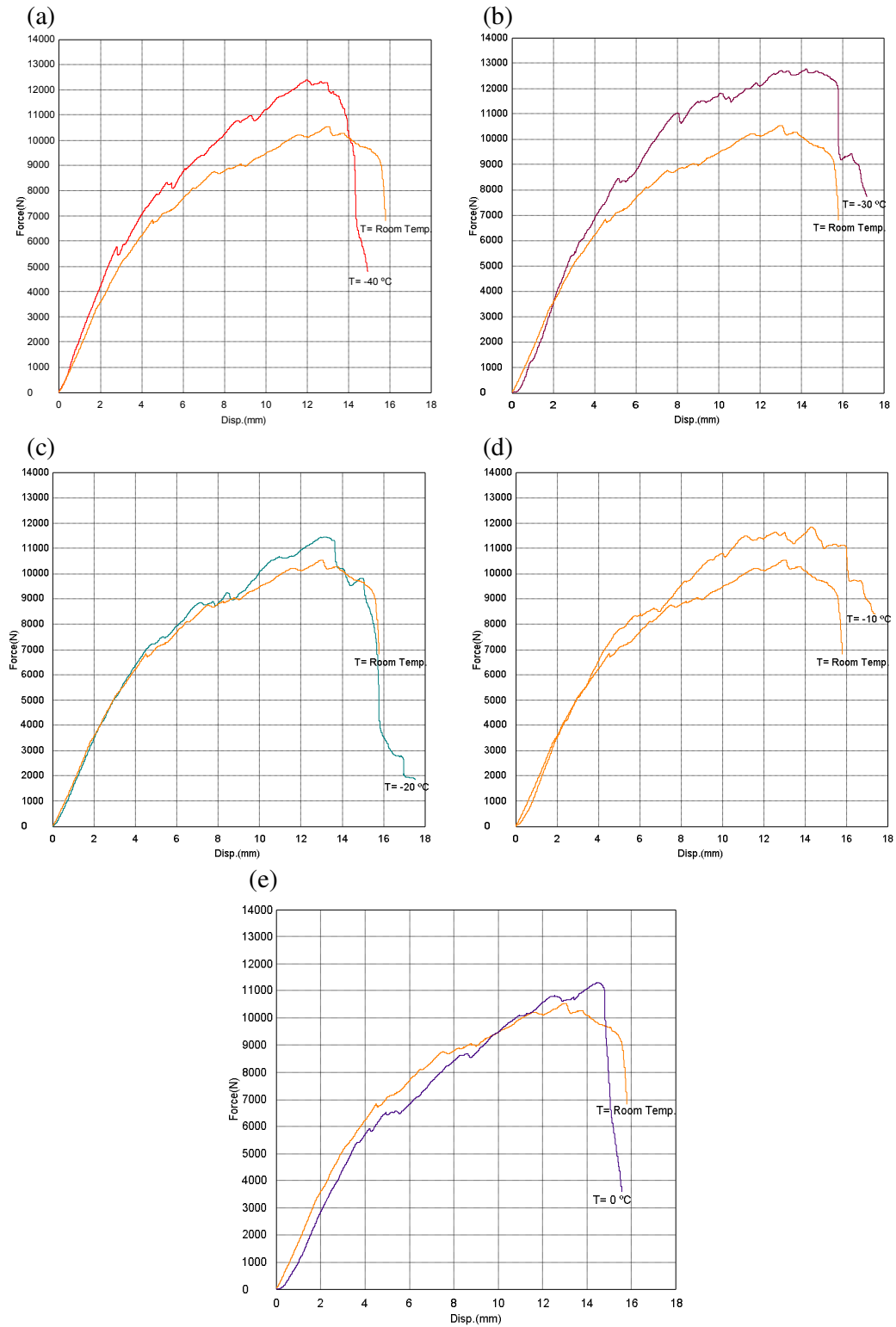|		Failure Loads (N)					
Temperature (ºC)		-40	-30	-20	-10	0	20
Tightening torques (Nm)	0	12847.4	12757.0	11839.3	11837.3	10932.1	10511.0
	6	14198.6	13837.0	13170.2	13027.8	13031.2	11209.9

Figure 8.3 The effect of temperature on load/displacement curves in tensile tests of bolted glass fiber / epoxy composite joint under M= 0 Nm tightening torque. Curves of (a) -40°C (b) -30 °C, (c) -20 °C, (d) -10 °C (e) 0 °C in comparison with that obtained at ~20°C (room temperature)

98
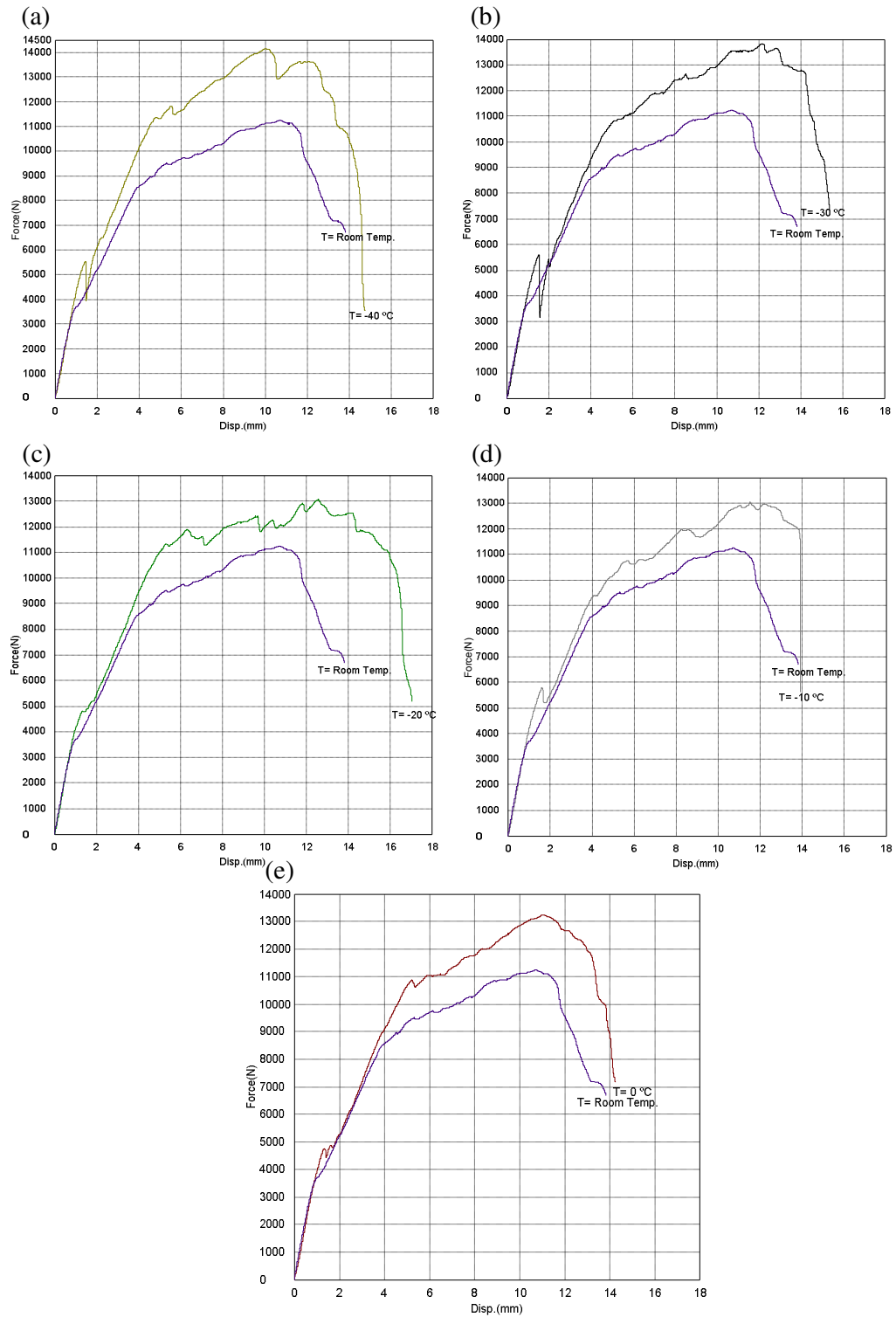

Figure 8.4 The effect of temperature on load/displacement curves in tensile tests of bolted glass fiber / epoxy composite joint under M= 6 Nm tightening torque. Curves of (a) -40°C   (b) -30 °C, (c) -20 °C, (d) -10 °C (e) 0 °C in comparison with that obtained at ~20°C (room temperature)
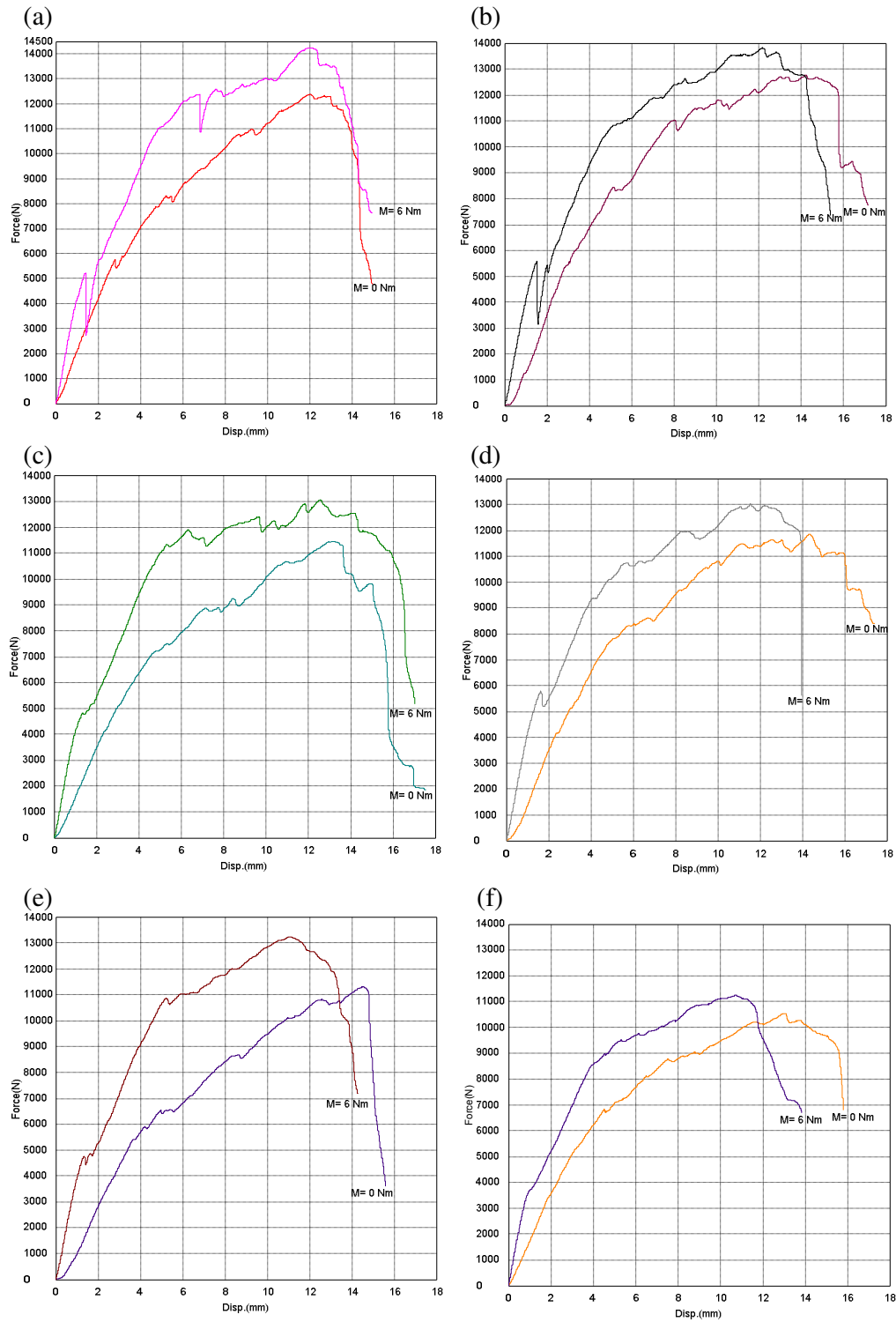
Figure 8.5 The effect of bolt tightening torques on load/displacement curves in tensile tests of bolted glass fiber / epoxy composite joint (a)-40°C, (b) -30 °C, (c) -20 °C, (d) -10 °C,(e) 0 °C (f) ~20°C (room temperature)
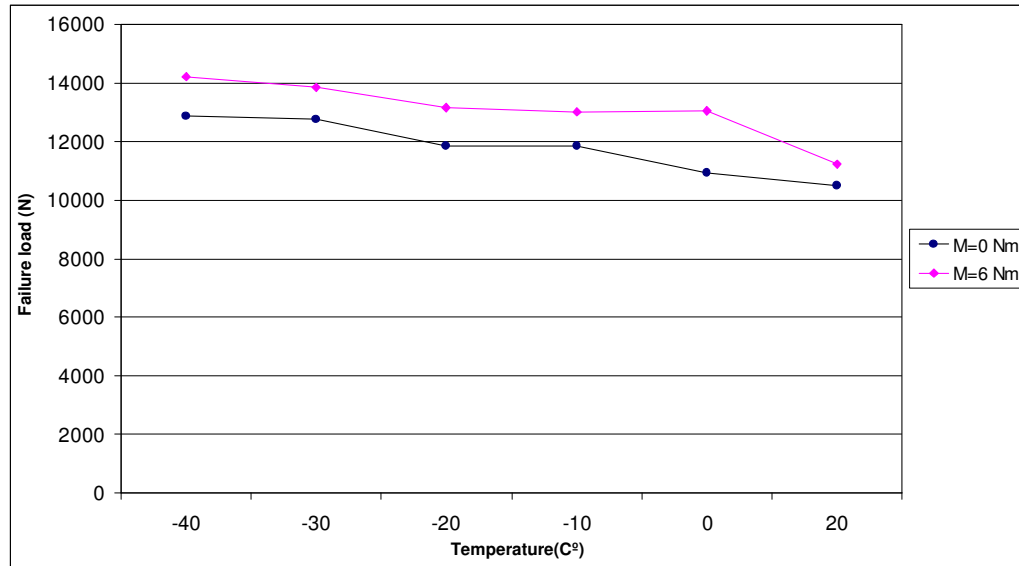
Figure 8.6 The effect of temperature and tightening torque on the failure loads

With the application of the preload moment, the clamping force produced by bolts plays an important role on the failure behavior of bolted joints in composite laminates. Tightening the bolt not only improves the joint stiffness but also takes the maximum bearing forces up to higher levels (Figure 8.5). When comparing with the assemblies of finger tightened bolts, an increase of 6.65 percent was obtained in failure loads of joints of which bolts were under M= 6 Nm tightening torque at room temperature. As the temperature decreased below zero degrees centigrade, the tightening torques seems to be more effective on failure loads rather than that observed at room temperature. In comparison with finger tightened ones, the average rise in failure loads of joints, tightened under M= 6 Nm is observed to be 11.9 percent at temperatures between 0 °C and -40 °C.

The post-deformation photos of the joints examined under M= 0 Nm and M= 6 Nm tightening torques are presented in Figures 8.7 and 8.8, respectively. As seen in these figures, the bearing failures for 6 Nm are slightly greater than the failures of 0 Nm. In the fastened joints with the torque of 6 Nm, even if smaller ultimate failure displacements occur compared to finger tightened ones, higher levels of stresses take place around the holes due to the frictional forces, acting in the vicinity of the hole boundary.
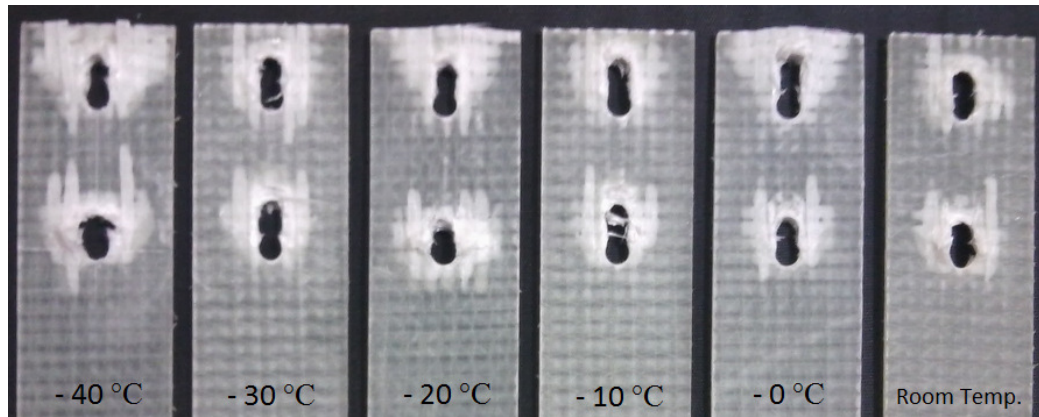
Figure 8.7 Photo of deformed composite specimens at various temperature levels in tensile tests under M= 0 Nm tightening torque.
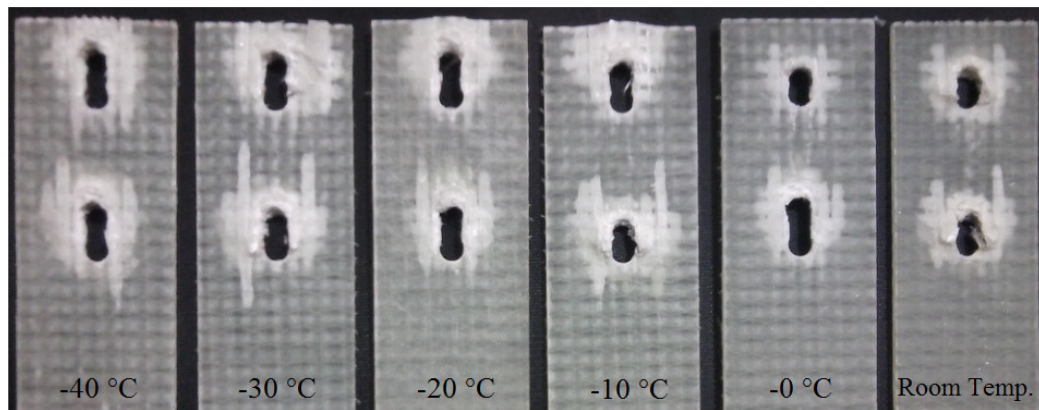

Figure 8.8 Photo of deformed composite specimens at various temperature levels in tensile tests under M= 6 Nm tightening torque.

CHAPTER NINE
CONCLUSIONS

Within the framework of the present study, experimental investigations were performed to obtain the effects of thermal conditions and preload moments on the failure behavior of single lap double serial mechanical fastener glass fiber / epoxy composite joints by means of static tensile tests.

In the first stage, experiments were performed by exposing the joints to five different high temperature levels (40, 50, 60, 70, 80 ℃), as has been discussed in detail in chapter eight. Subsequently, especially considering the freezing environment that the composite structural components of air vehicles are inevitably exposed, tests were conducted at five low temperature levels ranging from 0 ℃ down to -40 ℃ and results were comprehensively reported in chapter nine. Effects of exposing high and low temperatures on failure behaviors of bolted composite joints were discussed in comparison with those tests conducted at room temperature. The effects of preload applied to the fastener bolts and how this effect is influenced by temperature changes were also examined during tests. The following conclusions can be made based on the experimental results:

- Elevated temperatures significantly affect on failure loads of mechanically fastened composite joints. As the test temperature increases, the load-carrying capacity of the joint decreases to some extent depending on the temperature level exposed.

- Low temperature exposure has significant impact on failure loads in mechanically fastened composite joints. Joints exhibit relatively higher load-carrying capacity when decreasing temperature. When the temperature decreases from the room temperature to – 40 ℃, the failure load increases gradually.

- The torque applied to the fastener bolts remarkably affects the joint strength of composites. Higher failure loads are obtained for composite joints under preload

moment compared to the finger tightened ones. The increase in failure loads is getting much greater as the temperature decreases to subzero degrees centigrade. The positive influence of preload moment is experienced at elevated temperatures as well.

• Depending on the test temperature, there is no change in failure modes which are highly affected by material and geometrical parameters. Just as the bearing failure mode, which is the desirable mode, is observed at room temperature, so it is monitored at elevated temperatures and at low temperatures, too. Thus, the selected geometry and material properties are found to be suitable for even low and high temperature applications.

The following investigations can be performed in the future:

o   Hot water aging effects on mechanically fastened composite joints.
o   Effects of hot and cold environments on adhesively-bonded joints.

REFERENCES

Adams, D. O., Moriarty, J. M., Gallegos, A. M., & Donald F. Adams, D. F. (2003). *Development and evaluation of the v-notched rail shear test for composite laminates.* Atlantic City: Federal Aviation Administration.

Adams, D. (2005). *V-Notch Rail Shear test (ASTM D 7078-05).* Retrieved July 31, 2012, from http://www.compositesworld.com/articles/v-notch-rail-shear-test-astm-d-7078-05

Aktaş, A., İmrek, H. & Cünedinoğlu, Y. (2009). Experimental and numerical failure analysis of pinned joints in composite materials. *Composite Structures, 89* (3), 459-466.

Asi, O. (2010). An experimental study on the bearing strength behavior of al_2o_3 particle filled glass-fiber reinforced epoxy composite pinned joints. *Composite Structures, 92* (2), 354-363.

Baker, A., Dutton, S., & Kelly, D. (2004). *Composite Materials for Aircraft Structures* (2th ed.). USA: American Institute of Aeronautics and Astronautics.

Camanho, P.P., & Lambert, M. (2006). A design methodology for mechanically fastened joints in laminated composite materials. *Composites Science and Technology, 66* (15), 3004-3020.

Campbell, F. C. (2004). *Manufacturing processes for advanced composites* (1th ed.). UK, USA, JAPAN: Elsevier Ltd.

Campbell, F. C. (2011). *Joining – understanding the basics* (1th ed.). USA: ASM International.

Choo V. K. S. (1990). *Fundamentals of composite materials* (1th ed.). Delaware: Knowen Academic Press, INC.

Daniel, I. M., & Ishai, O. (1994). *Engineering mechanics of composite materials*.(1th ed.). NY: Oxford University Press

Dano, M.L., Gendron, G., & Picard, A. (2000). Stress and failure analysis of mechanically fastened joints in composite laminates. *Composite Structures, 50* (3), 287-296.

Ekh, J., & Schön, J.(2006). Load transfer in multirow, single shear, composite-to-aluminum lap joints. *Science and Technology, 66* (7-8), 875-885.

Gibson, R.F. (1994). *Principals of Composite Material Mechanics* (1th ed.). NY: McGraw-Hill.

Hirano N., Takao Y., & Wang W.X. (2007) Effects of temperature on the bearing strength of CF / epoxy pinned joints. *Journal of Composite Materials, 41* (3), 335-351.

Jones, R. M. (1999). *Mechanics of Composite Materials* (2th ed.). US: Taylor & Francis Inc.

Karakuzu R., Çalışkan C.R., Aktaş M., & İçten B.M. (2008). Failure behavior of laminated composite plates with two serial pin- loaded holes. *Composite Structures, 82* (2), 225-234.

Kaw, A. K. (2006). *Mechanics of composite materials.* (2th ed.). NY: Taylor & Francis Group, LLC.

Kelly G., & Hallström S. (2004). Bearing strength of carbon fiber/epoxy laminates: effects of bolt-hole clearance. *Composites: Part B, 35*, 331–343.

Kishore A.N., Malhotra S.K., & Prasad N.S. (2009). Failure analysis of multi-pin joints in glass fibre/epoxy composite laminates. *Composite Structures, 91* (3), 266–277.

Lie, S.T., Yu G., & Zhao, Z. (2000). Analysis of mechanically fastened composite joints by boundary element methods. *Composites: Part B, 31* (8), 693-705.

Ling, Y. (1986). An estimation method of bearing strength of bolted joints in fiber reinforced composite. *Applied Mathematics and Mechanics, 7* (1), 103-109.

Mallick, P. K. (1993). *Fiber-reinforced composites materials, manufacturing, and design,* (2 nd ed.). NY: Marcel Decker.

Matthews, F.L., & Rawlings, R.D. (1999). *Composite materials: engineering and science* (1th ed.). London, UK: Imperial College of Science, Technology and Medicine.

Messler, R.W. (2004). *Joining of materials and structures* (1th ed.). USA: Elsevier Butterworth-Heinemann.

Okutan, B. (2001). *Stress and failure analysis of laminated composite pinned joints.* PhD Thesis, Dokuz Eylül University, Izmir.

Okutan Baba, B. (2006). Behavior of pin-loaded laminated composites. *Experimental Mechanics, 46* (5), 589-600.

Ozen M., & Sayman O. (2011). Failure loads of mechanical fastened pinned and bolted composite joints with two serial holes. *Composites Part B, 42* (2), 264-274.

Park, H.J. (2001a). Bearing failure analysis of mechanically fastened joints in composite laminates. *Composite Structures, 53* (2), 199-211.

Park, H.J. (2001b). Effects of stacking sequence and clamping force on the bearing strengths of mechanically fastened joints in composite laminates. *Composite Structures, 53* (2), 213-221.

Pearce, M.G., Johnson, A.F., Thomson, R.S. & Kelly, D.W. (2010). Experimental investigation of dynamically loaded bolted joints in carbon fibre composite structures. *Appl. Compos Mater, 17* (3), 271-291.

Pekbey, Y. (2008). The bearing strength and failure behavior of bolted e-glass-epoxy composite joints. *Mechanics of Composite Materials, 44* (4), 397-414.

Peters, S. T. (1998). *Handbook of composites* (2th ed.). London: Chapman & Hall.

Sánchez-Sáez S., Gómez-del Río T., Barbero E., Zaera R., & Navarro C. (2002). Static behavior of CFRPs at low temperatures. *Composites: Part B, 33* (5), 383-390.

Sen, F., Pakdil, M., Sayman, O., & Benli, S. (2008). Experimental failure analysis of mechanically fastened joints with clearance in composite laminates under preload. *Materials and Design, 29* (6), 1159-1169.

Sen F., Komur M.A., & Sayman O. (2010). Prediction of bearing strength of two serial pinned / bolted composite joints using artificial neural networks. *Journal of Composite Materials, 44* (11), 1365-1377.

Sen F., & Sayman O. (2011). Failure response of two serial bolted joints in composite laminates. *Journal of Mechanics, 27* (3), 293-307.

Sheikh-Ahmad J.Y. (2009). *Machining of Polymer Composites* (1th ed.). NY: Springer Science + Business Media LLC.

Song M.H., Kweon J.H., Kim S.K., Kim C., Lee T.J., Choi S.M., & Seong M.S. (2008). An experimental study on the failure of carbon/epoxy single lap riveted joints after thermal exposure. *Composite Structures, 86* (1-3), 125-134.

Staab, G. H. (1999). *Laminar composites*. (1th ed.). USA.: Butterworth-Heinemann.

Thostenson, E.T., & Chou, T.W. (2008). Carbon nanotube-based health monitoring of mechanically fastened composite joints. *Composites Science and Technology*, *68* (12), 2557-2561.

Walker S.P. (2002). Thermal effects on the pin-bearing behavior of im7/peti5 composite joints. *Journal of Composite Materials, 36* (23), 2623-2651.